DISSERTATION

INVERSE COLLOIDAL CRYSTAL MEMBRANES: FORMATION, SURFACE

MODIFICATION AND APPLICATIONS

Submitted by

Xinying Wang

Department of Chemical and Biological Engineering

In partial fulfillment of the requirements

For the Degree of Doctor of Philosophy

Colorado State University

Fort Collins, Colorado

Fall 2010

Doctoral Committee:

    Department Chair: David S. Dandy

    Advisor: Ranil Wickramasinghe

    Scott M. Husson

    Travis S. Bailey

    Xianghong Qian

ABSTRACT

INVERSE COLLOIDAL CRYSTAL MEMBRANES: FORMATION, SURFACE
MODIFICATION AND APPLICATIONS

Inverse colloidal crystal (ICC) membranes have many advantages, such as highly
uniform pore size, fully interconnected pores, and high porosity, over commercially
available porous membranes as a selective barrier for ultrafiltration and microfiltra-
tion. However, making a ICC membrane which is applicable in separations using
reported ICC membrane formation methods has been still not successful yet. we
describe here a new ICC membrane formation method, vertical cell (VC) assembly
method, to make ICC separation membranes in a simple, low-cost way. The VC as-
sembly method is a versatile colloidal crystal assembly method which is specifically
designed for making ICC membranes.

Formation of colloidal crystal films(CCF), which is the first step in formation of
the inverse colloidal crystal membrane, to large extent determines how good the fi-
nal membrane properties. The vertical cell assembly method is described that yields
CCFs with surface areas up to 5 cm^2 and thicknesses up to 100 μm. The thickness
of the CCF can also be easily controlled by the spacer which is used.

Based on the new ICC membrane formation method, the ICC membranes have
been fabricated with a variation of pore-sizes and thicknesses. The membrane cast-

ing cell facilitates easy variation of membrane thickness. The membrane pore size is varied by changing the diameter of the silica spheres used to prepare the colloidal crystal template. By changing the composition of the reactive monomer solution, membranes have been fabricated with different hydrophobicities. The ICC membranes were tested in a commercially available stirred cell. Particle fractionation was studied in normal flow filtration experiments. The membrane produced from 835 nm particles and 100 μm spacer gives a good passage for 60 nm particles in 60-835nm bidisperse particle suspension while gives poor passage for the same size paritcles in 60-440 nm bidisperse particle suspension.

Fabrication of a UF membrane requires a much smaller pore size. However, for making the ICC membranes with pore size in UF range , it is hard to produce them relying on using small SiO_2 particles. This would lead to poor membrane mechanical strength. Here, I described a way to reduce the ICC membrane pore size by growing a unform poly (poly ethylene glycol methacrylate) (PPEGMA) nano-layer from the membrane surface using surface initiated atom transfer radical polymerization. The grafted membranes were characterized with SEM, XPS, ATR-FTIR and water contact angle measurement. Dextran rejection test was conducted on the modified membrane with modification time of 3hr. The rejection rate was obtained for dextran with Mw from 1 kDa through 2000 kDa. the tested membrane shows more than 80% rejection for Dextran with MW more than 100 kDa, and a partial rejection for Dextran with Mw from 10 kDa to 100 kDa, and a less than 20% rejection for Dextran with MW smaller than 10kDa.

ACKNOWLEDGEMENTS

I would never have been able to finish my dissertation without the guidance from my committee members, help from my friends, and support from my family.

I would like to express my deepest appreciation to my advisor, Dr. Ranil Wickramasinghe, for his excellent guidance, caring, patience, and providing me with an excellent atmosphere for doing research. I would like to thank my committee members, Dr. Husson, Dr. Qian, and Dr. Bailey for their constructive suggestions towards my research and the kind conversations over the years.

I would like to thank my fellow group members, David Grzenia for helping me a lot on HPLC operation and analysis, Justin Weaver for providing me with antibody and helping me a lot on FPLC, Heath Himstedt for helping organizing the lab, and the former group members Michael Becker, Emily Stump, Hailey Cutler, Shytyug Loh for their kind help during my PhD study.

My thanks also go to all the people who helped me during my PhD study.

TABLE OF CONTENTS

LIST OF TABLES

LIST OF FIGURES

1. BACKGROUND INTRODUCTION

Abstract

In this chapter, an overall introduction is given to inverse colloidal crystal materials. In the first section, inverse colloidal crystal material formation procedures are introduced including assembly of colloidal crystal template, infiltration of precursor, solidification of precursor, and removal of the template. The template assembling methods reported for ICCs and their precursors are summarized. In the second section, the reported ICC applications are described. In the following section, the reported ICC membrane formation methods are described in detail and their advantages and disadvantages for making ICC membranes are summarized. Finally, the motivation is stated for developing ICC membranes as separation membrane. My contributions to this work is described.

1.1   Introduction to the inverse colloidal crystal (ICC)

An inverse colloidal crystal (ICC) is a macro-porous material that has a three-dimensional ordered pore structure. The first report of making ICC material using colloidal crystal as template was in the late 1990's.[1] Since then, ICC has been extensively studied due to its special structures, including its highly periodical structure, high volume pores and uniform pore size.[2] Generally, making ICCs includes four steps, which are assembly of colloidal crystal template, infiltration of reactive precursor solutions, polymerization or solidification of the precursors, and the last, removal of colloidal crystal template. Some new publications give three steps in which assembly of template and infiltration of precursor are combined as one step. Figure 1.1 gives the illustration of the four steps for making ICCs. Every step has the flexibility to modify to make ICCs with desired properties.

Colloidal crystal template assembly, which is the first step to make ICCs, is the most important step among the four making steps because it determines the quality of the ICC structure. There are a variety of methods available to make colloidal crystal templates. The method classification is mainly based on the driving forces driving the colloidal particles close-pack together to form a colloidal crystal.

Table 1.1 summarizes the driving forces and their derived template assembling methods. The template assembly methods try to make colloidal crystals with long range ordered structure on which the ICC structure is based. Since the ICC was first made

from colloidal crystal template, the template assembly methods have been continuously updated. At the early stage, there were a few template formation methods available, such as gravitational and filtration assembly[1, 7, 8, 9]which were only for 3D templates. As a result, only 3D ICC can be produced from them. The new methods developed afterwards were much more versatile in making ICC and they are mostly to assemble 2D templates, which were mainly for making 2D ICCs.

The colloidal particles for making template are either inorganic or polymeric. The particles have to meet the following requirements before they can be served to make templates. First, the particle size needs to be uniform. Size derivation should be less than 5%.[1] Second, the particles need to be easily etched away physically or chemically. Based on the requirements, the most commonly used inorganic particles are silicon dioxide particles. They are able to be easily made through Stober method and be easily etched away by hydrofluoric acid. For polymeric particles, the most commonly used particles are polystyrene or poly methyl methacrylate(PMMA) particles which can be easily removed by solvent extraction or burning.

Subsequent to assembly of the colloidal crystal template, the following steps are infiltration of a fluid or a vapor precursor, solidification of the precursor, and removal of the template. Precursors determine the final ICC materials. So far, there are a variety of ICCs prepared using corresponding precursors. Table 1.2 gives the summary of ICCs and their precursors. The solidification of precursor is highly dependent on the precursor being used. For making metal oxide ICCs, precursors are usually metal

alkoxides, salt solution, and nano particles suspension. All these precursors can be solidified by hydrolyzing and heating. Thermo or UV initiated polymerization is the way to solidify monomer precursors to make polymer or hydrogel ICCs. Calcination of metal oxide precursors under H_2 flow is a way to make semiconductors and metal ICCs.

Template removal, the last step for making ICC membrane, is either by solvent extraction, calcination for polymer particles or etching away using hydrofluoric acid solution for silicon dioxide particles. Based on the application of the final ICCs, the four ICC production steps are specifically grouped together to produce the ICC with desired properties. In the following section, the applications of the ICCs are summarized

1.2   Applications of the ICCs

A number of applications for ICC materials have been reported so far and new applications are still emerging. The earliest application reported for ICC was in the optical area. The periodical structure of ICC causes it to be considered as a relatively inexpensive photonic crystal material that can be used to make optical devices. Photonic crystals are materials that show similar functions to photons as semiconductor to electrons. In a semiconductor, the periodic potential affects electron motion by defining allowing and forbidden electronic energy band. In photonic crystal, the periodic structure provides a diffraction grating for light with wavelength comparable

to the repeating unit size. Based on the application of ICC in optical area, ICC sensors for sensing temperature, humidity, pH etc have been fabricated. More and more new applications are still developing taking advantage of ICC's special structures. A summary is made in Table 1.3 for all reported applications of ICC.

As seen from Table 1.3, no report is found about ICC applied in separation area. As ICC is a macroporous material with fully interconnected and uniform pores, it is ideal for use as a selective barrier for size exclusion separation. However, there are several challenges for ICC materials to be made into a flat sheet membrane applicable in separations. First, the integral ICC membrane size needs to be big enough to fit the commercially available membrane holder with a size usually more than 10 mm in diameter. Second, the membrane mechanical strength needs to be strong enough to bear at least several psi pressure. Last, but not the least, pores on both sides of the membrane should be open because most ICC materials have closed pores on the surface due to the formation process. There are also a few ICC membrane formation methods reported to make ICC membranes. However, the membranes formed from the reported methods are hard to meet the requirements mentioned above. Therefore, no successful separation applications of the ICC membranes have been reported so far. In the following, I will summarize the reported ICC membrane formation methods.

1.3 Reported ICC membrane formation methods

1.3.1 Vertical deposition assembly

The vertical deposition assembly method to make ICC membrane was first reported by Jiang et.al.[3] In this method, a piece of glass slide is vertically placed into a beaker which contains particles suspension. As solvent, usually water, is vaporizing, particles will deposit onto the glass slide and assemble to form a colloidal crystal film by capillary force (see figure 1.2 (A)). Colloidal crystal film thickness can be controlled by the particle concentration in suspension. The formed colloidal crystal film is then covered by another slide to form a colloidal crystal 'sandwich' (figure 1.2 (B)) for monomer infiltration. As the distance between the two slides is only about 10 μm, the monomer solution can infiltrate colloidal film by capillary force in a very short time (in minutes). After infiltration, the monomer will be polymerized thermally or by UV irradiation. Afterwards, both slides are carefully separated to get the free standing composite film. To obtain the ICC membrane, the film is then soaked into a hydrofluoric acid solution to etch away the SiO_2 particles. Figure 1.2 (C) shows the SEM image of one side of ICC membrane obtained by VD method. As seen from the image, the surface and the cross section are highly porous. However, the other side of the membrane has always a condensed polymer layer (see figure 1.2 (D)) due to the space between the colloidal crystal film and the covering slide.

1.3.2   Physical confinement cell assembly

In this method, a confinement cell is first fabricated.[4, 9] Figure 1.3(A) shows the setup of the cell. It is composed of two pieces of glass substrates and a square frame as a spacer. The frame is treated by a photolithographic procedure to create microchannels on its surface to allow the solvent to flow out while keeping the particles in place. A glass tube is attached to a hole on the top glass substrate using epoxy adhesive. The cell is held together with clip binders. Subsequent to cell fabrication, the particle suspension is injected in through the tube by a syringe. Pressurized nitrogen is then applied to the tube to press out the solvent while keeping the particles inside of the cell. The particles will assemble to be a colloidal crystal film. After the template is obtained, monomer solution is injected through the same glass tube for monomer infiltration. The monomer solution is polymerized thermally or by UV irradiation. Subsequently, the template is etched away either by HF solution or solvent depending on the particles used. This method provides a way to make ICC membranes quickly. Figure 1.3(B) gives the published picture of ICC membrane produced from this method. As seen, the membranes made from this method are small and are not integral.

1.3.3   Particle assisted wetting method

Particle assisted wetting method is a way to make very thin ICC membranes.[5] In this method, a mixture of surface hydrophobic SiO_2 colloidal particles and non volatile

monomer which is trimethylolpropane trimethacrylate were suspended on water surface. The SiO_2 colloidal particles are embedded in the monomer layer. After the assembly, the monomer layer is polymerized under UV irradiation. Subsequently, the particle-polymer composite film is transfered into an HF solution for template removal. The resulting membranes have a regular porous structure. The membrane area can be made up to 23 cm^2 surface area. However, the thickness of the membrane is very hard to control. The maximum thickness of the membrane reported is 10 μm, which gives a poor mechanical strength for separation. Even worse, in the template assembling step, as particles tend to settle out of the film, stabilizing the particles requires great skill. Thus the particle assisted wetting method provides a method to make ICC membranes. However, Making ICC membrane is not easy and the ICC membranes obtained are not good enough to be used for separations.

1.3.4   Spin coating method

The spin coating method provides a method to make wafer sized ICC membranes quickly.[10] In this method, a spin coater is employed for assembly of the colloidal crystal template. Like the particle assisted wetting method, a mixture of SiO_2 colloidal particles and monomer solution are used. The mixture is dropped to the center of a silicon wafer which is placed on the spin coater. As the coater is rotating, the mixture will spread over the wafer and form a film. Figure 1.4 (A) is an illustration for this process. The thickness of the film is controlled by rotation speed. After the colloidal crystal film is formed, the monomer is polymerized by UV irradiation.

Then the ICC membrane is obtained after removal of the particles. However, the ICC membrane made from this method has a thin non-porous layer covering upper surface of the membrane. Thus plasma treatment is needed to get rid of the polymer layer. The spin coating method provides a way to make ICC membranes with wafer size quickly. The pore structure is very regular. However, membrane thickness control is still a problem. The maximum thickness reported for ICC membranes produced from this method is about 10 μm which will gives a poor mechanical strength. Some damages can even be seen in the ICC membrane picture published (figure 1.4 (B)).

1.4 Motivation for developing ICC membranes and our contributions

Membrane technologies have been widely used in producing protein products such as food, additives, enzymes, antibodies etc. Based on the applications of protein products, the protein purity requirements are different. The higher the protein purity requirement is, the higher the production cost is, and the higher percentage of cost goes to separation and purification step. For example, therapeutic protein products have an extremely strict purity requirement as they are injected into human body. As a result, the cost of producing such protein drugs is very high and up to 80% of its cost goes to the separation and purification step in which there may be a big space for membranes technologies applied to cut down the cost.[6] Therefore, the membrane possesses a high separation efficiency, in other words, the membrane has narrow pore size distribution, high porosity, fully interconnected pores and large surface area will largely cut down the protein drug production cost. However, most of

commercially available porous membranes which are produced from phase inversion method are suffering of broad pore size distribution and low porosity. The remaining porous membrane products, which are made from other methods such as sintering, stretching, and track etching method, may have high porosity, yet, at the same time they will lose pore uniformity, or have pore uniformity traded with porosity and pore interconnectivity.

Inverse colloidal crystals, introduced in previous sections, is a macroporous material with very uniform and fully interconnected pores, high porosity (up to 74% theoretically) and large surface area, which make it an ideal material for membrane chromatography, ultrafiltration and microfiltraion, all of which is very important in bioseparation. A number of applications for ICC material have been reported due to its unique structures. Nevertheless, no report for ICC material used in separation process exists because the ICC membranes made from the reported ICC membrane formation methods have problems being used as separation membranes.

In this work, the ICC membranes which are applicable in separation applications have been developed. The first step is making the colloidal crystal template which is very important in determining the properties of the ICC membrane. Chapter 2 focuses on making colloidal crystal template. Large-area colloidal crystal films with different thicknesses assembled from different size of polystyrene particles using a new-developed assembly method are investigated in this chapter.

Chapter 3 gives the details about making ICC membranes using the newly developed ICC membrane formation method. ICC membranes with a variation of thicknesses and pore sizes, and made of a variety of polymers are produced successfully. The application of ICC membrane in particles fractionation is also discussed in this chapter.

Chapter 4 describes the surface modification of ICC membranes using surface initiated atom transfer radical polymerization. The pore size of the membrane can be well controlled by the modification time. Dextran rejection test shows that the modification achieves the goal of decreasing membrane pore size and improving membrane surface hydrophocility.

List of tables

Tab. 1.1: Summary of the driving forces and their derived template assembling method

Driving Force	Assembling method	dimension
Gravitational force	Sedimentation assembling[7, 8]	3D
External pressure	Filtration assembling[1]	3D
	Confinement cell assembling[9]	2D
Centrifuge	Spin coating[10]	2D
Capillary force	Vertical deposition[11]	2D
	Capillary cell	2D
Electric static force	Electric field driving assembly[13]	2D
Buoyancy	Floating assembling[14]	3D
Surface tension	Particles assisted wetting[15]	2D
Temperature gradient	Thermally driven assembly[16]	2D

Tab. 1.2: Summary of reported ICC materials and their precursors

	ICC material	Precursor
Oxides	SiO_2[17] TiO_2[17] ZrO_2[18] WO_3[19]	Organometallic precusor,
	$Cr2O_3$[20] Mn_2O_3[20] Fe_2O_3[20] NiO[21]	metal alkoxides, salt
	Al_2O_3[22] Mg_2O_3[20] SnO_2[23]	
Ternary Oxides and Compositions	$BaTiO_3$[24] $PbTiO_3$[25] $LiFePO_4$[26]	Metal alkoxides, salt
	$LiCoO_2$[27] $LiNiO_2$[28] $LiNbO_3$[29]	
	$Li_4Ti_5O_{12}$[30] $LaFeO_3$[31]	
Non-oxides	Carbons[32] Diamond[33] $CaCO_3$[20]	Meltings, vapor, polymers, salt
Metals	Fe[34, 35] Co[36] Ni[21] Au[37] Zn[38] alloies[39]	Metal oxalate-latex composite, metal related acid
Semiconductors	Si[40] GaP[41] InP[41]	Vapor
Polymers	Polyurethane[42] polyacrylonitrile[43]	Monomer solution

Tab. 1.3: Summary of reported applications for ICCs

ICC structure	Field	Application
Periodical pore structure	Optical application	Photonic bandgap material[44]
		Pigments[45]
		Roman Spectroscopy[46]
	Sensors	Protein sensing[47]
		Humidity sensing[48]
		pH sensing[49]
		Temperature sensing[50]
		Gas sensing[51]
High surface area and fully interco- nnected pores	Catalysis	Catalysi[18, 31]
		Catalyst scaffold[52]
	Bioactive materials	Cell culture scaffold[53]
		Tissue engineering[54]
	Electrode and Battery	Electrode[55]
	Sorption media	Gas adsorption[56]
		Metal adsorption[57]

List of figures

Template assembly

Precursor Infiltration

Precursor solidification

Template removal
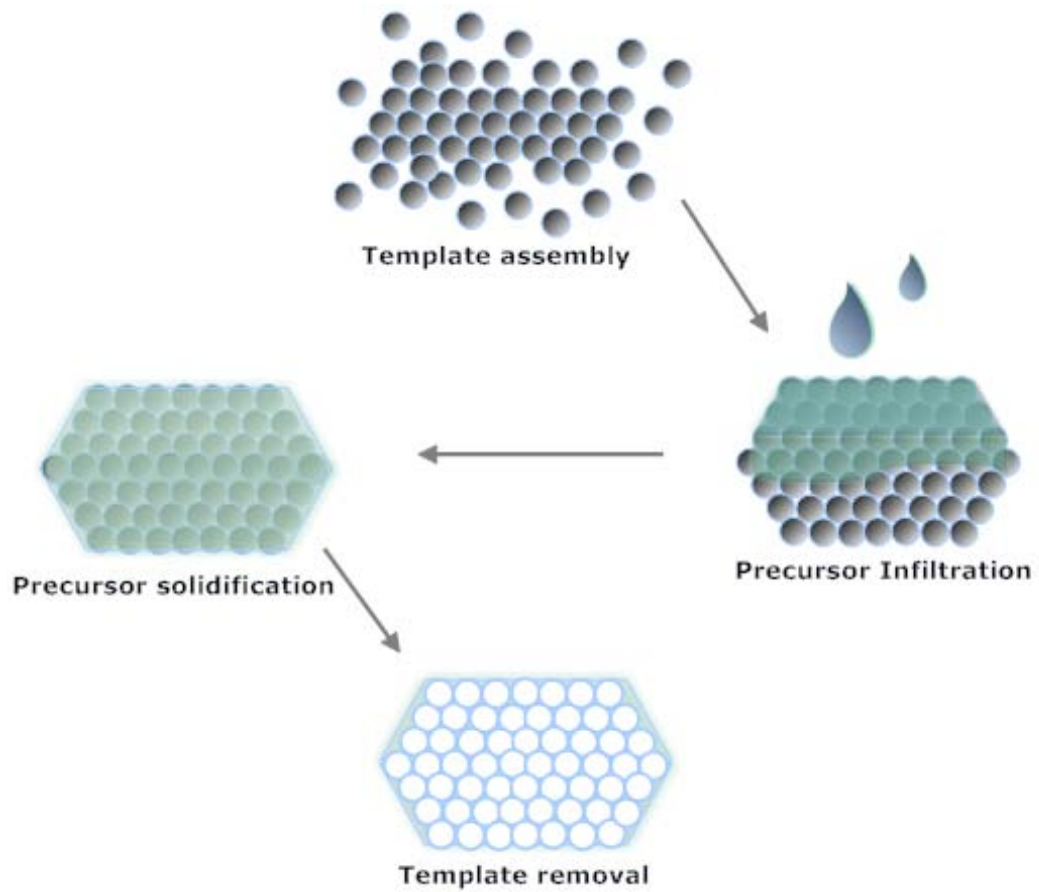
Fig. 1.1: Illustration of the four steps making ICCs
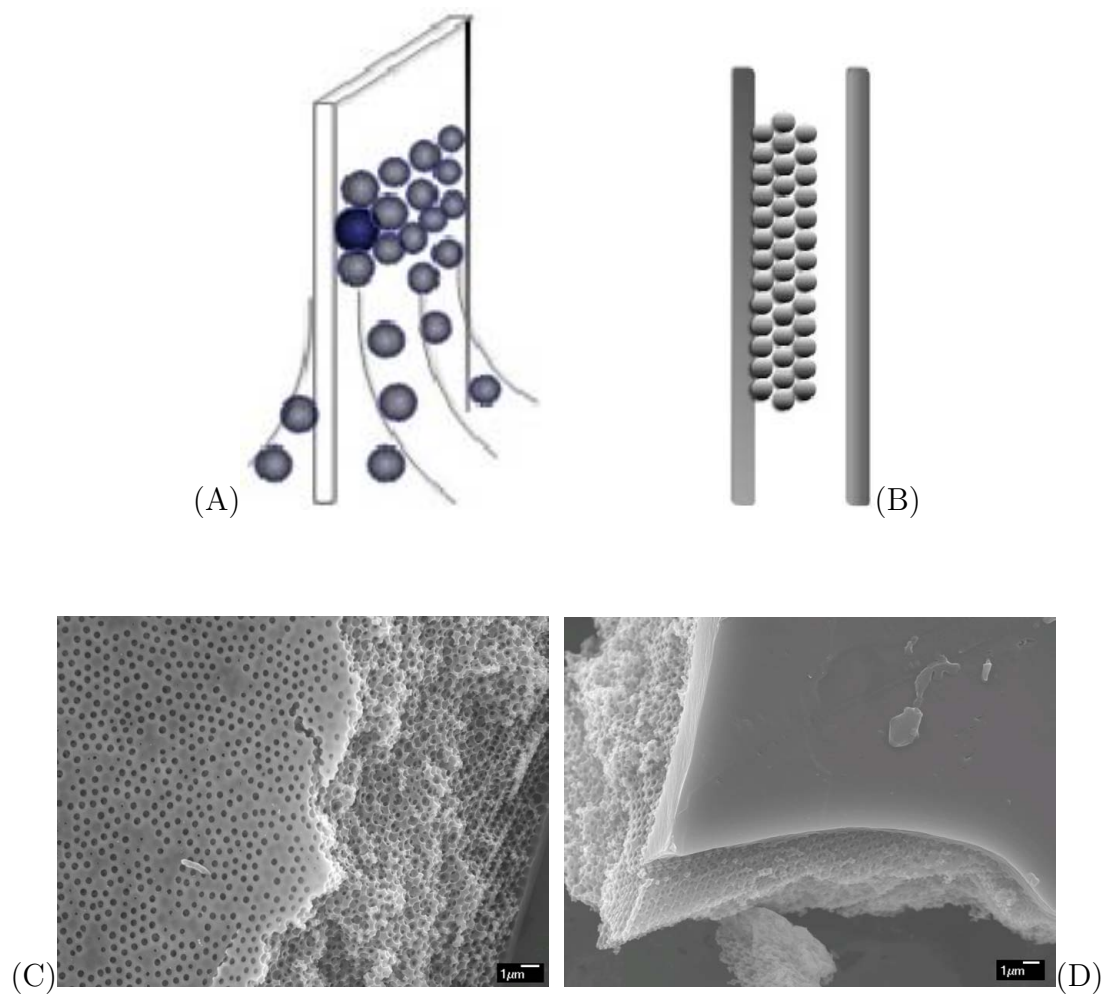
Fig. 1.2: Illustration of vertical deposition assembly method (A) template assembly process (B) template 'sandwich' for monomer infiltration (C) SEM image of top side of ICC membrane (D) SEM image of the bottom side of ICC membrane made from vertical deposition assembly method)

(A)

(B)
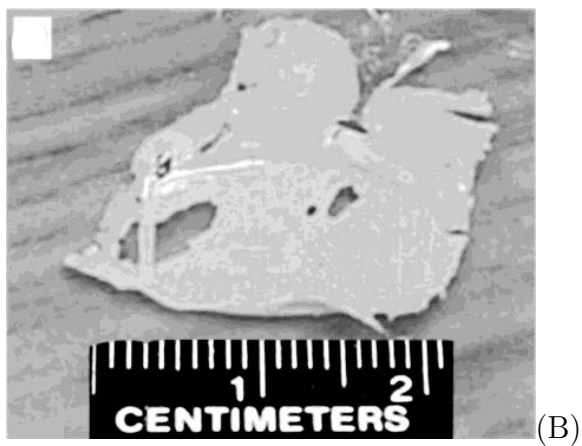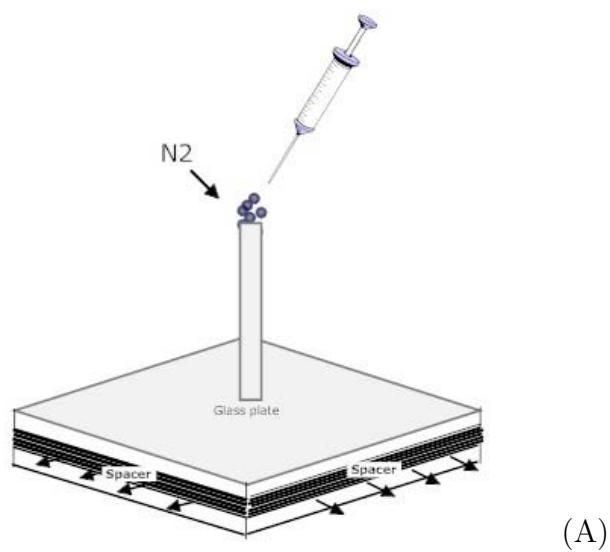
Fig. 1.3: (A)Illustration of particle assisted wetting assembly method (B) Picture of ICC membrane made from particle assisted wetting assembly method (F. Yan, W. A. Goedel, Adv. Mater. 16, 911 Copy right, John Wely)

(A)

(B)
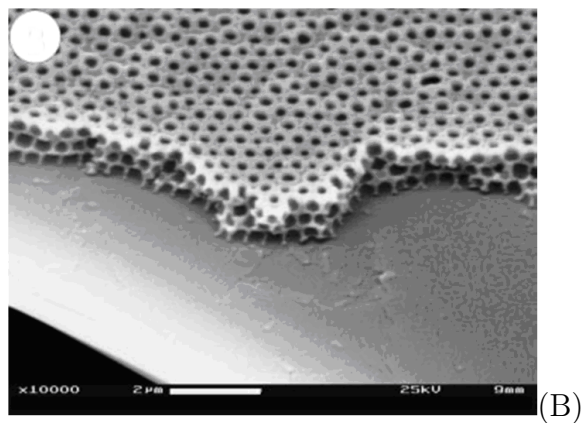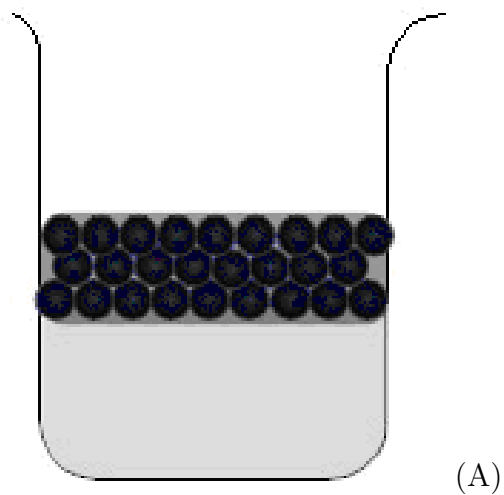
Fig. 1.4: (A)Illustration of confinement cell (B) Picture of ICC membrane made from confinement cell assembly method (B. Gates, Y. Yin, Y. Xia, Chem. Mater. 11, 2827, Copy right ACS)

(A)

2 cm (B)
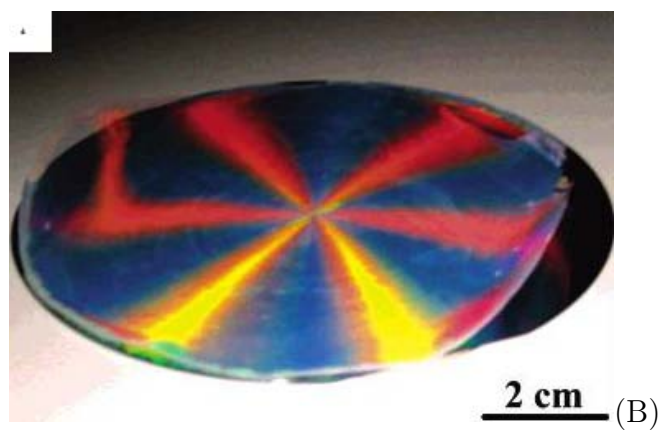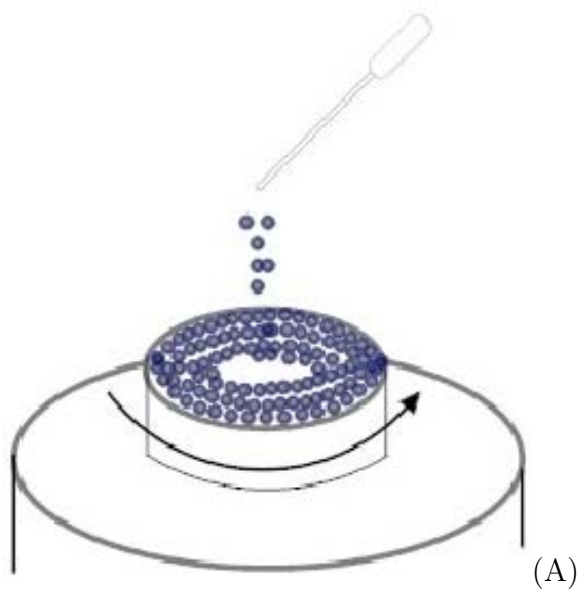
Fig. 1.5: (A)Illustration of spin coating assembly method (B) Picture of ICC membrane made from spin coating assembly method (P. Jiang, M.J. Mcfarland, J. Am. Chem. Soc. 126, 13778, Copy right ACS)

Bibliography

[1] B.T. Holland, C.F. Blanford, S. Stein, Synthesis of macroporous minerals with highly ordered three-dimensional arrays of spheroidal voids, Science 281 (1998) 538-540

[2] J. E. G. Wijnhoven, W. L. Vos, Preparation of photonic crystals made of air spheres in Titania, Science 281 (1998) 802-804

[3] P. Jiang, K. S. Hwang, D. M. Mittleman, J. F. Bertone, V. L. Colvin, Template-directed preparation of macroporous polymers with oriented and crystalline arrays of voids, J. Am. Chem. Soc. 121(1999) 11630-11637

[4] B. Gates, Y. Yin, Y. Xia, Fabrication and characterization of porous membranes with highly ordered three-dimensional periodic structures, Chem. Mater. 11(1999) 2827-2836

[5] F. Yan, W. A. Goedel, A simple and effective method for the preparation of porous membranes with three dimensional arranged pores, Adv. Mater. 16(2004) 911-915

[6] C.Charcosset, Purification of proteins by membrane chromatography, J. Chem. technol. Biotechnol. 71(1998) 95-110

[7] R. Mayoral, JS Requena, C.Lopez, A. Cintas, H. Miguez, F. Meseguer, L.Vazquez , M. Holgado, A. Blanco, Adv. Mater. 9(1997) 257

[8] O.D. Velev, T. A. Jede, R. F. Lobo, A. M. Lenhoff, Microstructured porous silica obtained via colloidal crystal templates, Chem. Mater. 10(1998) 3597

[9] B. Gates, Y. Xia, Fabrication and characterization of chirped 3D photonic crystals, Adv. Mater. 12(2000) 1329-1332

[10] P. Jiang, M.J. Mcfarland, Large-scale fabrication of wafer-sizecolloidal crystals, macroporous polymers and nanocomposites by spin-coating, J. Am. Chem. Soc. 126(2004) 13778-13786

[11] Z.Z. Gu, A. Fujishima, S. Sato, Fabrication of high-quality opal films with controllable thickness, Chem. Mater. 14(2002) 760-765

[12] H. L. Li, F. Marlow, Controlled arrangement of colloidal crystal strips, Chem. Mater. 17(2005) 3809-3811

[13] R. C. Hayward, D. A. Saville, I. A. Aksay, Electrophoretic assembly of colloidal crystals with optically tunable micropatterns, Nature, 404(2000) 56-58

[14] Y. Zhang, S. Wang, M. Eghtedari, M. Motamedi, N. A. Kotov, Inverted-colloidal-crystal hydrogel matrices as three-dimensional cell scaffolds, Adv. Funct. Mater. 15(2005) 725-731

[15] H. Xu, W. A. Goedel, Particle-assisted wetting, Langmuir, 19(2003) 4950-4952

[16] A. Toyotama, J., Yamanaka, M. Yonese, T. Sawada, F. uchida, Thermally driven unidirectional crystallization of charged colloidal silica, J. Am. Chem. Soc. 129(2007) 3044-3045

[17] N.P. johnson, D. W. Mccomb, A. Richel, B. M. Treble, R. M. Delarue, Synthesis and optical properties of opal and inverse opal photonic crystals, Synthetic Met. 116(2001) 469-473

[18] M.A. Al-Daous, A. Stein, Preparation and catalytic evaluation of macroporous crystalline sulfated zirconium dioxide templated with colloidal crystals, Chem. Mater. 15(2003) 2638-2645

[19] S.L. Kuai, G. Bader, P.V. Ashrit, Tunable electrochromic photonic crystals, Appl. Phys. Lett. 86(2005) 221110-221113

[20] H. Yan, C. F. Blanford, B. T. Holland, W. H. Smyrl, A. Stein, General synthesis of periodic macroporous solids by templated salt precipitation and chemical conversion, Chem. Mater. 12(2000) 1134-1141

[21] H. Yan, C.F. Blanford, B.T. Holland, M. Parent, W. H. Smyrl, A. Stein, A chemical synthesis of periodic macroporous NiO and metallic Ni, Adv. Mater. 11(1999) 1003-1006

[22] S. Sokolow, D. Bell, A. Stein, Preparation and characterization of macroporous alpha-alumina, J. Am. Ceram. Soc. 86(2003) 1481-1486

[23] R. W. J. Scott, S. M. yang, G. Chabanis, N. Coombs, D. E. Williams, G. A. Ozin, Tin dioxide opals and inverted opals: near-ideal microstructures for gas sensors, Adv. Mater. 13(2001) 1468-1472

[24] I. Soten, H. Miguez, S. m. Yang, S. Petrov, N. Coombs, N. Tetreault, N. Matsuura, h. E. Ruda, G. A. Ozin, Barium titanate inverted opals-synthesis, characterization, and optical properties, Adv. Funct. Mater. 12(2002) 71-77

[25] G. Gundiah, C. N. R. Rao, Macroporous oxide materials with three-dimensionally interconnected pores, Solid State Sci. 2(2000) 877-882

[26] J. Lu, Z. Tang, Z. Zhang, W. Shen, Preparation of LiFePO4 with inverse opal structure and its satisfactory electrochemical properties, Mater. Res. Bull. 40(2005) 2039-2046

[27] N.S. Ergang, J. C. Lytle, A. Stein, F. Zhang, W. Smyrl, The effect of a macropore structure on cycling rates of LiCoO2, J. Electrochem. Soc. 152(2005) A1989-A1995

[28] H. Yan, S. Sokolov, J. C. lytle, A. Stein, F. Zhang, W. Smyrl, Colloidal-crystal-templated synthesis of ordered macroporous electrode materials for lithium secondary batteries, J. Electronchem. Soc. 150(2003) A1102-A1107

[29] D. Wang, F. Caruso, Lithium niobate inverse opals prepared by templating colloidal crystals of polyelectrolyte-coated particles, Adv. Mater. 15(2003) 205-210

[30] E. M. Sorensen, S. J. Barry, H. K. Jung, J. R. Rondinelli, J.T. Vaughey, K. R. Poeppelmeier, Three-dimensionally ordered macroporous Li4Ti5O12: effect of wall structure on electrochemical properties, Chem. Mater. 18 (2006) 482-489

[31] M. Sadakane, T. Asanuma, J. Kubo, W. Ueda, Facile procedure to prepare three-dimensionally ordered macroporous (3DOM) perovskite-type mixed metal oxides by colloidal crystal templating method, Chem. Mater. 17(2005) 3546-3551

[32] M. W. Perpall, K. P. U. Perera, J. Dimaio, J. Ballato, S. H. Foulger, D. W. Smith, Novel network polymer for templated carbon photonic crystal structures, Langmuir 19(2003) 7153-7156

[33] A. A. Zakhidov, R. H. Baughman, Z. Iqbal, C. Cui, I. Khayrullin, S. O. Dantas, J. Marti. V. G. Ralchenko, Carbon structures three-dimensional periodicity at optical wavelengths, Science 282(1998) 897-901

[34] P.N. Bartlett, M. A. Ghanem, I.S. El Hallag, P. DeGroot, A. Zhukov, Electrochemical deposition of macroporous magnetic networks using colloidal templates J. Mater. Chem. 13(2004) 2596-2602

[35] T.S. Eagleton, P.C. Searson, Electrochemical Synthesis of 3D Ordered Ferromagnetic Nickel Replicas Using Self-Assembled Colloidal Crystal Templates, Chem. Mater. 16(2004) 5027-5032

[36] H. Yan, C.F. Blanford, J. C. Lytle, B. Carter, W. H. Smyrl, A. Stein, Influence of processing conditions on structures of 3D ordered macroporous metals prepared by colloidal crystal templating, Chem. Mater. 13(2001) 4314-4321

[37] J. E. G. Wijnhoven, S. J. M. Zevenhuizen, M. A. Hendriks, D. Vanmaekelbergh, J. J. Kelly, W. L. Vos, Electrochemical assembly of ordered macropores in gold, Adv. Mater. 12(2000) 888-890

[38] B.H. Juarez, C. lopez, C. Alonso, Formation of zinc inverted opals on Indium Tin oxide and silicon substrates by electrochemical deposition, J. Phys. Chem. B 108(2004) 16708

[39] H. Yan, C. F. Blanford, J. C. Lytle, B. Carter, W. H. Smyrl, A. Stein, Influence of processing conditions on structures of 3D ordered macroporous metals prepared by colloidal crystal templating, Chem. Mater. 13(2001) 4314-4321

[40] Y. A. Vlasov, X. Z. Bo, J. C. Sturm, D. J. Norris, On-chip natural assembly of silicon photonic bandgap crystals, Nature 414(2001) 289-293

[41] H.M. Yates, D. E. Whitehead, M. G. Nolan, M. E. Pemble, E. Palacios-Lidon, S. Rubio, F. J. Meseguer, C. lopex, Growth and formation of inverse GaP and InP opals, Proc. Electrochem. Soc. 3(2003) 967-974

[42] Y. Xu, G. J. Schneider, E. D. Wetzel, D. W. Prather, Centrifugation and spin-coating mehtod for fabrication of three-dimensional opal or inverse opal structures as photonic crystal, J. Microlith. Microsys. 3(2004) 168-173

[43] H. Bu, J. Rong, Z. Yang, Template synthesis of polyacrylonitrile-based ordered macroporous materials and their derivatives, Macromol. Rapid Comm. 23(2005) 460-464

[44] E. Palacios-Lidon, A. Blanco, M. Ibisate, F. Meseguer, C. Lopez, J. Sanchez-Dehesa, Optical study of the full photonic band gap in silicon inverse opals, Appl. Phys. Lett. 81(2002) 4925-4927

[45] Z. Z. Gu, h. uetsuka, K. Takahashi, R. Nakajima, H. Onishi, A. Fujishima, O. Sato, Structural color and the lotus effect, Angew. Chem Int. Ed. 42(2003) 894-897

[46] D. M. Kuncicky, S.D. Christensen, O. D. Velev, Role of the micro-and nanostructure in the performance of surface-enhanced raman scattering substrates assembled from gold nanoparticles, Appl. Spectrosc. 59(2005) 401-409

[47] W. Qian, Z. Gu, A. Fujishima, O. Sato, Three-dimensionally ordered macroporous polymer materials: an approach for biosensor applications, Langmuir 18 (2002) 4526-4529

[48] R. A. Barry, P. Wiltzius, Humidity-sensing inverse opal hydrogels, Langmuir 22(2006) 1369-1374

[49] Y. J. Lee, P.V. Braun, Tunable inverse opal hydrogel pH sensors, Adv. Mater. 15(2003) 563-556

[50] J. H. Kang, J.H. Moon, S.K. Lee, S. G. Park, S. G. Jang, S. Yang, S.M Yang, Thermoresponsive hydrogel photonic crystals by three-dimensional holographic lithography, Adv. Mater. 20(2008) 3061-3065

[51] M. Acciarri, R. Barberini, C. Canevali, M. Mattoni, C. M. Mari, F. Morazzoni, L. Nodari, S. Polizzi, R. Ruffo, U. Russo, M. Sala, R. Scotti, Ruthenium(Platinum)-doped Tin dioxide inverted opals for gas sensors: synthesis, electron resonance, mssbauer, and electrical investigation, Chem. Mater. 17(2005) 6167-6171

[52] B. J. S. Johnson, A. Stein, Surface modification of mesoporous, macroporous, and amorphous silica with catalytically active polyoxometalate clusters, Inorg. Chem. 40(2001) 801-808

[53] Y. Zhang, S. Wang, M. Eghtedari, M. Motamedi, N. A. Kotov, Inverted colloidal crystal hydrogel matrices as three dimensional cell scaffolds. Adv. Func. Mater. 15(2005) 725-731

[54] K. Zhang, h. Yan, D. C. Bell, A. Stein, L.F. Francis, Effects of materials parameters on mineralization and degradation of sol-gel bioactive glasses with 3D-ordered macroporous (3DOM) structures, J. Biomed. Mater. Res. 66A(2003) 860-869

[55] J. W. Long, B. Dunn, D. R. Rolison, H. S. White, Three-dimensional battery architectures, Chem. Rew. 104(2004) 4463-4492

[56] S. Kang, J. S. Yu, M. Kruk, M. Jaroniec, Synthesis of an ordered macroporous carbon with 62 nm spherical pores that exhibit unique gas adsorption properties, Chem. Commun. (2002) 1670-1671

[57] R. C. Schroden, M. Al-Daous, S. Sokolov, B.J. Melde, J. C. Lytle, A. Stein, M. C. Carbajo, J. T. Fernandez, E. E. Rodriguez, Hybrid macroporous materials for heavy metal ion adsorption, J. Mater. Chem. 12 (2002) 3261-3267

2. COLLOIDAL CRYSTAL TEMPLATE ASSEMBLY

This chapter is based on the following published paper:

Xinying Wang, Scott M. Husson, Xianghong Qian, S. Ranil Wickramasinghe,

Abstract

Formation of colloidal crystal films (CCFs) is the first step in the fabrication of inverse colloidal crystals, a class of three-dimensionally ordered, macroporous materials. A new vertical cell assembly method is described that yields CCFs with thicknesses up to 100 μm. The cell consists of two microscope cover glasses separated by a thin polymeric spacer. The lower edge of the cell is placed in a colloidal dispersion. Particles are transported to the top of the cell by capillary force and self-assemble into CCF as the solvent evaporates. This novel vertical cell assembly method is well suited for fabrication of large-area CCFs with controllable thickness that could be further processed into ICC filters for size-based separations of molecules and particles.

2.1   Introduction

Colloidal crystals (photonic crystals) are highly-ordered, three-dimensional structures of close-packed, uniform spheres. Natural opals are an example of colloidal crystals. Photonic crystals display a dielectric constant that varies with a periodicity similar to that of visible light resulting in a partial photonic band gap.[1] Consequently, they are of great interest as photonic band gap materials.[2, 3] Colloidal crystal films (CCFs) may be processed into inverse colloidal crystals (ICCs), which are three-dimensionally ordered macroporous structures, where air fills the spaces originally occupied by the colloidal particles. ICCs could potentially display a complete photonic band gap, as they meet the theoretical requirement that the ratio of the maximum to minimum refractive index within the material be more than 2.9 for materials with high refractive indices such as Si and Ge . Thus, ICCs are also of great interest in photonics.[2, 4, 5, 6, 7] Here, I focus on the fabrication of CCFs. Production of defect-free CCFs is essential in order to fabricate ICC films that are suited ideally for size based filtration applications. Unfortunately, fabrication of large area, defect-free CCFs is often problematic.[8]

Numerous methods have been described for fabrication of CCFs. Sedimentation in a gravitational field or assisted by an additional force,e.g. an oscillatory shear,[9] suction due to filtration,[10] has been used frequently. However, sedimentation methods suffer from lack of control over the surface morphology and the thickness of the film, both essential for filtration media. Other methods include spin coating,[11] floating self-assembly,[12] electric field-induced self-assembly,[13, 14] vertical deposition[15, 16, 17, 18] and

injection cell based methods.[8, 19, 20, 21, 22, 23] Controlling CCF thickness using these methods is difficult. The vertical cell method I describe allows simple control over the CCF thickness.

2.2 Material and methods

2.2.1 Fabrication of the CCF

Uniform polystyrene spheres with diameters of 0.42, 1 and 2 μm were used to fabricate CCFs. The 0.42 μm particles with size derivation less than 5% were prepared according to Ceska et al.[24] Typically, 20mL styrene (aluminum oxide column purified), 1g acrylic acid (vacuum distilled), 0.2g potassium persulfate and 100mL DI water were charged into a 250 mL flask. The reaction was conducted at 60°C for 5hrs under agitation. The resulting particles were centrifuged for 10 min at 10,000 rpm. The solvent was decanted and DI water was added to resuspend the particles using ultrasonic bath. The particles were washing for three time using the centrifugation cycles. Then the particles were dispersed in water. The 1 and 2 μm particles with size derivation of 1% were purchased from Duke Scientific. All particles were produced or received as an aqueous suspension. Prior to use, they were centrifuged at 10000 rpm for 10 min and washed with ethanol three times. Particles were resuspended in ethanol.

The vertical cell used to form the CCFs comprised two microscope cover glasses separated by two strips of Mylar film (Grafix, USA) (shaded strips in Fig. 2.1 (A)).

The cell was held together by a clip at the bottom and placed vertically in a beaker (30 mL) that contained the dispersion (20 mL) of polystyrene spheres in ethanol. Three dispersions were used: 15, 4 and 6 wt % for 0.42, 1 and 2 μm spheres, respectively. The spheres were transported to the top of the vertical cell by capillary forces (Fig. 2.1 (A)). As the ethanol evaporated, the particles self assembled in the vertical cell over a 5-7 day period. For making CCFs with heterostructures, the vertical cell was first placed in one beaker which contains one size of particles suspension. After certain time, a strip of CCF was obtained. Subsequently, the film dried and then put into another beaker in which suspension of particles with different size to the previous assembling particles. The new particles will be assembled into CCF alone the old strip of CCF. Finally, the complex CCF structure was obtained.

2.2.2   Characterization

CCFs were characterized by field emission scanning electron microscopy (FESEM; Model JSM-6500F, JEOL, Japan) equipped with an in-lens thermal field emission electron gun. All samples were coated with 10nm gold layer before they were imaged at a voltage of 15kV. The UV-Vis absorption spectra of the CCFs were recorded using a UV-visible-near infrared double beam spectrometer (UV-Vis, Cary 500, Varian, USA)and unpolarized light at nearly normal incidence in the 700C3300 nm spectral range.

2.3   Results and discussion

Using the vertical cell shown in Fig. 2.1 (A) I fabricated CCFs ranging from 25-100 μm in thickness by varying the thickness of the polymer spacer. Fig. 2.1 (B-D) are photographs of CCFs fabricated from 0.42, 1 and 2 μm spheres with spacer thickness of 25, 50 and 100 μm, respectively. The CCFs in Fig. 2.1 (B-C) appear colored under white light illumination due to the presence of a partial photonic band gap. The CCF in Fig. 2.1 (D) appears white, suggesting that the larger particle size yields a less ordered structure lacking a well-defined photonic band gap.

Fig. 2.2 gives FESEM images of top view of of the CCFs made from particle with different sizes. Fig. 2.2 (A-C) shows the surface and a high magnification inset of 25 μm thick CCFs consisting of 0.42, 1, and 2 μm spheres respectively. Since the 0.42 m particles gave the most regular CCF, these films were studied in more detail. Fig. 2.3 (A-C) gives cross-sectional views of CCFs fabricated using 25, 50 and 100 μm thick spacers, fabricated with 0.42 μm particles. The FESEM images indicate that the film thickness is similar to the spacer thickness. Thus, the thickness of the CCF can be adjusted easily. Finally, Fig. 2.4 (A-B) shows the bottom edge of the CCF obtained using 0.42 μm particles and a 100 μm spacer. Fig.2.4 (B) is a higher magnification image of Fig. 2.4(A). The surface and the cross sectional images show that the CCF has essentially close-packed face-centered cubic (fcc) structure.

Analyzed together, images in Fig. 2.2 indicate that larger particles yield more de-

fects in the CCF. Previous investigators also note that obtaining defect-free colloidal crystals using micron-sized particles is difficult[25] . Formation of a defect-free CCF depends on uniform self-assembly of the spheres, which depends on a balance between capillary and gravitational forces, as well as Brownian motion. While colloidal crystals with particle sizes ranging from < 1 nm to 10 μm have been described,[5] using large or very small particles is problematic. In the case of large particles, sedimentation often leads to defect formation.

There are several methods reported to make colloidal crystal heterostructures in which two or more sizes of particles assembled together.[21, 26] However, using a simple self-assembly method without preformed templates to make colloidal crystal into a more complex structure has not been reported yet. Here, the vertical cell method not only is a versatile method to make monostructure CCFs but also provides a straightforward way to make such complex structure CCFs. I have made two heterostructure CCFs using our new developed method. Fig 2.5 (A) and (B) present the pictures for CCFs made from 1 μm-0.42 μm and 2 μm-0.42 μm, respectively. The top sections in both pictures are CCFs made from bigger particles, while the bottom sections are CCFS made from 0.42 μm. Under white light illumination, the CCF regions made from 0.42 μm demonstrate beautiful iridescence while the region made from 1 μm particles shows a little color and no color for the region made from 2 μm particles. Fig 2.6 (A) and (B) give the SEM images for the two complex CCFs, 1 μm-0.42 μm and 2 μm-0.42 μm. From the images, both films show the clear interface for the regions assembled from different particles.

Fig. 2.7 gives UV-Vis spectra of CCFs fabricated with 0.42, 1 and 2 μm spheres. A sharp absorbance peak is observed for the CCF formed with 0.42 μm spheres. The peak shifts to larger wavelengths and becomes broader for CCFs comprising larger spheres. A broad peak indicates a less regular, less periodic structure. The hetro-structure CCF of 0.42-1 μm gives two peaks in the UV-Vis spectra. The positions of the two peaks appear at the same position as monostructure CCF of 0.42 μm and 1 μm.

Waterhouse and Waterland[1] estimate the position of the photonic band gap max for fcc photonic crystals:

$$\lambda_{max} = 1.633 D \sqrt{n_{avg}^2 - \sin\theta^2} \qquad (2.1)$$

where D is the sphere diameter; $\theta$is the angle between incident light and the normal to the CCF surface, and n_{avg} is the average refractive index. I estimate $n_{avg} = n_{PS}f_{PS} + n_{air}f_{air}$, where f_{PS} and fair denote the volume fractions of polystyrene spheres and void space. Assuming an fcc structure (see Fig. 2.2(G)), f_{PS}=0.74. At room temperature, $n_{PS} = 1.589^{26}$ and n_{air}=1.000. For θ=0, the calculated λ_{max} are 991, 2330 and 4685 nm for CCFs fabricated from 0.42, 1 and 2 μm spheres. The measured (Fig. 2.7) and calculated max agree well for the CCFs fabricated using 0.42 and 1 μm particles. However, the agreement is poor for the CCF fabricated using 2 μm particles, likely due to the disordered structure obtained using large particles.

2.4 Conclusion

A vertical cell assembly method has been developed for fabrication of large area CCFs with adjustable thickness. Assembly of CCFs using larger spheres results in less ordered structures. The resulting CCFs could be used as templates for the production of ordered, macroporous filtration media.

List of figures
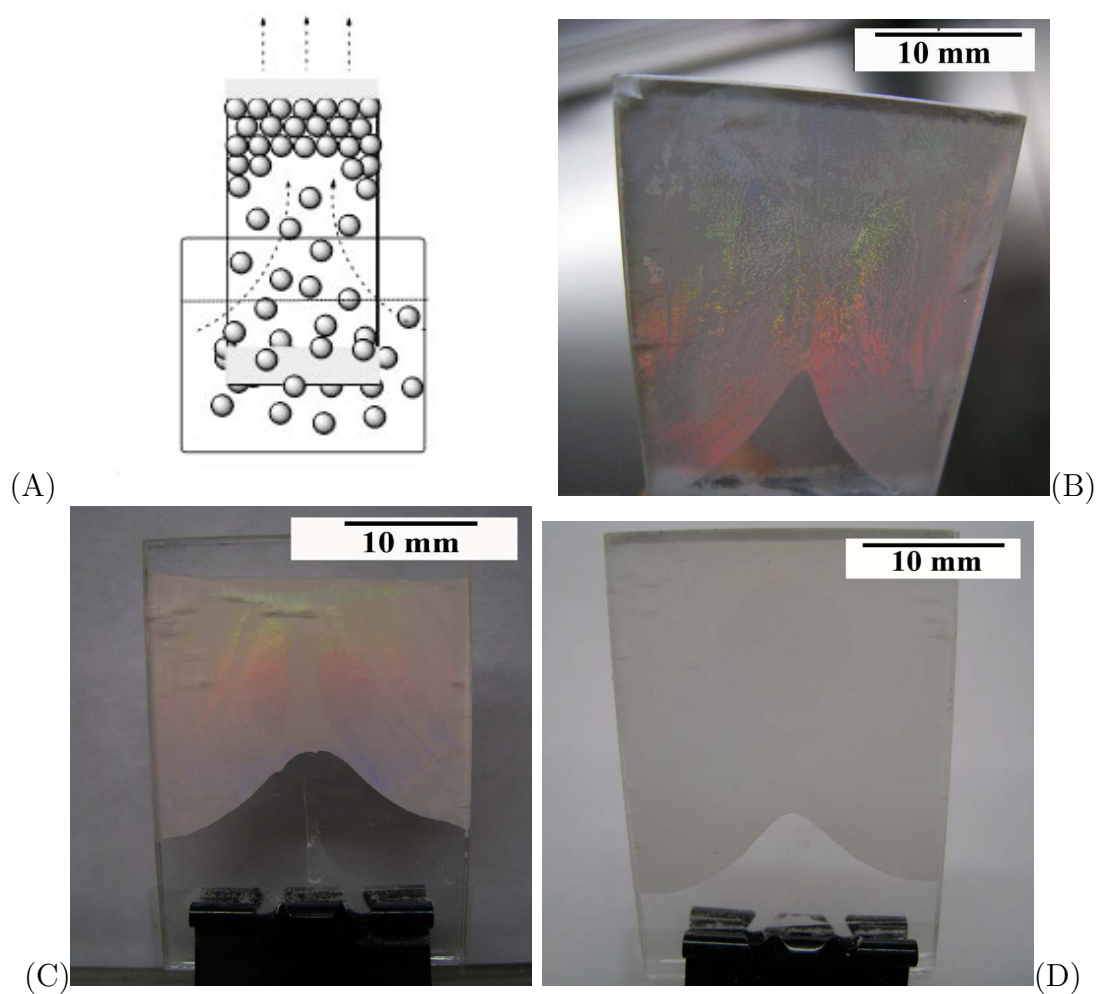
Fig. 2.1: (A) Schematic representation of the vertical cell used to fabricate CCFs. (B-D) photographs of CCFs fabricated from 0.42, 1 and 2 μm spheres, respectively.
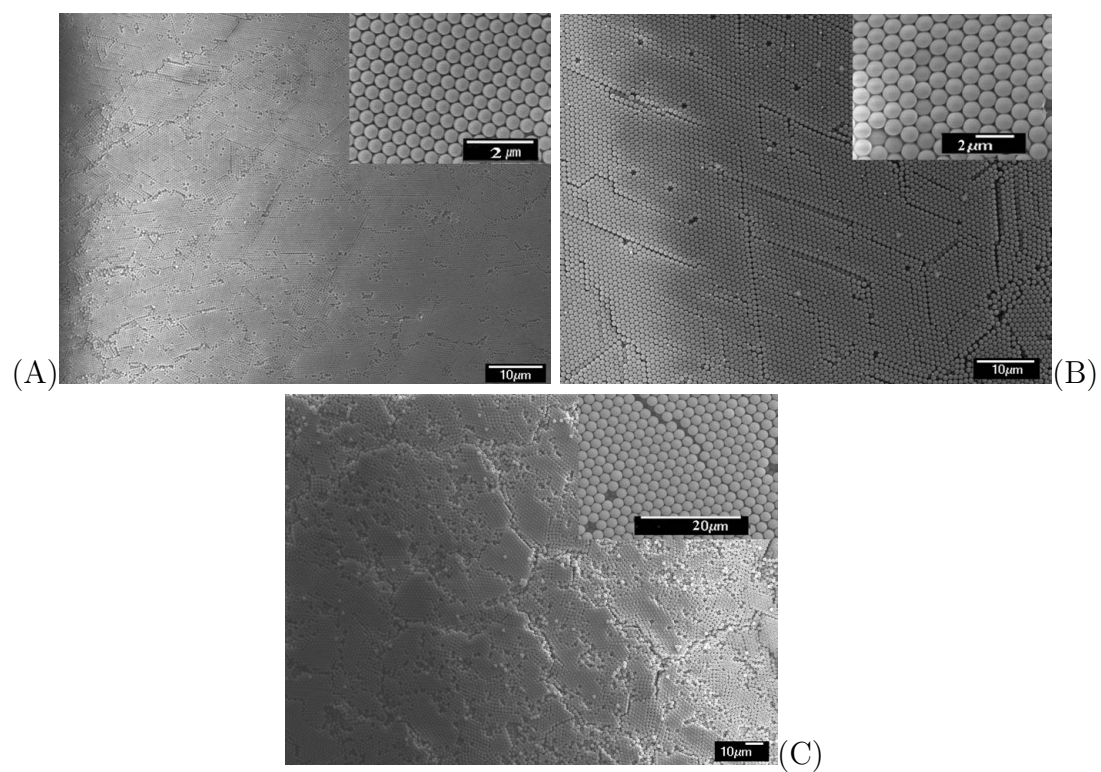
Fig. 2.2: FESEM images of colloidal crystal films. Top surface and high magnification inset of CCFs fabricated using (A)0.42, (B)1 and (C)2 μm spheres, respectively.

(A)

(B)

(C)
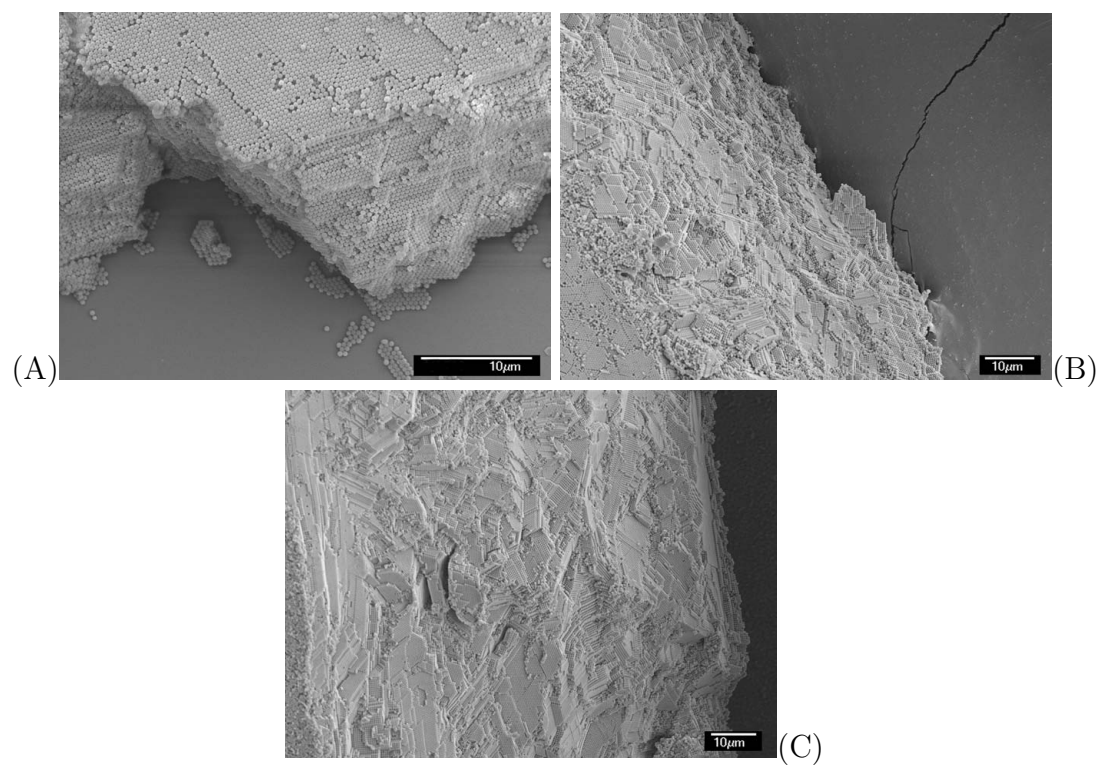
Fig. 2.3: Cross-sectional images of CCFs assembled with 0.42 μm spheres with thicknesses of (A)25, (B)50 and (C)100 μm, respectively.
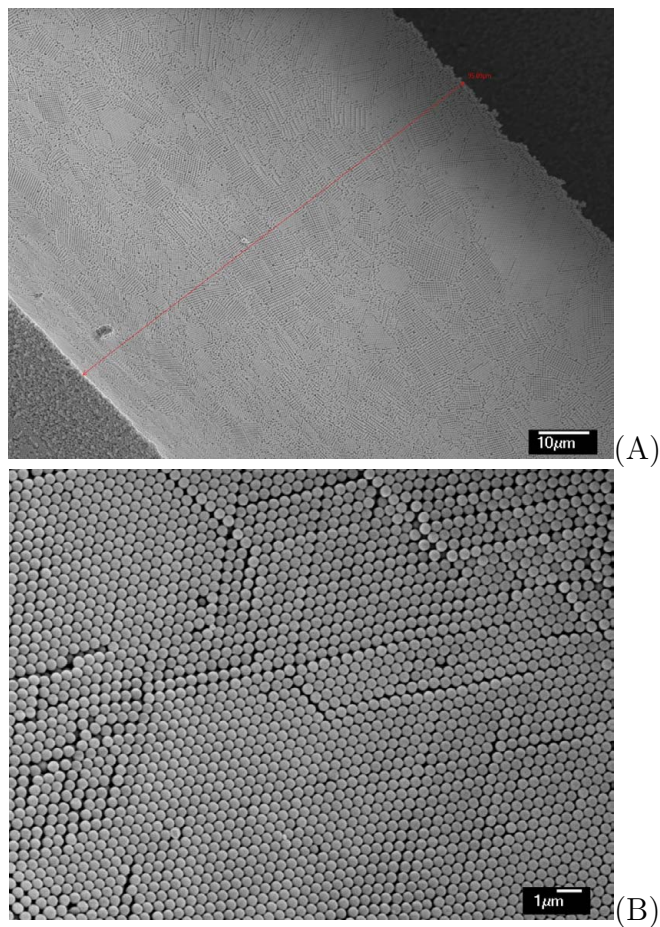
Fig. 2.4: (A) Bottom edge of CCF fabricated with 0.42 μm spheres and 100 μm spacer. (B) High-magnification image of (A).
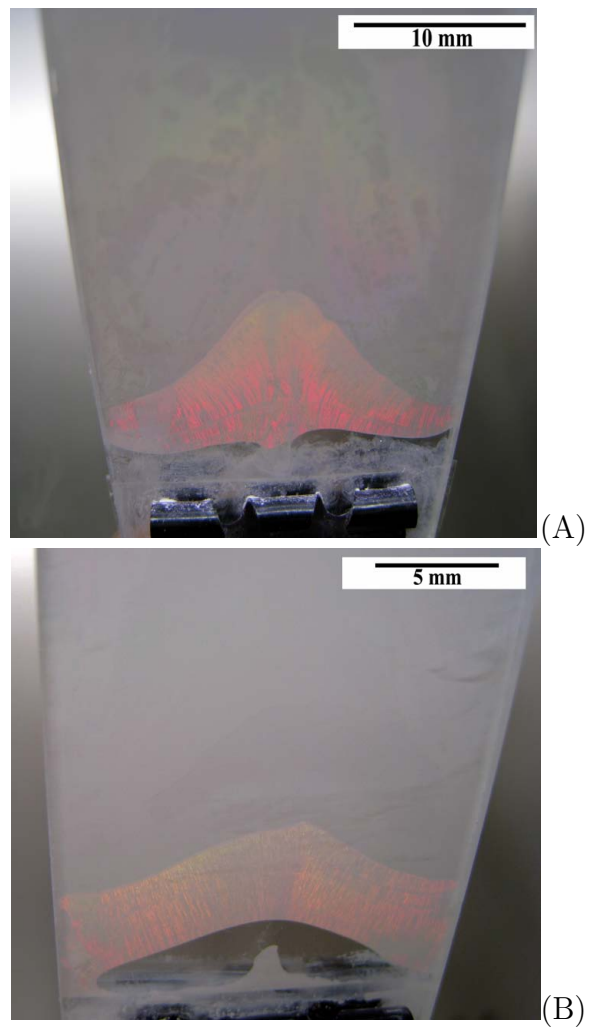
Fig. 2.5: Pictures of heterostructure CCFs (A) 1 m-0.42 μm (B) 2 μm-0.42 μm under white light illumination
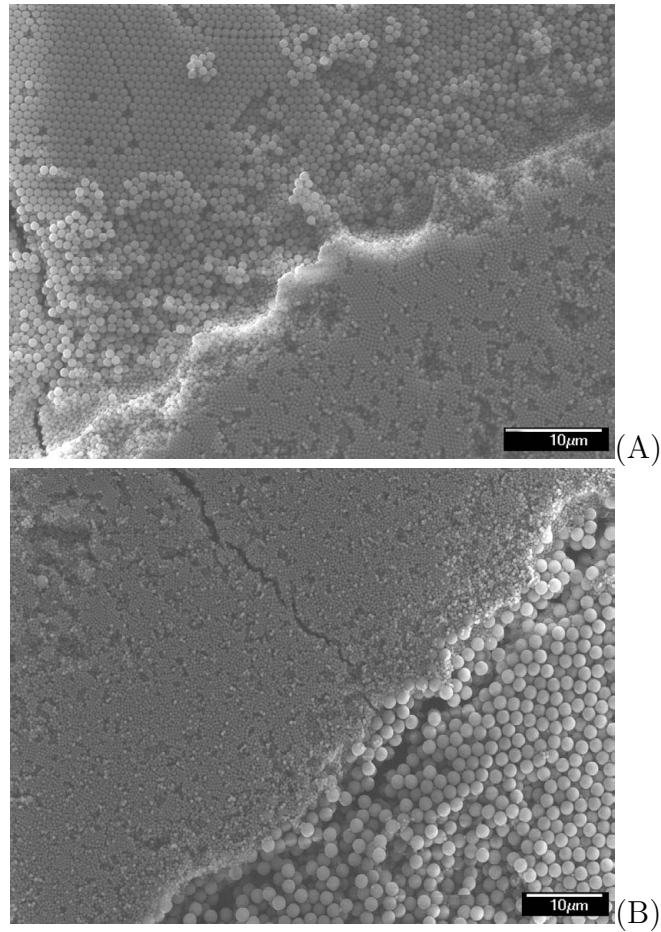
Fig. 2.6: Figure 2.6 SEM images of heterostructure CCFs (A) 1 μm-0.42 μm (B) 2 μm-0.42 μm
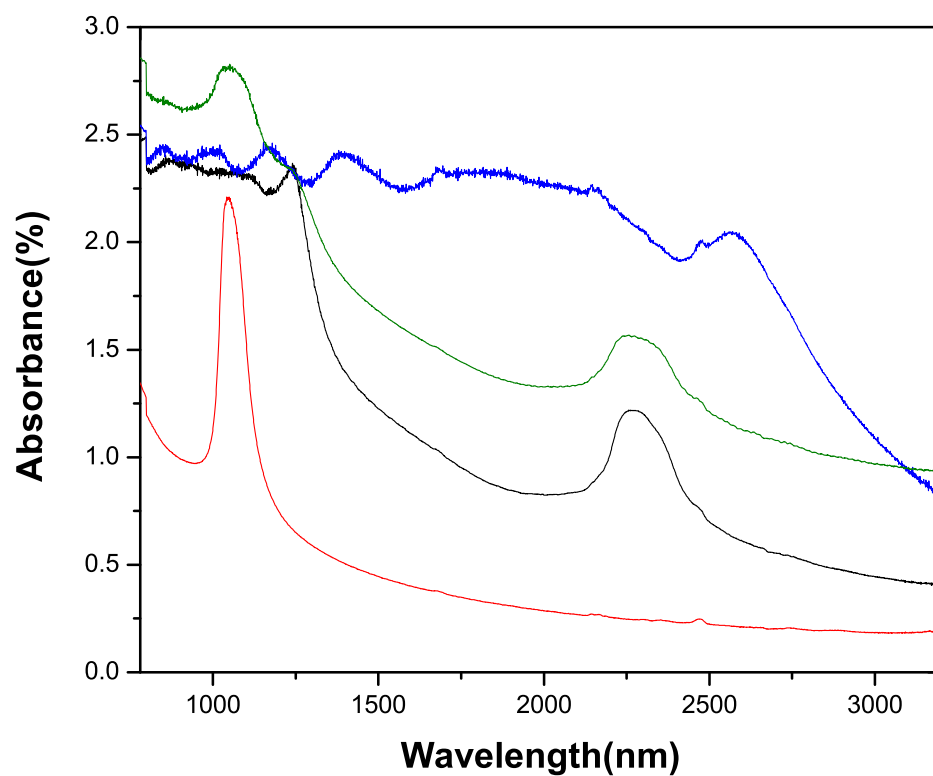
Fig. 2.7: UV-Vis spectra of CCFs fabricated with different size spheres. Absorbance peaks occur at 1100, 2300 and 2700 nm for CCFs fabricated with 0.42 (red line), 1 (black line), 2 (blue line), and 0.42-1 (green line) μm spheres, respectively.

Bibliography

[1] G.I.N Waterhouse, M.R. Waterland, Opal and inverse opals photonic crystals: fabrication and characterization, Polyhedron 26(2007) 356-68.

[2] C. Lopez, Materials aspects of photonic crystals, Adv. Mater. 15(2003) 1679-704.

[3] A. A. Zakhidov, R. H. Baughman, Z. Iqbal, C.X. Cui, I. Khayrullin, S.O. Dantas, I. Marti, V. G. Ralchenko, Carbon structures with three-dimensional periodicity at optical wavelengths, Science 282(1998) 897-901.

[4] J.M. Weissman, H.B. Sunkar, A.S. Tse, S.A. Asher, Thermally switchable periodicities and diffraction from mesoscopically ordered materials. Science 274(1996) 959-60.

[5] Y.N. Xia, B. Gates, Y.D. Yin, Y. Lu, Monodispersed colloidal spheres: old materials with new applications, Adv. Mater. 12(2000) 693-713.

[6] O. Painter, R.K. Lee, A. Scherer, A. Yariv, J. D. O'Brien, P.D. Dapkus, I. Kim, Two-dimensional photonic band-gap defect mode laser, Science 284(1999) 1819-21.

[7] H. Fudouzi, Y.N. Xia. Colloidal crystals with tunable colors and their use as photonic papers, Langmuir 19(2003) 9653-60.

[8] B. Gates, Y. Yin, Y. Xia. Fabrication and characterization of porous membranes with highly ordered three-dimensional periodic structures, Chem. Mater. 11(1999) 2827-36.

[9] O. Vickreva, O. Kalinina, E. Kumacheva, Colloid crystal growth under oscillatory shear. Adv. Mater. 12(2000) 110-2.

[10] B.T. Holland, C.F. Blanford, A. Stein, Synthesis of macroporous minerals with highly ordered three-dimensional arrays of spheroidal voids. Science 281(2) 538-40.

[11] P. Jiang, M.J. McFarland, Large-scale fabrication of wafer-size colloidal crystals, macroporous polymers and nanocomposites by spin-coating, J. Am. Chem. Soc.; 126(2004) 13778-86.

[12] Y. Liu, S. Wang, J.W. Lee, N.A. Kotov, A floating self-assembly route to colloidal crystal templates for 3D cell scaffolds. Chem. Mater. 17(2005) 4918-24.

[13] M. Trau, D. A. Saville, I.A. Aksay, Field-induced layering of colloidal crystals. Science 272(1996) 706-9.

[14] R.C. Hayward, D.A. Saville, I.A. Aksay, Electrophoretic assembly of colloidal crystals with optically tunable micropatterns. Nature 404(2000) 56-9.

[15] P. Jiang, J.F. Bertone, K.S. Hwang, V.L. Colvin, Single crystal colloidal multi-layers of controlled thickness, Chem. Mater. 11(1999) 2132-40.

[16] Z.Z. Gu, A. Fujishima, O. Sato, Fabrication of high-quality opal films with controllable thickness. Chem. Mater. 14(2002) 760-5.

[17] Z. Zhou, X.S. Zhao, Opal and inverse opal fabricated with a flow-controlled vertical deposition method. Langmuir 21(2005) 4717-23.

[18] L.M. Goldenberg, J. Wagner, J. Stumpe, B.R. Paulke, E. Grnitz. Ordered arrays of large latex particles organized by vertical deposition. Langmuir 18(2002) 3319-23.

[19] B. Gates, Y. Xia, Fabrication and characterization of chirped 3D photonic crystals. Adv. Mater. 12(2000) 1329-32.

[20] H.L. Li, W. Dong, H.J. Bongard, F. Marlow, Improved controllability of opal film growth using capillaries for the deposition process, J. Phys. Chem. B 109(2005) 9939-45.

[21] H.L. Li, F. Marlow. Controlled arrangement of colloidal crystal strips. Chem. Mater. 17(2005) 3809-11.

[22] H.L. Li, F. Marlow, Solvent effects in colloidal crystal deposition. Chem. Mater. 18(2006) 1803-10.

[23] M. Ishii, H. Nakamura, H. Nakano, A. Tsukigase, M. Harad,. Large-domain colloidal crystal films fabricated using a fluidic cell, Langmuir 21(2005) 5367-71.

[24] G.W. Ceska, The effect of carboxylic monomers on surfactant-free emulsion copolymerization, J. Appl. Polym. Sci. 18(1974) 427-37.

[25] J.C. Lytle, A. Stein, Annual reviews of nanoresearch, New Jersey: World Scientific; 2006.

[26] X.Y. Ma, J.Q. Lu, R.S. Brock, K.M. Jacobs, P. Yang, X.H. Hu. Determination of complex refractive index of polystyrene microspheres from 370 to 1610 nm, Phys. Med. Biol. 48(2003) 4165-72

[27] S.M. Yang, H. Mguez, G.A. Ozin, Opal circuits of lightplanarized microphotonic crystal chips, Adv. Func. Mater. 12(2002) 425-431

3. INVERSE COLLOIDAL CRYSTAL MICROFILTRATION MEMBRANES

Abstract

Uniform pore size, high porosity membranes are important for applications such as microfiltration and ultrafiltration, as well as for use as membrane adsorbers. In this work, uniform pore size, high porosity microfiltration membranes were developed using three dimensionally ordered macroporous templates. A membrane casting cell which was described in Chapter 2 was used for self assembly of silica spheres into a colloidal crystal template. The resulting close-packed colloidal crystal was infiltrated with a reactive monomer solution. After polymerization, the silica spheres were etched away, resulting in an inverse colloidal crystal (ICC) membrane with high

porosity and uniform pores that are highly interconnected.

ICC membranes have been fabricated with a range of pore sizes and thicknesses. The membrane casting cell facilitates easy variation of membrane thickness. The membrane pore size is varied by changing the diameter of the silica spheres used to prepare the colloidal crystal template. By changing the composition of the reactive monomer solution, membranes have been fabricated with different hydrophilicities. Following synthesis, the ICC membranes were tested in a commercially available stirred cell. Particle fractionation was studied in normal flow filtration experiments.

3.1 Introduction

Microfiltration is used frequently for solid-liquid separations involving aqueous streams.[1] It is used in the biotechnology, electronics, chemical and food industries to separate particulate matter from the suspending liquid.[2] Microfiltration may be run in either tangential flow or dead-end mode. Typical applications include rejection of bacteria and colloids in the production of drinking water, rejection of microparticles in the production of ultrapure water and other liquid streams in the semiconductor industry, rejection of pyrogens in sterile filtration applications, and validation of virus clearance in the manufacture of biopharmaceutical products. In all of these applications, the desired product is the permeate stream that passes through the membrane pores.

In addition to particle clearance, particle fractionation by microfiltration has been studied by several groups. For example, Leivisk et al.[3] investigated the use of 8, 3,

0.45 and 0.22 μm nominal pore size membranes for fractionation of wood extractives, lignin and trace elements in pulp and paper mill wastewater. Gan et al.[4] investigated beer clarification by microfiltration. Here the process requirements involve rejection of colloidal particles such as yeast cells, flocs etc and passage of large macromolecules such as carbohydrates proteins, flavor and color compounds. Wakeman and Akay[5] have investigated concentration and fractionation of latex particles, while Kromkamp et al.[6] studied concentration and fractionation of model fluorescent particles. Brans et al.[7] have developed micro-machined membranes or microsieves with carefully controlled pore size, geometry and porosity. They indicate that by carefully controlling pore geometry, size and porosity, one can optimize processes aimed at either complete rejection of particles or fractionation of particles, while maximizing permeate flux. In a more recent study Brans et al.[8] investigated transmission and fractionation of micron-sized particles in both tangential flow and normal flow filtration.

Optimization of microfiltration processes involves maximizing membrane capacity, productivity and selectivity.[9] Membrane capacity refers to the maximum volume of feed that can be treated before the permeate flux drops to unacceptably low values. In the case of tangential flow filtration, filtration is stopped and the membrane cleaned; while, for normal flow filtration, the membrane usually is replaced. Membrane productivity refers to the rate at which the feed can be processed (i.e., maximum sustainable permeate flux). Selectivity refers to the ability to yield high product recovery and removal of unwanted particulate matter.

Here I focus on normal flow microfiltration, as used in the biopharmaceutical industry for sterile filtration and virus clearance applications.[2] Ho and Zydney have investigated the effects of membrane morphology on membrane capacity during normal flow microfiltration.[10, 11, 12, 13, 14] They indicate that membrane morphology can have a significant effect on flux decline due to membrane lateral permeability. For membranes with non-connected straight through pores, the rate of flux decline tends to vary inversely with membrane porosity but becomes independent of porosity at higher porosities due to the possibility of a single particle blocking more than one pore. The rate of flux decline for isotropic membranes with highly interconnected pores is much slower than for membranes with non-connected pores, even for membranes with similar porosity. Pore interconnections allow fluid to flow around a deposited particle as it passes through the membrane. Thus, blockage of a pore mouth does not result in blockage of the entire pore. This result highlights the importance of lateral permeability within the membrane.

Ho and Zydney note that for asymmetric membranes with a tight skin layer, the flux decline is often similar to a membrane with non-interconnected pores. For a thin, tight skin layer, the flow has insufficient time to pass around blocked pores resulting in a behavior similar to a membrane consisting of non-interconnected pores. They discuss the effect of a membrane support structure in a composite membrane on flux decline due to the different lateral permeabilities of the different layers.[14]

These previous studies highlight the benefits of fabricating microfiltration membranes

with a high porosity, regular pore structure and high lateral permeability (highly interconnected pore network). This contribution describes the use of colloidal crystal templates for the development of such a membrane. Colloidal crystals or photonic crystals are three dimensionally periodic structures formed from monodisperse colloids.[15] Self-assembly of the colloidal spheres into a close-packed arrangement results in a colloidal crystal that displays a periodically modulated dielectric constant with a period similar to that of visible light (380-790 nm), resulting in a partial photonic band gap.[16, 17] Natural opals are an example of a colloidal crystal composed of face-centered arrays of amorphous silica spheres.

Conceptually, colloidal crystals may be easily converted into inverse colloidal crystals or inverse opals, which are three dimensionally ordered macroporous (3DOM) materials. The close-packed colloidal crystal is infiltrated with a reactive monomer solution. After polymerization, the colloidal particles are removed by thermal processing, solvent extraction or chemical etching. The resulting 3DOM structure will have a very regular pore size, high porosity and high level of pore interconnectivity. Numerous potential application for inverse colloidal crystals have been described[18] including photonic crystals and optical devices,[17, 19, 20] sensors,[21, 22, 23, 24] catalysts,[25, 26] magnetic materials,[27, 28] electrodes and batteries[29] and bioactive materials.[30]

Here I have developed inverse colloidal crystal (ICC) microfiltration membranes. Previous studies report the use of colloidal crystal templates as sieves for separation applications.[31, 32, 33] A few investigators also have described fabrication of ICC mem-

branes. Though numerous methods have been described for the preparation of very small surface area colloidal crystal templates, fabrication of ICC membranes requires self assembly of a large defect-free template that can be fabricated into a defect-free membrane. Park and Xia,[34, 35] and Gates et al.[36] describe the fabrication of ICC membranes using polystyrene and silica particles. They measured permeabilities of various solvents and found Darcy's law to be applicable. However, given the very small membrane surface areas they were able to fabricate, they needed to custom design an apparatus to measure membrane permeability. Yan and Goedel[37] and Jiang and McFarland[38] describe the formation of much larger surface area ICC membranes. However their fabrication method leads to very thin membranes that lack the mechanical stability for testing in commercially available stirred cells, which limits their practical applicability.

I have developed a method for fabrication of ICC microfiltration membranes. These defect-free membranes are mechanically stable and large enough to be tested in a commercially available stirred cell. Here, I describe a method for self assembly of the colloidal crystal template and then fabrication of the membrane. Permeate fluxes have been determined for a number of membranes with different pore sizes and thicknesses. In addition, particle fractionation using ICC membranes has been investigated.

3.2   Material and methods

3.2.1   Materials

The following chemicals were obtained from Sigma Aldrich (St Louis, MO): ethylene glycol dimethacrylate (EGDMA, 98%); hydroxybutyl methacrylate, mixture of isomers (HBMA, 94%); 2-hydroxyethyl methacrylate (HEMA, 97%); benzoin isobutyl ether (BIE, 90%); hydrofluoric acid (HF, 40%); tetraethylorthosilicate (TEOS, 99%); hydrogen peroxide (30%); sulfuric acid (95-98%) and ammonium hydroxide (28-30%). EGDMA, HBMA and HEMA were passed through a neutral Al_2O_3 column to remove polymerization inhibitors prior to use. TEOS was vacuum distilled prior to use. BIE and HF were used as received.

Ethanol (200 proof) was obtained from Pharmaco Products (Brookfield, CT) and used as received. Microscope cover glasses (24×50×0.1 mm) were obtained from VWR International (West Chester, PA) and cleaned using a mixture of 1:3 hydrogen peroxide-sulfuric acid before use. Mylar films with thicknesses of 25, 50 and 100 μm (to produce membranes with thicknesses of 25, 50 and 100 μm) were obtained from Grafix (Cleveland, OH) and cut into strips (25×10 mm). In some experiments, polyethersulfone microfiltration membranes (pore size 0.22 μm, thickness 100 μm, Pall Corp., NY) were used instead of Mylar. Silica particles (60 nm, 20% in water) were obtained from Allied High Tech (Rancho Dominguez, CA). All other silica particles were made as described below. A Millipore 8010 stirred cell (Millipore Corp., MA) was used for normal flow microfiltration experiments.

3.2.2   Preparation of monodisperse silica particles

Monodisperse silica particles were prepared based on the method by Stober-Fink-Bohn.[39] Ethanol (210 mL) was added to a 500 mL flask. HPLC water (17 mL), ammonium hydroxide solution (11 mL), and TEOS (11 mL) were added sequentially. The reaction was conducted at room temperature for 4 hours with agitation of 400 rpm. The contents of the flask were centrifuged at 5,000 rpm for 10 min. The solvent was then decanted, and a 20 mL 50:50 (v/v) mixture of ethanol-water was added to each of total 6 centrifugation tubes to resuspend the particles. The suspension in six tubes was then concentrated into two centrifugation tubes. The suspension was centrifuged at 5,000 rpm for 10 min. The solvent was decanted and the particles again resuspended in a 30 mL 50:50 (v/v) mixture of ethanol-water and centrifuged as before. This procedure was repeated two times to wash the particles.

Laser diffraction light scattering (Beckman Coulter LS 230, Fullerton, CA), was used to determine the particle size distribution. The resulting mean particle diameters were found to be 300-500 nm. Though there is batch-to-batch variation in the mean particle diameter, for a given batch, the standard deviation of the particle size distribution was less than 5% of the mean diameter.

Larger particles were prepared by following the method described above, except that an additional 11 ml TEOS and 10 ml water were added to the beaker after the initial

4 hr reaction time. The contents of the flask were again agitated for 4 hours to allow further reaction. This procedure was repeated until the desired particle size was obtained. After washing as described above, the particle dispersions were diluted to 1-5 wt% with absolute ethanol and added to a 30 mL beaker

3.2.3   Self assembly of colloidal crystal template and fabrication of ICC membrane

Self assembly of the colloidal crystal templates was conducted in the 'membrane casting' cell. The method developed here involved the use of two microscope cover glasses cut into 24×30 mm rectangles separated by two strips of either Mylar film or microfiltration membrane at the top and bottom (see Fig.3.1). The casting cell was placed vertically in the beaker containing the colloidal dispersion. This 'vertical cell' assembly of colloidal crystal films has been described in detail in chapter 2. Briefly, silica particles are transported to the lower surface of the upper spacer (Fig. 3.1) by capillary forces. As the solvent (ethanol) evaporates, the particles self assemble into a close-packed structure. In this work, both Mylar and microfiltration membranes have been used as spacers. The later yielded a more rapid self assembly of the colloidal crystal template due to faster ethanol evaporation through the microfiltration membrane.

The colloidal crystal template formed in 1 day using fresh-made suspension. The particle suspension was being reused to get as many as possible membranes. Therefore, the particle concentration will be getting lower over the time as more membrane

produced. As the assembly time exceeds more than 24 hours, I will replace the old suspension with new one. The thickness of the template and, therefore, the corresponding membrane depends on the thickness of the spacer. After formation of the colloidal crystal template, the template was dried at room temperature for 12 hours and infiltrated with the monomer solution.

The following monomer solutions were used to cast membranes: 2.0 g HEMA, 0.2 g EGDMA and 0.03 g BIE; 1.5 g HEMA, 0.5 g HBMA, 0.2 g EGDMA and 0.03 g BIE; 1.0 g HEMA, 1.0 g HBMA, 0.2 g EGDMA and 0.03 g BIE; 0.5 g HEMA, 1.5 g HBMA, 0.2 g EGDMA and 0.03 g BIE; 2.0 g HBMA, 0.2 g EGDMA and 0.03 g BIE. The monomer solution within the colloidal crystal template was polymerized using a UV lamp (30 W with wavelength 254 nm) by irradiating for 15 min. Following polymerization, the casting cell was immersed in 10 wt% HF solution to etch away the template and the microscope cover glasses. The membrane was characterized by field emission scanning electron microscopy (FESEM; Model JSM-6500F, JEOL, Japan) equipped with an in-lens thermal field emission electron gun. All samples were coated with 10nm gold layer before they were imaged at a voltage of 15kV. FESEM gives qualitative information for membrane surface morphologies.

3.2.4   Membrane testing

Permeate fluxes were determined using the Millipore stirred cell. The stirred cell also was used for the particle fractionation studies. An ICC membrane was placed

in the stirred cell. Two bi-disperse particle suspensions were prepared by mixing 60 and 835 nm silica particles, both at 0.36 % (w/w), and 60 nm and 440 nm silica particles at 0.31 and 0.28% (w/w). Particle fractionation tests were conducted at a feed pressure of 3.5 kPa using compressed nitrogen. The initial feed volume was 10 mL. Filtration was continued until about 8 mL of permeate were recovered. Laser diffraction light scattering was used to determine the particle size distribution in the feed and retentate.

3.3   Results

Figure 3.1 shows our newly designed membrane casting cell used to self assemble the colloidal crystal template. Features of the casting cell include ability to fabricate integral membranes that are large enough to be tested in a commercially available Millipore stirred cell and easy control over the membrane pore size and thickness. Figure 3.2(a) is a photograph of the colloidal crystal template formed using 400 nm particles and a 100 μm Mylar spacer. The colloidal crystal template appears colored under white light illumination due to the presence of a partial photonic band gap.

Figure 3.3 shows the resulting inverse colloidal crystal membrane. The membrane was formed by reacting 0.5 g HEMA, 1.5 g HBMA, 0.2 g EGDMA and 0.03 g BIE. Like the colloidal crystal template (Figure 3.2), the membrane also appears colored under white light illumination due to the presence of a partial photonic band gap. The FESEM image of the ICC membrane and the higher magnification inset indicate a very uniform, 3DOM structure where there appears to be a high level of pore in-

terconnectivity.

Figure 3.4 shows membranes fabricated with various ratios of HEMA:HBMA. Figures 3.4(A-E) show membranes formed from 2.0 g HEMA, 1.5 g HEMA:0.5 g HBMA, 1.0 g HEMA:1.0 g HBMA, 0.5 g HEMA:1.5 g HBMA and 2.0 g HBMA, respectively. For all membranes, 0.2 g EGDMA and 0.03 g BIE were used as the cross linker and initiator, respectively. The corresponding colloidal crystal template was created using 440 nm silica particles using the microfiltration membrane as a 100μ spacer. These FESEM images of the membrane cross section show the existence of a 3DOM structure. A high level of pore interconnectivity is evident.

Figure 3.5 shows the effect of varying the spacer thickness and, hence, membrane thickness. FESEM images are given for membranes cast using 25, 50 and 100μm Mylar spacers. The membranes were formed from 0.5 g HEMA, 1.5 g HBMA, 0.2 g EGDMA and 0.03 g BIE using 400 nm silica particles. The FESEM images indicate that the membrane thickness accurately matches the thickness of the spacer used, thus allowing us to easily control membrane thickness.

The membrane pore size is easily changed by changing the diameter of the silica particles used to form the colloidal crystal template. Figure 3.6 gives top view and cross-sectional FESEM images of membranes fabricated from 210, 375, 440 and 835 nm silica particles. Membranes were formed using 0.5 g HEMA, 1.5 g HBMA, 0.2 g EGDMA and 0.03 g BIE.

ICC membranes display three characteristic pore sizes. The larger pore size (e.g. see Figure 3.6) represents the diameter of the silica particles used to create the colloidal crystal template. The 'smaller' pore size represents the neck between two primary pores. It represents the volume between the silica spheres where the reactive monomer solution does not infiltrate. This smaller pore diameter will control the permeate flux. The surface pore size represents the volume between the silica sphere and the cover glass. The diameter of surface pore is in between the smaller pore size and the larger pore size. Figure 3.7 gives the surface pore and 'smaller' pore diameter as a function of the silica particle diameter used to form the inverse colloidal crystal template. The pore diameter was determined by measuring the pore size of at least 100 pores from FESEM images of the membrane cross section.

Deionized water fluxes as a function of applied pressure were determined for the membranes shown in Figure 3.4. Though all five membranes were fabricated using 440 nm silica particles and a common membrane thickness of 100μ, Figure 3.8 indicates the water fluxes at a given pressure vary significantly. Increasing the relative amount of HEMA used to fabricate the membrane leads to a decrease in water flux at a given pressure. Since HEMA is far more hydrophilic then HBMA, increasing the HEMA content of the membrane will lead to membranes that swell more in water. This swelling, in turn, leads to lower pore sizes and explains the observed dependence of water flux on HEMA content of the membrane.. This result appears somewhat contradictory to the observation that membrane swelling often leads to an increase in

pore size and a decrease in rejection. However it is important to realize that after polymerization the membranes are immersed in 10 wt% HF to etch away the template. Thus while the template is being etched away, the membrane polymer swells. This is somewhat different to the observed swelling of other membranes described in the literature where swelling does not occur during pore formation.

Figure 3.9 shows the variation of denionized water flux with feed pressure for the membranes fabricated using silica particles with diameters of 375, 440 and 835 nm (Figure 3.6). Using larger silica particles to form the colloidal crystal template leads to membranes with larger pore sizes, which, in turn, leads to higher fluxes at a given feed pressure.

Figure 3.10 gives particle fractionation results for a membrane fabricated using 835 nm silica particles and a 100μ microfiltration membrane as the spacer. The reactive monomer solution comprised 0.5 g HEMA, 1.5 g HBMA, 0.2 g EGDMA and 0.03 g BIE. The percentage by volume of a given particle diameter is plotted against the particle diameter. Figure 3.10(A) gives the particle size distribution in the feed and retenate for a feed stream consisting of 60 and 440 nm silica particles. Little fractionation of the particles appears to take place. Figure 3.10(B) gives the particle size distribution in the feed and retentate for a feed stream consisting of 60 and 835 nm silica particles. In this case, the retentate is enriched in the larger particles.

3.4   Discussion

I have developed a membrane casting cell that enables us to fabricate inverse colloidal crystal microfiltration membranes that can be tested in a commercially available stirred cell. In addition, the membrane thickness and pore size can be adjusted easily by changing the thickness of the spacer (Figure 3.5) and the diameter (Figure 3.6) of the silica particles used to form the colloidal crystal template. Membrane thickness will affect both the resistance to permeate flow and the mechanical stability of the membrane. Here isotropic membranes have been fabricated. Thicknesses less than 25μm lead to the formation of membranes that lacked mechanical stability and could not be tested in a Millipore stirred cell. In addition, the higher magnification insets in Figure 3.6 indicate that as the membrane thickness increases, the pore structure becomes less regular. This loss of order is due to the fact that I rely on capillary forces acting against the gravitational force to form the colloidal crystal template.

Since ICC membranes are 3DOM structures, they display a very regular morphology. While the membrane porosity could be has high as 74% for ICC membranes produced from close packed colloidal crystal templates, actual porosities are typically around 50-60%. The high porosity of the membrane results from the closed packed arrangement of the silica particles used to fabricate the colloidal crystal template. While there is a very high level of pore interconnectivity, as indicated in the FESEM images, the membranes may be characterized using two pore sizes. The 'smaller' pore size, due to contact between two silica particles, will control the permeate flow

through the membrane for a given feed pressure.

The smaller pore size is determined by the size of the silica particle used to form the colloidal crystal template and the viscosity of the reactive monomer solution. A more viscous monomer solution will lead to less effective infiltration into the spaces between the silica particles and will lead to a less mechanically stable membrane. For the reactive monomer solution used here, use of silica particle less then 200 nm in diameter led to membranes that were not sufficiently robust for testing in the Millipore stirred cell. In addition, these membranes contained many defects due to poor infiltration of the reactive monomer solution into the spaces between the silica particles. Optimization of the smaller pore size will be essential to maximize flux and to ensure the membranes are robust enough for practical applications.

Generated using FESEM images, Figure 3.7 gives the measured smaller pore sizes and surface pore size for membranes fabricated using 210, 375, 440 and 835 nm silica particles. Error bars represent the range of values measured. The much larger range for the membranes fabricated with 210 nm silica particles is due to less efficient infiltration of the reactive polymer solution. While colloidal crystal templates have been self assembled with particle varying from <1 nm to 10μm,[40] using very large or small particle often leads to colloidal crystal templates containing many defects. Formation of an ICC membrane also depends on efficient infiltration of the reactive monomer solution, which is more difficult for colloidal crystal templates containing very small particles. In our earlier work, I showed that sedimentation effects lead to less reg-

ular colloidal crystal templates self assembled using our vertical cell assembly method.

Applications for new membranes often are limited by membrane surface properties such as hydrophobicity.[41] It is therefore important to fabricate ICC membranes from a variety of monomers using a variety of methods. Here I present results for membrane fabrication using photoinitiated polymerization. I show (Figures 3.4 and 3.8) that using different ratios of HEMA:HBMA leads to membranes that display different water fluxes at the same feed pressure. The more hydrophilic membranes were found to swell more leading to a narrowing of the membrane pore size and lower water fluxes. One way to limit this response of the membrane and retain membrane hydrophilicity is to increase the amount of cross linking agent used (EGDMA in this work). Our results indicated that membranes fabricated from 0.5 g HEMA, 1.5 g HBMA, 0.2 g EGDMA and 0.03 g BIE gave the best properties in terms of membrane robustness, hydrophilicity and brittleness.

In this work I focused on membranes fabricated from HEMA, HBMA, and EGDMA using BIE for initiation. Nevertheless, the method used to cast ICC membranes may be used for other reactive monomer solutions. For example, I have fabricated membranes of polyurethane, polystyrene, and poly(methyl methacrylate) and used azobisisobutyronitrile as initiator. Polymerization was induced thermally at 60 °C for 2 hours, again highlighting the flexibility of our membrane fabrication process. The details for this work is listed in Appendix.

Permeate fluxes for feed pressure up to 70 kPa shown in Figure 3.9 indicate that using larger silica particle to fabricate the colloidal crystal template leads to larger pores and, hence, higher permeate fluxes at a given feed pressure. Flux data for the membrane fabricated with 210 nm silica particles (Figure 3.6A) are not given in Figure 3.9, as I were not able to test the membrane over the entire range of feed pressures. As explained above, inefficient infiltration of the reactive monomer solution leads to the formation of a weak membrane that collapsed at higher pressures.

Barns et al.[8] have investigated fractionation of bi-disperse particle suspensions in normal flow filtration. They indicate that, if the smaller particle size is less than the membrane pore size, transmission depends on the ratio of the larger to smaller particle sizes. They note that permeate flux and transmission decrease for all combinations of particle size with time. As a cake layer consisting of rejected larger particles forms on the membrane surface, it tends to reject smaller particles. In fact, Barns et al.[8] indicate that the smaller particles need to be at least 7 times smaller than the larger particles to move through the cake layer of larger particles.

The particle fractionation results given in Figure 3.10 are consistent with these earlier observations. Figures 3.10(A) and (B) indicate rejection of 440 and 835 nm particles. From Figure 3.7 the surface pore size and the smaller pore size for the membrane fabricated using 835 nm silica particles should be less then 350 nm and 200 nm, respectively. The ratio of larger to smaller particle size in the feed streams used in Figure 3.10(A) and (B) are about 7 and 14, respectively. The retentate particle

size distribution after the feed volume is reduced from 10 to about 2 mL indicates significant rejection of the 60 nm particles in the presence of 440 nm particles, but significant passage of 60 nm particles in the presence of 835 nm particles.

3.5   Conclusion

High porosity, uniform pore size microfiltration membranes with highly interconnected pores have been fabricated based on the three dimensionally ordered macroporous structure present in inverse colloidal crystals. A membrane casting cell has been developed that allows self assembly of silica spheres with a range of diameters. The casting cell also allows easy variation of membrane thickness. Using our casting cell, inverse colloidal crystal membranes have been fabricated and tested in a commercially available stirred cell. The membrane fabrication method I have developed may be used to fabricate membranes from a range of monomers.

Permeate fluxes have been determined for membranes with different pore sizes and hydrophilicities. Fraction of bi-disperse particle suspensions also has been investigated. The structure of inverse colloidal crystal membranes could be ideally for microfiltration applications. A major challenge will be scale up of the membrane fabrication process.

List of figures

MF membrane or
Mylar film

Microscope cover glass

Binder clip

(A)

MF membrane or
Mylar film

Microscope cover glass

Binder clip

(B)
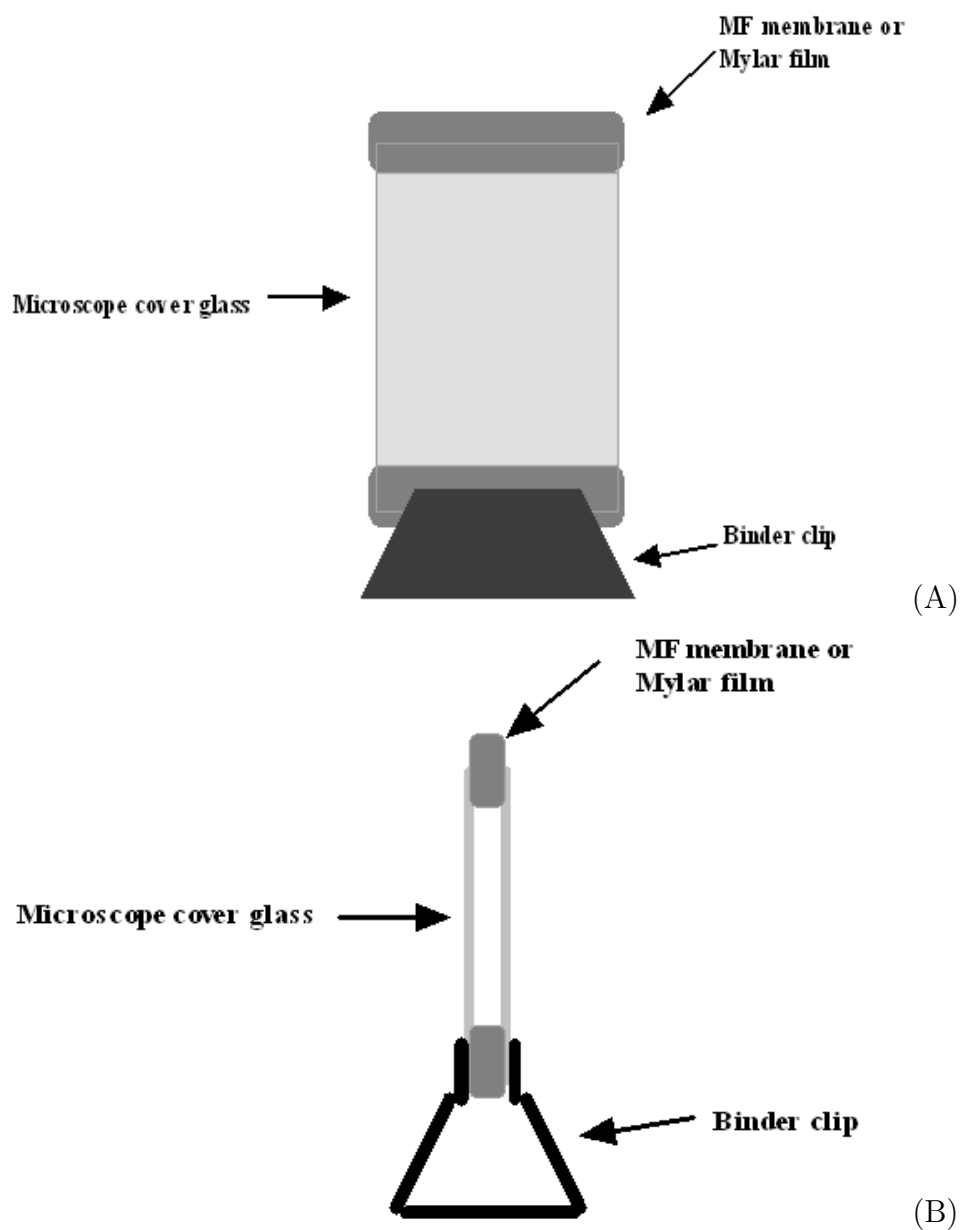
Fig. 3.1: Membrane casting cell used to self assemble the colloidal crystal template: (A) front view, (B) side view.

(A)

(B)
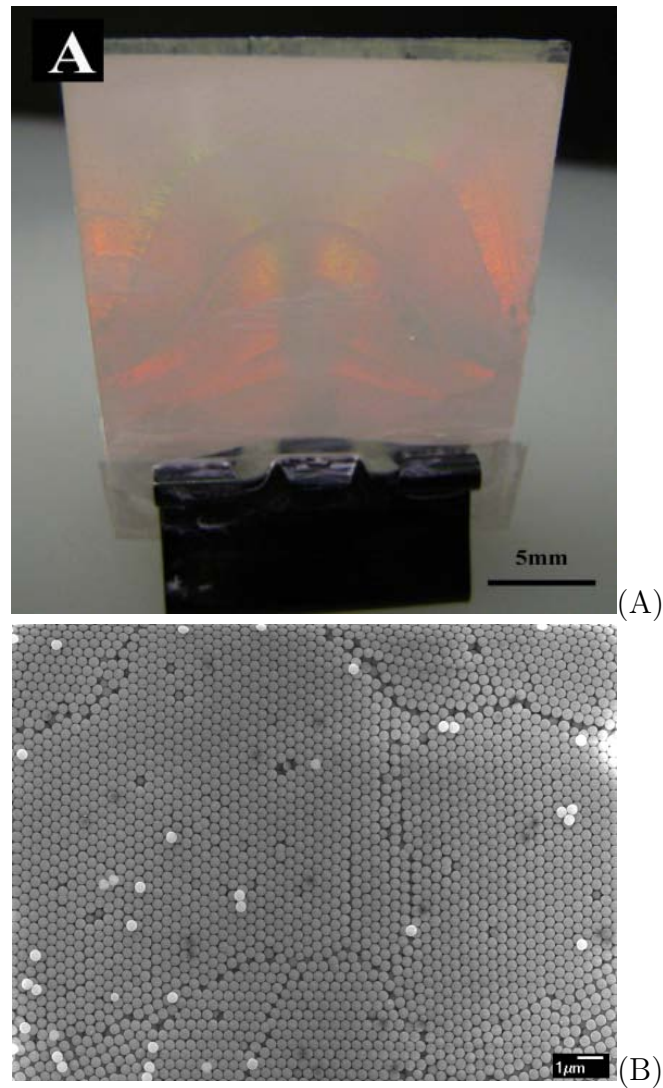
Fig. 3.2: Colloidal crystal template (A) under white light illumination and (B) FESEM image, formed using 400 nm silica particles and a 100 μm Mylar spacer.
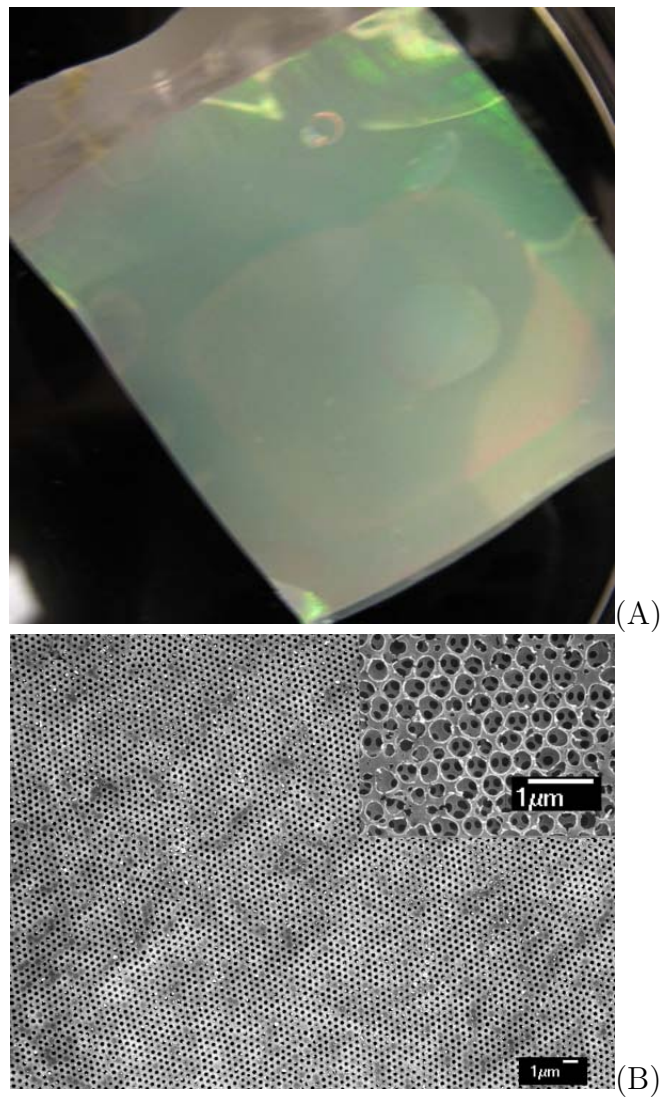
Fig. 3.3: Inverse colloidal crystal membrane formed from the template shown in Figure 3.2. (A) Under white illumination the membrane appears colored. (B) FESEM image of the membrane indicates a 3DOM structure with highly interconnected pores.
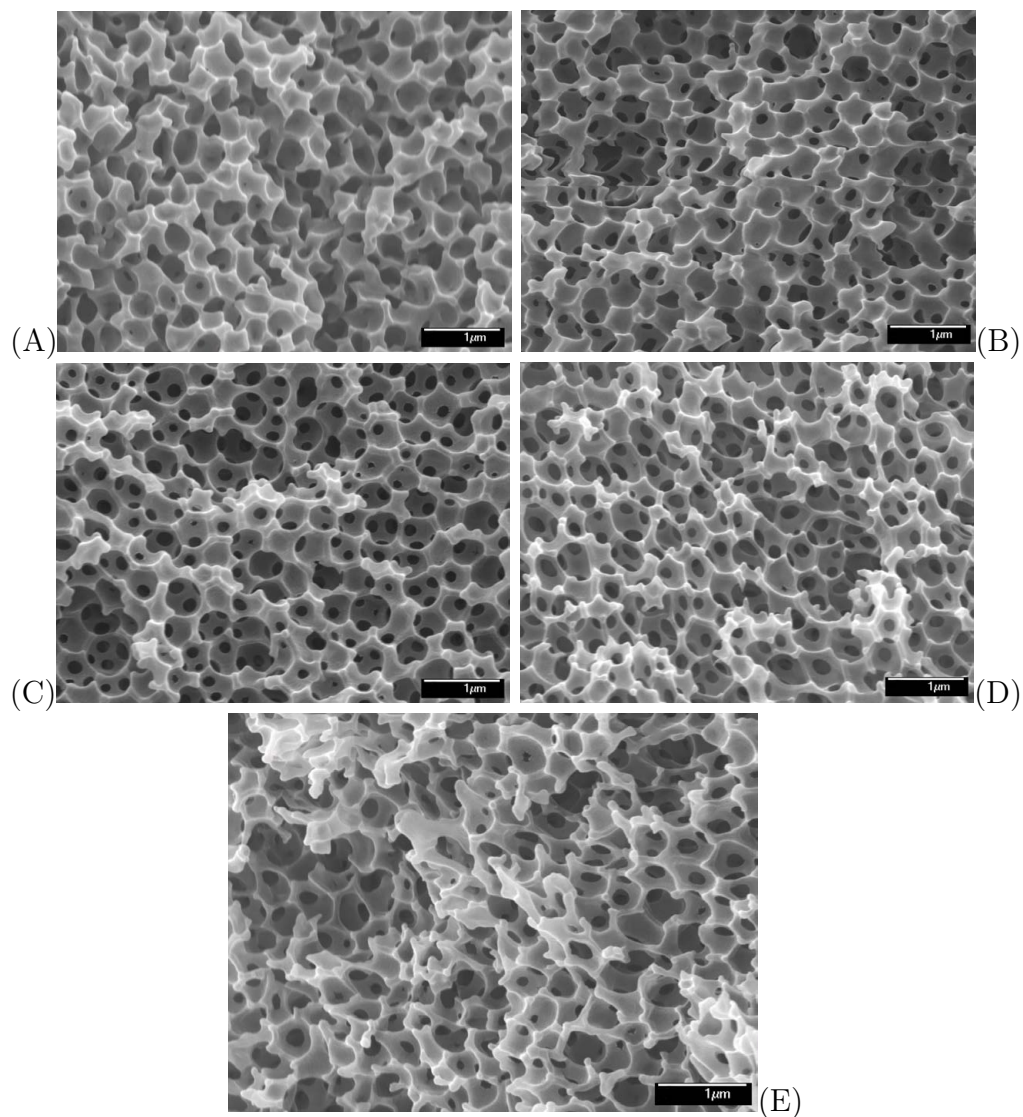
Fig. 3.4: FESEM image of inverse colloidal crystal membranes formed from colloidal crystal templates containing 440 nm silica particles. The microfiltration membrane was used as a 100 m spacer. Membranes were fabricated using (A) 2.0 g HEMA; (B) 1.5 g:0.5 g HEMA/HBMA; (C) 1 g:1 g HEMA/HBMA; (D) HEMA/HBMA 0.5 g:1.5 g; (E) 2.0 g HBMA. In all cases, 0.2 g EGDMA and 0.03 g BIE were used as the cross linker and initiator.
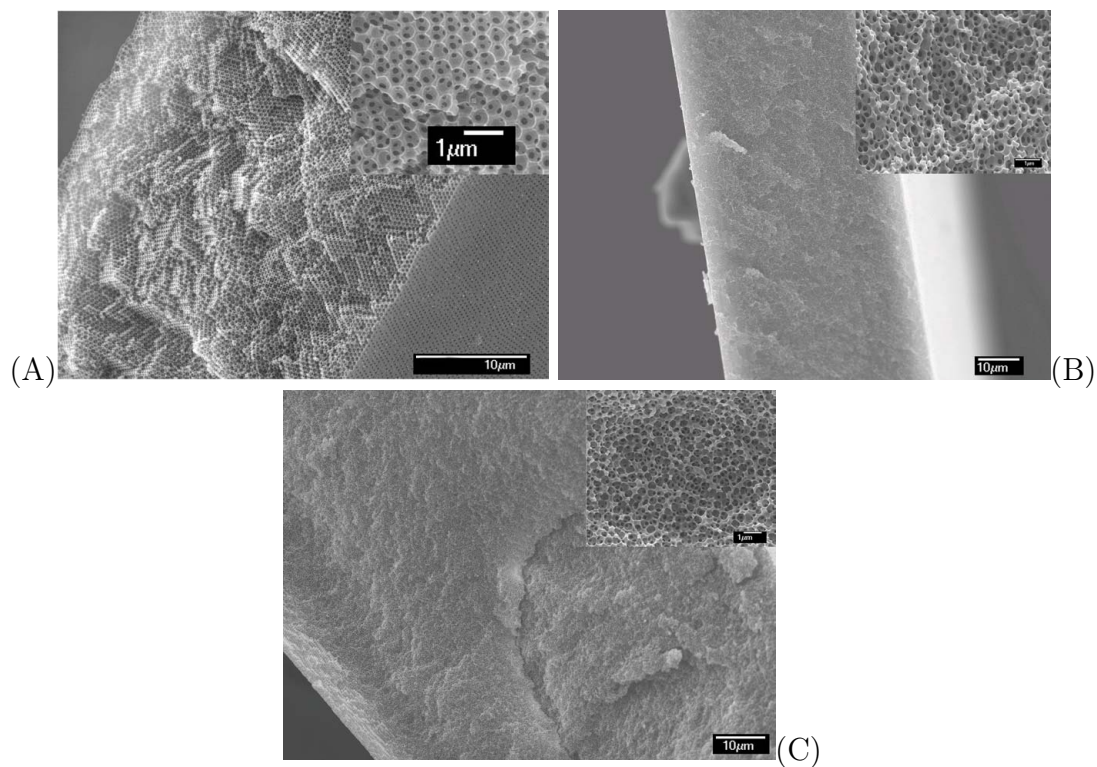
Fig. 3.5: Effect of spacer thickness on membrane thickness. All membranes were formed using 400 nm silica particles and 0.5 g HEMA, 1.5 g HBMA, 0.2 g EGDMA and 0.03 g BIE. (A) 25 μm thick membrane using 25 μm Mylar spacer; (B) 50 μm thick membrane using 50 μm Mylar spacer; (C) 100 μm thick membrane using 100 μm Mylar spacer.
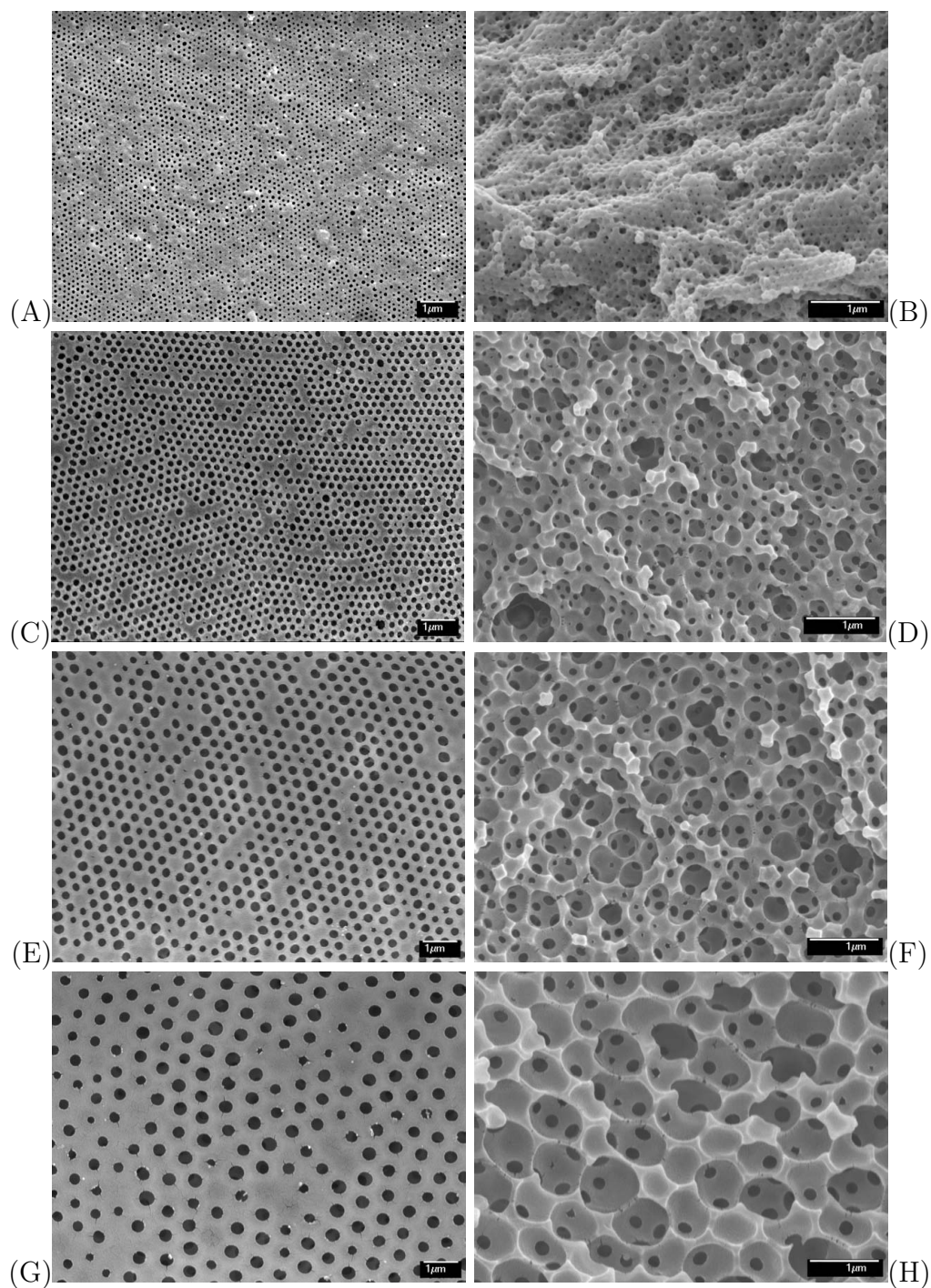
Fig. 3.6: Effect of silica particle diameter on membrane surface pore and 'smaller' pore size. Membranes were fabricated using 0.5 g HEMA, 1.5 g HBMA, 0.2 g EGDMA and 0.03 g BIE. The colloidal crystal template was formed using (A)(B) 210, (C)(D) 375 (E)(F) 440 and (G)(H) 835 nm silica particles. The microfiltration membrane was used as a 100 μm spacer.
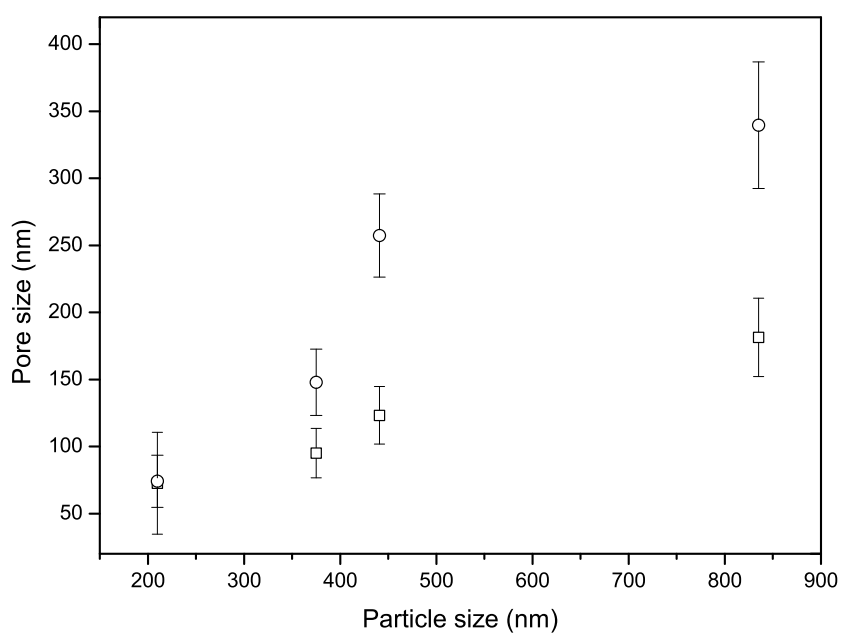
Fig. 3.7: Variation of the 'smaller'(open square) and surface (open circle) pore diameter of the colloidal crystal membrane, due to contact among the silica particles in the colloidal crystal template, with the silica particle diameter used to form the colloidal crystal template.
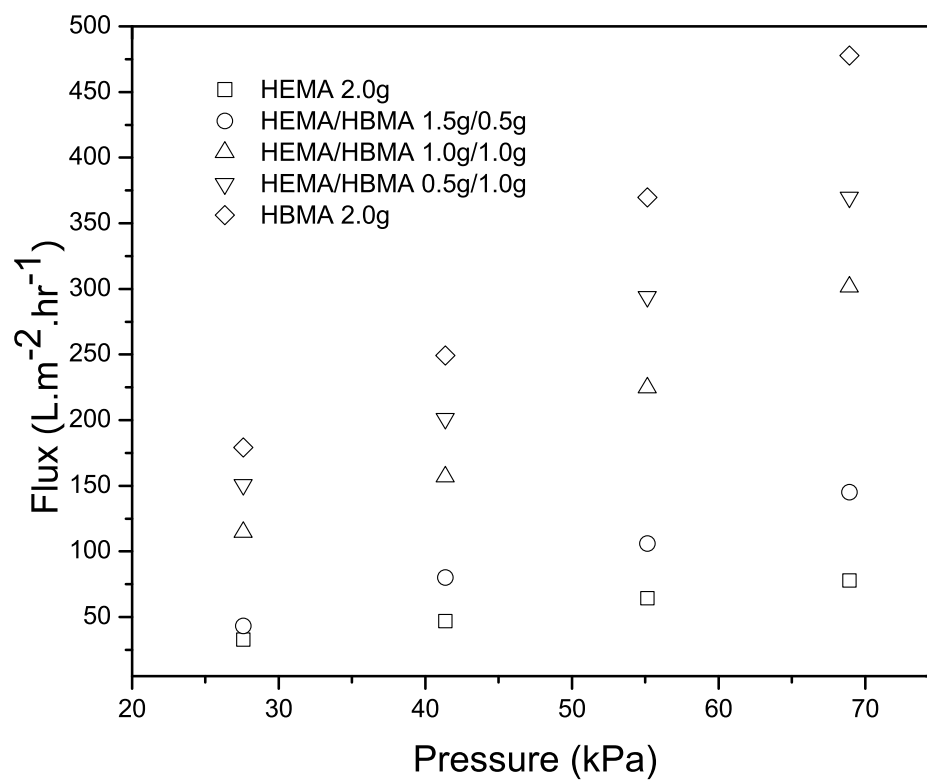
Fig. 3.8: Deionized water fluxes for membranes shown in Figure 3.4. The greater the mass of HEMA used to form the membrane, the lower the permeate flux.
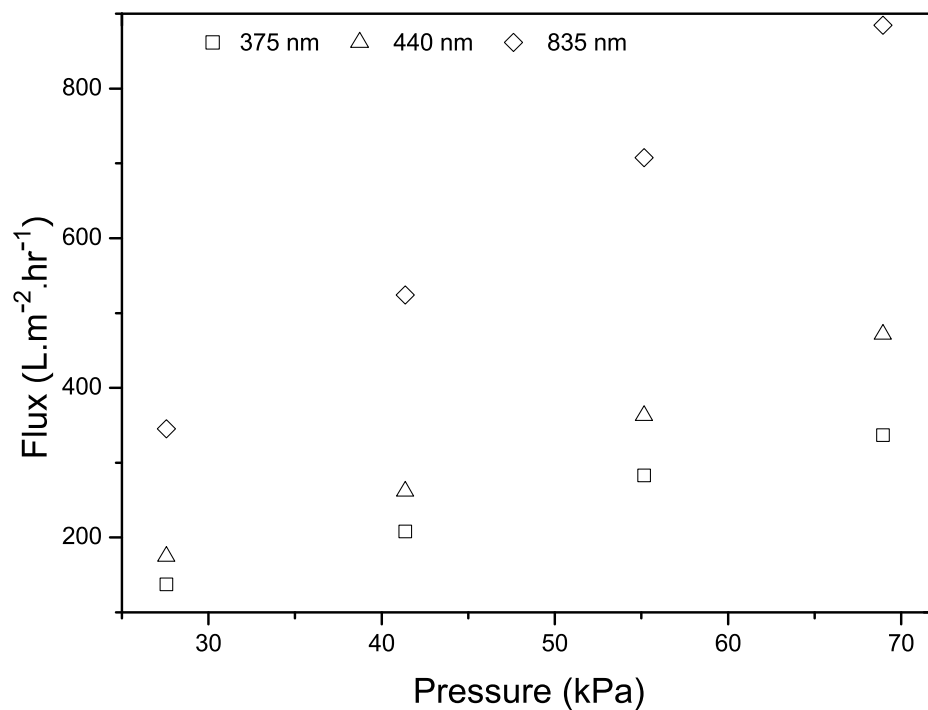
Fig. 3.9: Deionized water fluxes for membranes fabricated using 375, 440 and 835 nm silica particles. Using larger silica particles leads to higher permeate fluxes at a given feed pressure.
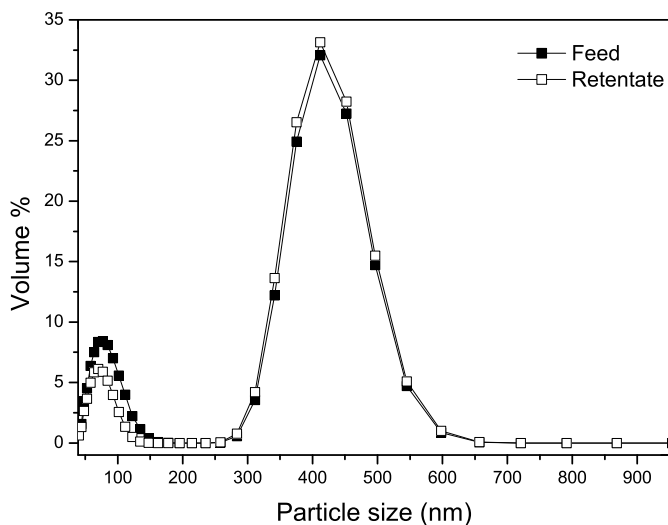
(A)
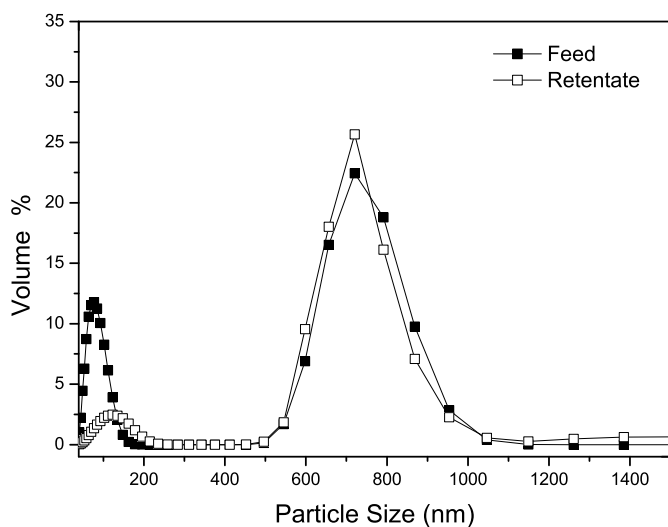
(B)

Fig. 3.10: Percentage by volume of a given particle size for the feed and retentate streams. (A) Feed stream consisted of 60 and 440 nm silica particles. (B) Feed stream consisted of 60 and 835 nm silica particles. The membranes used were formed using 835 nm silica particles and a 100 μm microfiltration membrane as the spacer. The reactive monomer solution consisted of 0.5 g HEMA, 1.5 g HBMA, 0.2 g EGDMA and 0.03 g BIE.

Bibliography

[1] N. Kubota, T. Hashimoto, Y. Mori, Microfiltration and ultrafiltration, in Advanced Membrane Technology and Applications, Eds: N. N. Li, A. G. Fane, W. S. W. Ho, T. Matsura, Wiley, Hoboken, NJ, 2008.

[2] R. van Reis, A. L. Zydney, Review: Bioprocess membrane technology, J. Membr. Sci. 297 (2007) 16-50.

[3] T. Leivisk, J. Rm, H. Nurmesniemi, R. Pyki, T. Kuokkanen, Size fractionation of wood extractives, lignin and trace elements in pulp and paper mill wastewater before and after biological treatment, Water Research 43 (2009) 3199-3206.

[4] Q. Gan, J. A. Howell, R. W. Field, R. England, M. R. Bird, C. L. O'Shaughnessy, M. T. MeKechinie, Beer clarification by microfiltration - product quality control and fractionation of particles and macromolecules, J. Membr. Sci. 194 (2001) 185-196.

[5] R. J. Wakeman, G. Akay, Concentration and fractionation of polyvinyl alcohol-anionic surfactant stabilized latex dispersions by microfiltration, J. Membr. Sci. 106 (1995) 57-65.

[6] J. Kromkamp, F. Faber, K. Schroen, R. Boom, Effects of particle size segregation on crossflow microfiltration performance: control mechanism for concentration polarisation and particle fractionation, J. Membr. Sci. 268 (2006) 189-197.

[7] G. Brans, R. G. M. van der Sman, C. G. P. H. Schron, A. van der Padt, R. M. Boom, Optimization of the membrane and pore design for micro-machined membranes, J. Membr. Sci. 278 (2006) 239-250.

[8] G. Brans, A. van Dinther, B. Odum, C. G. P. H. Schron, R. M. Boom, Transmission and fractionation of micro-sized particle suspensions, J. Membr. Sci. 290 (2007) 230-240.

[9] S.T. Loh, U. Beuscher, T. K. Poddar, A. G. Porter, J. M. Wingard, S. N.. Husson, S. R. Wickramasinghe, Interplay among membrane properties, protein properties and operating conditions on protein fouling during normal-flow microfiltration, J. Membr. Sci. 332 (2009) 93-103.

[10] C. C. Ho, A. L. Zydney, Theoretical analysis of the effect of membrane morphology on fouling during microfiltration, Separation Science and Technology 34 (1999) 2461-2483.

[11] C. C. Ho, A. L. Zydney, Effect of membrane morphology on the initial rate of protein fouling during microfiltration, J. Membr., Sci. 155 (199) 261-275.

[12] C. C. Ho, A. L. Zydney, Measurement of membrane pore interconnectivity, J. Membr. Sci. 170 (2000), 101-112.

[13] C.-C. Ho, A. L. Zydney, Protein fouling of Asymmetric and composite microfiltration membranes, Ind. Eng. Chem. Res. 40 (2001) 1412-1421.

[14] A. L. Zydney, C. C. Ho, Effect of membrane morphology on system capacity during normal flow microfiltration, Biotechnology and Bioengineering 83 (2003) 537-543.

[15] P. Jiang, M. J. McFarland, Large-scale fabrication of wafer-size colloidal crystals, macroporous polymers and nanocomposites by spin-coating, J. Am Chem. Soc. 126 (2004), 13778-13786.

[16] J. M. Weissman, H. B. Sunkara, A. S. Tse, S. A. Asher, Thermally switchable periodicities and diffraction from mesoscopically ordered materials, Science 274 (1996) 959-960.

[17] G. I. N. Waterhouse, M. R. Watrland, Opal and inverse opal photonic crystals: fabrication and characterization, Polyhedron 26 (2007) 356-368.

[18] J. C. Lytle, A. Stein, Recent progress in syntheses and applications of inverse opals and related macroporous materials prepared by colloidal crystal templating, In Annual Review of Nanomaterials, Vol. 1; Cao, G.; Brinker, C. J., Ed.; World Scientific Publishing Company, Hackensack, NJ, 2006.

[19] E. A. Kanmenetzky, L. G. Magliocco, H. P. Panzer, Structure of solidified colloidal array laser filters studied by cryogenic transmission electron microscopy structure of solidified colloidal array laser filters studied by cryogenic transmission electron microscopy, Science 263 (1994) 207-210.

[20] A. Blanco, E. Chomski, S. Grabtchak, M. Ibisate, S. John, S.W. Leonard, C. Lopez, F. Meseguer, H. Miguez, J. P. Mondia, G. A. Ozin, O. Toader, H. M. Van Driel, Large-scale synthesis of a silicon photonic crystal with a complete three-dimensional bandgap near 1.5 micrometres, Nature 405 (2000) 437-440.

[21] J. H. Holtz, S. A. Asher, Polymerized colloidal crystal hydrogel films as intelligent chemical sensing materials, Nature 389 (1997) 829-832.

[22] S. A. Asher, V. L. Alexeev, A. V. Goponenko, A. C. Sharma, I. K. Lednev, C. S. Wilcox, D. N. Finegold, Photonic crystal carbohydrate sensors: low ionic strength sugar sensing, J. Am. Chem. Soc. 125 (2003) 3322-3329.

[23] O. D. Velev, E.W. Kaler, In situ assembly of colloidal particles into miniaturized biosensors, Langmuir 15 (1999) 3693-3698.

[24] A. C. Sharma, T. Jana, R. R. Kesavamoorthy, L. J. Shi, M. A. Virji, D. N. Finegold, S. A. Asher, A general photonic crystal sensing motif: Creatinine in bodily fluids. J. Am. Chem. Soc. 126 (2004) 2971-2977.

[25] R. C. Schroden, C. F. Blanford, B. J. Melde, B. J. S. Johnson, A. Stein, Direct synthesis of ordered macroporous silica materials functionalized with polyoxometalate clusters, Chem. Mater. 13 (2001) 1074-1081.

[26] B. J. S. Johnson, A. Stein, Surface modification of mesoporous, macroporous, and amorphous silica with catalytically active polyoxometalate clusters, Inorg. Chem. 40 (2001) 801-808.

[27] P. N. Bartlett, M. A. Ghanem, I. S. El Hallag, P. De Groot, J. J. Zhukov, Electrochemical deposition of macroporous magnetic networks using colloidal templates, Mater. Chem. 13 (2003) 2596-2602.

[28] A. A. Zhukov, A. V. Goncharov, P. A. J. de Groot, P. N. Bartlet, M. A. J. Ghanem, Magnetic antidot arrays from self-assembly template methods, Appl. Phys. 93 (2003) 7322-7324.

[29] W. A. Long, B. Dunn, D. R. Rolison, H. S. White, Three-dimensional battery architectures, Chem Rev. 104 (2004) 4463-4492.

[30] Y. Liu, S. Wang, J. W. Lee, N. A. Kotov, A floating self assembly route to colloidal crystal templates for 3D cell scaffolds, Chem. Mater. 17 (2005) 4918-4924.

[31] L. Liu, P.S. Li, S.A. Asher, Entropic trapping of macromolecules by mesoscopic periodic voids in a polymer hydrogel, Nature 397(1999) 141-144.

[32] D. Nykypanchuk, H.H. Strey, D. A. Hoagland, Brownian motion of DNA confined within a two-dimensional array, Science 297(2002) 987-990.

[33] Y. Zeng, D. J. Harrison, Self-assembled colloidal crystal arrays as three dimensional nanofluidic sieves for separation of biomolecules on microchips, Anal. Chem. 79 (2007) 2289-2295.

[34] S. H. Park, Y. Xia, Macroporous membranes with highly ordered and three-dimensionally interconnected spherical pores, Adv, Mater. 10 (1998) 1045-1048.

[35] S. H. Park, Y. Xia, Fabrication of three-dimensionally macroporous membranes with assemblies of microspheres as templates, Chem. Mater. 10 (1998) 1745-1747.

[36] B. Gates, Y. Yin, Y. Xia, Fabrication and characterization of porous membranes with highly ordered three dimensional periodic structures, Chem. Mater. 11 (1999) 2827-2836.

[37] F. Yan, W. A. Goedel, A Simple and Effective Method for the Preparation of Porous membranes with three-dimensionally arranged pores, Adv. Mater. 16 (2004) 911-915.

[38] P. Jiang, J. M. McFarland, Large-scale fabrication of wafer-size colloidal crystals, macroporous polymers and nanocomposites by spin-coating, J. Am. Chem. Soc. 126 (2004) 13778-13786.

[39] W. Stober, A. Fink, E. Bohn, Controlled growth of monodisperse silica spheres in the micron size range, J. Colloid Interf. Sci. 26 (1968) 62-69.

[40] Y. Xia, B. Gates, T. D. Yin, Y. Lu, Monodispersed colloidal spheres: old materials with new applications, Adv. Mater. 12 (2000) 693-713.

[41] B. Van der Bruggen, Chemical modification of polyethersulfone nanofiltration membranes, J. App. Poly. Sci. 114 (2009) 630-642.

4. SURFACE MODIFICATION OF ICC MEMBRANES USING ATRP

Abstract

This chapter describes the work of growing a poly(poly ethylene glycol methacrylate) nano-layer from inverse colloidal crystal membranes using atom transfer radical polymerization. The modification decreases the membrane pore size and increases the membrane surface hydrophilicity. The surface modifications are investigated under a variety of modification times and variety of monomer concentrations. The grafted membranes are characterized using SEM, XPS, ATR-FTIR and water contact angle measurement. The DI water flux measurement is conducted on unmodified membrane and modified membranes with modification time of 0.5, 1, 2, and 3hr. The Dextran rejection test is conducted on modified membrane with modification time of 3hr. Based on the rejection rate obtained for dextran with Mw from 1 kDa through 2000 kDa, the tested membrane appears more than 80% rejection for Dextran with Mw more than 100 kDa, and a less than 20% of rejection for Dextran with Mw smaller than 10kDa. The diameter of the small pores in cross section, which are the limited pores for separation, can be reduced from 110-130nm to 5-15nm.

4.1 Introduction

Ultrafiltration(UF), which is a size-exclusion, pressure-driven membrane separation process, has been widely used in biochemical, biopharmaceutical, food and beverage industries. UF membranes with pore size in the range of 1-100 nm are mostly made of polymeric materials which are easily casted into any shape. Traditionally, most of UF membrane materials are prepared through phase inversion method that can be divided into four ways. They are precipitation from vapor phase, precipitation by evaporation, immersion precipitation and thermal precipitation.[1] Newer membrane making methods are also developed or under developing to get UF membranes with narrow pore size distribution. Stretching method make membranes by stretching a polymer film at normal or elevated temperature in order to produce desired size pores.[2] Track etching is a way to make membrane by exposing a polymeric film to laser beams or to a beam of charged particles to get uniform pores within polymer matrix.[3] However, the membranes produced by these new methods have either broad pore size distribution or low porosity.

Fouling of UF membrane, in particularly, protein fouling, which is foulant readily adsorbing onto the membrane surface and pore walls leading to the formation of the secondary barrier resulting in the decrease of membrane performance, is another concern during the operation.[4, 5] Previous study has elucidated that the membrane fouling is contributed by three factors. They are material properties, the feed characteristics and the operating conditions. Among them, the material properties plays

a major role in determining how easily the membrane get fouled.[6, 7, 8, 9, 10] Therefore, to prevent fouling, new membranes with anti-fouling property have been explored by either synthesis of brand new membrane materials or surface modification of existing membranes.[11, 12] The later way, surface modification of existing membranes, has drawn extensive attention because it is more versatile and easy than exploring a new membrane material.

In this chapter, I am aiming to develop a new ultrafiltraion membrane which has narrow pore size distribution, hydrophilic membrane surface, interconnected pores and controllable pore size. Inverted colloidal crystals (ICC), a porous material, are composed of high percentage of volume of ordered array of pores or holes which are left behind after removal of colloidal crystals.[13] A detailed introduction to ICC materials has been discussed in previous chapters. I have developed the ICC membranes successfully through a new ICC membrane formation method, vertical cell method. Uniform silicon dioxide particles are self-assembled into colloidal film within a planer cell which are composed of two cover glasses separated with two strips of spacer. Then the colloidal film is used as template to get the monomer infiltrated and polymerized. The ICC membrane is produced after Etching of the silica film together with the microscope cover glasses.

The ICC membranes made in our group are excellent microfiltration membrane as they have narrow pore size distribution, fully interconnected pores and high surface area (5 times higher than PVDF microfiltration membrane with the similar pore size).

The membranes had been tested with fractionation of micron-size particles. However, for the application of ICC membrane in UF for bioseparation, membrane pore size needs to be less than 20 nm to reach the same magnitude as protein or virus. The pore size of ICC membranes is mainly determined by the silica particles used for making templates. The smallest pore size of the ICC membrane I made was about 75nm which was from the silica particles with particle size of 210 nm. But the mechanical strength of such membrane were very low due to the high porosity of membranes made from smaller particles. Therefore making small pore size ICC membranes by solely using small silica particles is very hard.

Atom transfer radical polymerization (ATRP) has been extensively used to grow polymer brush from the membrane surface. ATRP involves reversible redox activation of a dormant alkyl halide (I Br Cl) terminated polymer chain end by a halogen transfer to a transition metal (Cu Ni) complex to keep a low concentration of controlled radicals through the whole polymerization process. Since ATRP was first reported by Wang, Matyjaszewski and Percec in 1995,[14, 15] it has been proven to be an excellent technique to make well-defined polymer brush on membrane surfaces. So far, extensive work has been done on membrane surface modification based on ATRP either for improving membrane surface hydrophilicities to prevent fouling or controlling the membrane pore size.

Ningh et al. grew poly (poly ethyleneglycol)methacrylate (PPEGMA) brush from the surface of regenerated cellulose UF membranes using ATRP to control the membrane

pore size.[16] Different MW cutoff of the modified membrane under different modification times were obtained. Zhu et al. reported the modification of chloromethylated poly (phthalazione ether sulfone ketone) membranes to prevent membrane fouling.[17] They grew PPEGMA, a hydrophilic polymer, brush from the membrane with ATRP and membranes showed good anti-fouling property after modification. Chen et al. grafted poly (methyl methacrylate) and PPEMGA brush from poly (vinylidene fluoride) (PVDF) microfiltration membrane surfaces with reverse ATRP to improve the anti-fouling property of PVDF membrane.[18] The modified membrane showed slower flux drop than unmodified membrane when testing the membranes with bovine serum albumin (BSA) solution.

In this chapter, I will use ATRP to graft a PPEGMA layer from the surface of ICC membranes for two purposes. One is to decrease the membrane pore size to make the ICC membrane applicable in UF for bioseparation area without trading off the membrane mechanical strength. The other is to increase the membrane surface hydrophobicity for anti-fouling.

4.2   Material and methods

4.2.1   Materials and reagents.

The following chemicals were obtained from Sigma Aldrich (St Louis, MO): Cu(I)Cl (99.995%); $Cu(II)Cl_2$ (99.999%); 2,2'-bipyridyl(99%); triethylamine(99.9%); 4 dimethylamino pyridine (DMAP, 99%); 2-bromoisobutyryl bromide (BIB) ; acetonitrile (99.9%);

(poly ethyleneglycol)methacrylate (PEGMA,hydroxyl-terminated, Mn 360, 97%); ethylene glycol dimethacrylate (EGDMA, 98%); hydroxybutyl methacrylate, mixture of isomers (HBMA, 94%); 2-hydroxyethyl methacrylate (HEMA, 97%); benzoin isobutyl ether (BIE, 90%); hydrofluoric acid (HF, 40%); tetraethylorthosilicate (TEOS, 99%); hydrogen peroxide (30%); sulfuric acid (95-98%) and ammonium hydroxide (28-30%). PEGMA, EGDMA, HBMA and HEMA were passed through a neutral Al_2O_3 column to remove inhibitors prior to use. TEOS was vacuum distilled prior to use. BIE and HF were used as received. Ethanol (200 proof) was obtained from Pharmaco Products (Brookfield, CT) and used as received. Microscope cover glasses (24×50×0.1 mm) were obtained from VWR International (West Chester, PA) and cleaned using mixture of 1:3 hydrogen peroxide-sulfuric acid before use. Microfiltration membrane with pore size 0.22μm and thickness 100 μm was obtained from Pall (New York).

Ethanol (200 proof) was obtained from Pharmaco Products (Brookfield, CT) and used as received. Microscope cover glasses (24×50×0.1 mm) were obtained from VWR International (West Chester, PA) and cleaned using a mixture of 1:3 hydrogen peroxide-sulfuric acid before use. Mylar films with thicknesses of 25, 50 and 100 μm (to produce membranes with thicknesses of 25, 50 and 100 μm) were obtained from Grafix (Cleveland, OH) and cut into strips (25×10 mm). In some experiments, polyethersulfone microfiltration membranes (pore size 0.22 μm, thickness 100 μm, Pall Corp., NY) were used instead of Mylar. Silica particles (60 nm, 20% in water) were obtained from Allied High Tech (Rancho Dominguez, CA). All other silica par-

ticles were made as described below. A Millipore 8010 stirred cell (Millipore Corp., MA) was used for normal flow microfiltration experiments.

4.2.2   Fabrication of ICC membrane

Preparation of SiO_2 particles, assembly of template and fabrication of ICC membrane has been discussed in chapter 3. The ICC membrane made from 440 nm particles, 100 μm thickness spacer and monomer solution of HEMA/HBMA 1/3 (w/w) is used through this chapter.

4.2.3   Surface modification of ICC membranes with ATRP

4.2.4.1 Initiator immobilization

The ICC membrane sample was placed into a 50 mL dry beaker after wipe out water drops on the membrane surface with a tissue. 30 mL acetonitrile was charged into the beaker containing membrane sample. The membrane was incubated for 10 minutes to extract the water in the sample. After incubation, the acetonitrile was decanted. Another 30 mL fresh acetonitrile was charged in, and subsequently the sample was incubated for another 10 minutes. This procedure was repeated for three times to remove most of the water in the membrane. Because of the residue water trapped in the membrane after extraction and the noticeable amount water coming with acetonitrile (0.05wt%), suggested amount of BIB in the literatures used for initiator immobilization was not working well in this work for the further ATRP modification. I increased the amount of BIB to compensate the BIB loss to the residue

water remaining after extraction and the water coexisting with acetonitrile. Following

the extraction, the ICC membrane was placed into a new dry 50 mL beaker. 30 mL

fresh acetonitrile, triethylamine 350mM, DMAP 50mM and BIB 300mM were added

in and the beaker was sealed with parafilm. Subsequently the beaker was placed on

a shaker for 3hr to get the initiator reacted with the membrane. After reaction, the

membrane was washed with 30 mL acetonitrile for three times and then stored in

DI water. After initiator immobilized, the membrane is very brittle and weak due to

the increase in membrane surface hydrophobicity. Thus gentle handling is needed for

keeping the membrane integral.

4.2.4.2 ATRP modification

Figure 4.1 gives the scheme of the ATRP setup. A vacuum trap rather than a flask

as the reaction vessel is needed because the trap has a big neck to introduce the

membrane in without bending the sample as the bending might damage the mem-

brane. As well known, ATRP is very sensitive to oxygen as the living radicals are

easily terminated. Thus, keeping the system oxygen-free is very important for the

successfulness of the modification. In our modification, argon was bubbling through

the reaction solution to remove the oxygen. The outlet of the trap is sealed with

water to keep the oxygen in atmosphere from diffusing back. This setup can modify

3 samples in parallel.

Initiator immobilized ICC membrane was placed in a vacuum trap and then 30 mL

solution of PEGMA (0.05M), Cu(II)Cl2(0.2mM) and 2,2'-bipyridyl (3mM) in HPLC

water was charged in. Afterwards, the reaction solution was degassed by bubbling Argon for 30 minutes before adding Cu(I)Cl 10 mg (3mM) to let the modification start. The reaction was carrying on for desired time under protection of Argon. After modification, the membrane was quickly placed in 30 mL 0.3M $CuCl_2$ solution, and incubated for 20 min to terminate the reaction. Then the membrane was rinsed with HPLC water. The pure water flux was measured right after the wash. After flux obtained, the membrane was took out from the UF cell and then put into the vacuum trap for another desired time of ATRP modification with the same modification condition. The procedure was repeated to obtain modified ICC membrane with variation of grafting time. For better comparison, two initiator immobilized ICC membranes were modified in the same trap at same time. One membrane sample is for filtration test and the other is for characterization.

4.2.4   Instrumental characterization of modified ICC membranes

4.2.5.1 Field emission scanning electronic microscope (SEM)

Unmodified and ATRP modified ICC membranes were imaged using field emission scanning electronic microscope (FESEM, JSM 6500F, JOEL Ltd, Japan) equipped with an in-lens thermal field emission electron gun. All samples were coated with 10nm gold layer before they were imaged at a voltage of 15kV or 10kV depending on sample charging condition. FESEM gives qualitative information on the membrane surface morphologies.

4.2.5.2 X-ray photoelectron spectroscopy (XPS)

Surface chemistry of unmodified and modified ICC membranes was characterized using a Physical Electron 5800 ultrahigh vacuum XPS-Auger spectrometer (Chanhassen, MN). This system has a monochromatic Al Ka X-ray source ($h\nu$=1486.6 eV), hemispherical analyzer, and multichannel detector. For each measurement, a spot size of 250 μm×1000 μm was measured and 10 survey scans over the range 0-1100 eV were averaged. High resolution C1s spectra were acquired at analyzer pass energy of 23.5 eV with 0.1 eV steps.

4.2.5.3 Attenuated total reflectance Fourier-transform infrared (ATR-FTIR)

ATR-FTIR characterization was conducted on non-porous membranes which is produced from vertical cell without colloidal crystal template.The empty cell was directly infiltrated with the same monomer solution for ICC membrane. The following steps are the same as formation of ICC membranes. I use non-porous membranes for ATR-FTIR characterization because real ICC membranes are very brittle after being dried. Unmodified and modified non-porous membranes were examined with ATR-FTIR spectroscopy (Nicolet Magna 760, Thermo Electron Corp., WI) equipped with a mercury-cadmium-tellurium (MCT) detector with resolution of 4cm^{-1}. ATR-FTIR spectra were recorded over a range of 600-4000 cm^{-1} at room temperature and a total of 512 scans were averaged for each spectral measurement.

4.2.5.4 Water contact angle measurement

The water contact angle measurement was also conducted on non-porous membrane due to the reason mentioned above. The water contact angles of unmodified and modified membranes were measured using a KRÜS DSA10 Drop Shape Analysis system (Germany). A dynamic measuring method was used and the contact angle value was calculated using Circle Fitting method. The reported values represent the average of 100 measurements during 10 seconds.

4.2.5.5 Permeate flux measurement

The DI water fluxes were obtained for unmodified and modified membranes using the setup showed in figure 4.2. A Millipore 8010 stir cell (Millipore, Billerica, MA)was used with a membrane holder which fits a membrane with size of 18mm in diameter. The stir cell was attached to a pressurized nitrogen cylinder which supplies pressures up to 690 kPa. The fluxes were measured at increasing pressures between 6.9 kPa and 27.6 kPa. Once reached the desired pressure, the pressure was kept for 5 minutes for equilibrium and then followed by collecting 3 minutes permeate weighed with a electronic balance. Then the pressure was set to another point and the procedure was repeated.

4.2.5.6 Dextran rejection test

The Dextran rejection test was conducted using the same setup as water permeate flux test. The composition of dextran solution is listed in table 4.1. The composition of dextran solution is listed in table 1. Zydney and Xenopoulos have reported that

using the Dextran concentrations listed in table 1 yields a uniform concentration of dextrans over a wide range of MWs.[23] All the solutions were prefiltrated using a 0.22 μm microfiltration membrane.

The modified ICC membrane used for dextran rejection test was the modified membrane with 3hr modification time. Total 10 mL dextran solution was used as feed solution. Gentle stirring was applied to the feed solution through the rejection test. The pressure was set at 10 psi. Before taking sample for HPLC analysis, the membrane was equilibrated by circulating 2 mL feed through charging every 0.5 mL collected permeate back to the feed. The total circulat time was about 4 hours. After the membrane was equilibrated and the tubing was primed, 1 mL permeate and 1 mL retentate were collected for HPLC analysis. All the dextran samples were analyzed using an HPLC (Agilent Technologies Model 1050, Palo Alto, CA) equipped with HP 1047A RI detector. A gel permeate column (SB-806M HQ, Showa Denko, Japan) and a guard column (SB-G, Showa Denko, Japan) were used for analysis. The mobile phase was 0.05M sodium phosphate buffer with pH 4.5 and flow rate of 0.6 mL/min. The operation temperature was 40ºC.

4.3   Results and discussion

4.3.1   Membrane characterization

Unmodified and modified membranes were characterized using FESEM, XPS, ATR-FTIR and water contact angle measurement. Figure 4.3 gives the SEM images of unmodified ICC membrane and modified ICC membranes with a variety of modifica-

tion time. For better comparison, all modified membrane samples imaged by SEM are from exactly the same control membrane. Figure 4.3 (A) and (B)) are the top view and cross-section of unmodified ICC membrane produced from 440 nm particles and 100 μm spacer. As we seen, there are three kinds of pores, pores on the top (POT), small pores in the cross-section(SPCS) and big pores in the cross-section(BPCS). Here I only focus on POT and SPCS because they determines the cutoff of the membrane.

Figure 4.3 (C) and (D) gives the SEM images for the top view and cross-section of modified ICC membrane with modification time of 0.5hr. Compared to unmodified control membrane (figure 4.3(A) and (B)), the POT (figure4.3(C)) and SPCS(figure 4.3 (D)) show a slight shrink. As the modification is carrying on up to 3hrs, the POT and SPCS drop apparently (see figure 4.3 (E), (F), (G), (H), (I) and (J)) compared to unmodified membrane. From figure 4.3 we can see that the POT and SPCS can be well controlled by the modification time. However the pore shrinking rates for POT and SPCS are not the same.

The pore diameters of POT and SPCS were measured based on SEM images. At least 100 pores were sampled. Figure 4.4 gives the pore diameter of POT and SPCS for unmodified membrane and modified membranes. The decreasing rate for POT can be estimated from the figure 4.4 to be about 50nm/hr while the rate for SPCS is about 30nm/hr. The reason is due to the monomer concentration gradient through the membrane generated during the modification. At the beginning, the monomer concentration inside and outside of the membrane were the same. As reaction was

going, the monomer inside of the membrane was exhausting. However, the monomer molecules outside of membrane were easily captured by the growing sites at the membrane surface and captured before they diffuse into the membrane. Therefore the monomer concentration inside of membrane was lower than the outside of membrane as the reaction carrying on.

To further investigate the polymer growing rate variation inside and outside of membrane, I increased the monomer concentration while fix the modification time to be 0.5 hr. Figure 4.5 gives the SEM images of the modified ICC membrane with the same grafting time but different monomer concentration. Figure 4.5(A) (B) gives the top view and cross-section of the modified membrane using 0.1M monomer solution. Compared to the modified membrane from 0.05M monomer, it shows smaller POT but similar SPCS.

As I increased the monomer concentration to 0.2M (see figure 4.5 (C) (D)), all POT is closed while some of SPCS are still open. Thus at higher monomer concentration, the variation of polymer growing rate inside and outside of the membrane is more obvious. I also tried 0.5M monomer concentration (see figure 4.5 (E) (F)). As we seen, all the POT and SPCS are closed due to the high monomer concentration.

Figure 4.6 gives the XPS full scan spectra for unmodified ICC membrane (figure 4.6 (A)), initiator immobilized (figure 4.6 (B)), ATRP modified membranes with modification time of 0.5 hr (figure 4.6 (C)) 1hr (figure 4.6 (D)) and 3hr (figure 4.6 (E)). For

unmodified membrane, the XPS full scan spectra shows two strong peaks which are O1s (543 eV) and C1s (284 eV), respectively. There are two small peaks at 696 eV and 409 eV as well, which are attributed to F1s and N1s respectively. The fluorine element appearing in spectra is the residue HF from the HF solution which is for removing templates and cover glasses. The nitrogen element is from the impurities because of the tiny amount. For initiator immobilized membrane, four new peaks, which are 257eV, 189eV, 182eV and 70eV in correspondence to Br3s, Br3p1/2, Br3p3/2 and Br3d, respectively, appear. The initiator I am using is BIB which supplies bromine element for initiator immobilized membrane.

The XPS full scan spectra showed successfulness of reacting initiator to the membrane. In the spectra of ATRP modified membrane with modification time of 0.5hr, the four peaks for bromine have gone. Meanwhile, a tiny peak at 200 eV which is attributed to Cl2p show up. The penetration depth of XPS is only about 10 nm. From the SEM images, the thickness of the polymer layer after 0.5 hr modification has exceeded the penetration limit of the XPS. It attribute most to the disappearance for the four Br peaks. Besides, the replacement of bromine by chlorine over the time is another reason for the disappearance of the Br perks. However, the relative molar amount of chorine was too small because one chorine atom caps on the end of each polymer chain. Yet, the chlorine is becoming less available as the modification time increases due to the growing polymer chain termination (couple termination and terminated by trace amount of free radicals in the solution). Therefore, we can see from the full scan spectra of modified membrane with 0.5hr modification time that

the peak at 200 eV is very small, and as the modification time increases up to 3hr , this peak disappears (see figure 4.6 (D) and (E)) due to the relative amount of the chorine becomes too small to be detected by the XPS machine.

I also investigated the high resolution C1s peak for the unmodified, initiator immobilized and ATRP modified ICC membranes. The XPS Peak 4.1 software was used to fit the C1s peaks. Figure 4.7 (A) gives the high resolution of C1s peak for unmodified ICC membrane. There are three fitted peaks which are attributed to C=O (288.5 eV), C-O (286 eV) and C-C (284 eV), repectively. Compared to figure 4.7 (A), figure 4.7 (B), which is the fitted spectra for initiator immobilized membrane, shows bigger peak area for C=O and C-C peak while the C-O peak area keeps almost the same. The reason is that after reacted with initiator, more carbonyl groups from the initiator molecules are introduced onto the membrane surface.

Figure 4.7 (C) gives the ATRP modified membranes with modification time of 3hr. Compared to unmodified and initiator immobilized membranes, the C-O peak area for modified membranes increases dramatically due to the polymer chain has lots of poly ethylene glycol side chains. The C-C peak area decreases dramatically because the C-C bonds exist in the polymer backbone which is relative too small comparing to ethylene glycol side chains.

Figure 4.8 gives the ATR-FTIR spectra for unmodified, initiator immobilized and ATRP modified membranes with modification time of 0.5hr, 1hr and 3hr. There

are no characteristic peaks for initiator immobilized membrane due to the low molar amount initiator molecules. However compared to unmodified membrane, the peak intensity at 3500 cm^{-1}, which attributed to hydroxyl group,[20] get weaker due to part of the hydroxyl groups on the membrane reacted with the initiator. As the PPEGMA polymer layer thickness increases, this peak is getting diminish in intensity and a new peak is showing up around 3400 cm^{-1} which is attributed to non-hydrogen-bonded hydroxyl groups in poly ethylene glycol side chains.[16, 21]

Figure 4.9 gives the water contact angle value for unmodified control, initiator immobilized, ATRP modified membranes for up to 3 hours. The contact angle value for unmodified membrane is 60 degree. After initiator immobilized, the contact angle increased up to 64 degree. The reason is the molar amount of the hydroxyl group on the membrane surface becomes lower due initiator immobilization reaction. The increase in membrane surface hydrophobicity could also be visualized. After the reaction, the initiator immobilized membrane is always floating on water surface. The water is hard to spread on the membrane. The contact angle value illustrates the change in membrane surface hydrophobicity before and after the initiator immunization as well.

After 0.5 hour modification, the contact angle of the surface drops to be 57 degree and even lower to be 48 degree after 3 hours modification, which means the membrane surface turns to be more and more hydrophilic as the modification time is getting longer. The contact angle value of pure PPEGMA was measured as well. The value, 47.4 degree, is presented in figure 4.9 as well. The modified membrane with modi-

fication time of 3 hr gives a quite similar hydrophobicity with pure PPEGMA. The trend of the membrane surface hydrophobicity change shows good match with the investigation by Ningh et al.[16]

4.3.2 Pure water flux

Figure 4.10 gives the pure water fluxes for unmodified membrane and modified membranes with modification time up to 3 hours. As seen from figure 4.10, the fluxes for both unmodified and modified membranes increase linearly as the pressure increases. As I expect, the fluxes for modified membranes decrease steadily as polymerization time increases due to the pore size shrinking. However, as seen, the decrease in flux as polymerization time increase is not linear. There is a big drop for modified membrane with 0.5 hour polymerization time.

I did a calculation using Hagen-Poiseuille equation to predict the flux drop for modified ICC membranes. The equation is showed bellow.

$$J = \frac{n_p \pi r_p^4 \, \triangle P}{8 \mu l} \tag{4.1}$$

Assuming laminar flow through uniform cylindrical non-interconnected pores. Where n_p denotes total number of pores; r_p denotes the pore radius; $\triangle P$ denotes the transmembrane pressure; μ denotes the water viscosity; l denotes the membrane thickness.

the pore radius is using SPCS pore size which is approximated to be 55nm and 35nm for membranes with modification time of 0.5hr and 1hr respectively based on figure 4. The effective membrane surface area in the stirred cell is 4.1 cm^2 according to the manufacturer. The n_p is 4.709×10^{12}. Assuming the viscosity of water is 1×10^{-3} Pa.s for a 100 μm thick membrane. The pressures are 275760, 206820, 137880, and 68940 pa. The calculated fluxes for membranes with modification time of 0.5hr and 1hr are plot in the figure (figure 4.10) of experimental fluxes. The solid square dots represent the fluxes for modified membrane with 0.5 hr modification at various pressures while the solid diamond dots represent modified membrane with 1 hr. As seen, the calculated flux value for modified membrane with 0.5 hr modification is little lower than experimental value. However, the differential is in reasonable range. But for modified membrane with 1 hr modification time, the calculated flux value is even lower compared to experimental flux.

In the calculation, the total number of pores n_p is actually the total number of pores on the membrane surface. However, the flux is limited by the SPCS. The number of SPCS is higher than the number of POT. Nevertheless, the number of SPCS for the total membrane area in duty is very hard to be approximated because the SEM images are only able to give a cross section view. Thus I used the total number of POT instead of SPCS to approximate the flux which would be a little lower than the calculated flux if using total number of SPCS as n_p.

The calculated flux value for modified ICC membrane with modification time of 0.5 hr

gives a better approximation than modified membrane with 1 hr modification time. The reason is not clear, but I think it is due to the fully interconnectivity of the SPCS. When some pores get too small, the flux will just by pass it by the bigger pores. However, more future work needs to be proposed to elucidate the mechanism of flux decrease profile as modification time increase.

4.3.3   Dextran rejection

To investigate if the pore size of the membrane can be reduced to be small enough for rejection of macromolecules after modification, the Dextran rejection test which is a widely used method for measuring rejection cut-off of ultrafiltration membranes was conducted on the modified membrane with modification time of 3 hr . Figure 4.11 demonstrates the HPLC absorption signal strength versus elution time for the feed solution and the individual Dextrans which have the concentrations the same as they are in the feed.

Figures 4.12 gives the HPLC absorption signal strength versus elution time for retentate and permeate. As we seen, the Dextran with molecule weight of 2000 kDa shows significant rejection. The specific rejection rate for dextran with certain Mw is calculated based on figure 4.12. The result is given in figure 4.13. From 4.13, significant rejection for the Dextran with Mw higher than 100 kDa can be found. For the Dextran with Mw between 10 kDa and 100 kDa, the rejection rate shows a linear increase. From table2[22] , which gives the hydrodynamic radius for T10, T40,

T70, T500, and T2000, respectively, I can estimate the pore size for the modified

ICC membrane with 3 hour modification time to be 5 nm-15 nm. However, the SEM

image for this modified membrane shows closed pores in cross section. The reason

is due the gold coating to make the sample being visible under electron beam. The

thickness of the gold layer deposited on the sample surface is 10 nm. Therefore, if

the pore size smaller than 20 nm, they will not be able to visualized by SEM.

As we seen from figure 4.13, the diameter of SMCS could be decreased from 110-130

nm to 5-15 nm using ATRP modification. It means I can convert a MF membrane

to be a UF membrane by growing a polymer layer from the membrane. However, the

modification does not improve the pore size distribution from the rejection curve. Be-

sides, the water flux drops dramatically due to the dramatic shrinkage pore size. Nev-

ertheless, I developed a protocol for growing a polymer layer from the new-developed

membrane. This way will extend the application of the ICC membrane to UF and

membrane chromatography area.

4.4 Conclusion

A protocol of surface modification of new-developed ICC membrane using ATRP

has been developed. The ICC membranes were surface modified using ATRP under

variation of modification times and variation of PEGMA concentrations. The success-

fulness of the modification was demonstrated by SEM, XPS, ATR-FTIR and water

contact angle measurement. The dextran rejection test was conducted on the modi-

fied ICC membrane with 3 hours modification time. The rejection curve demonstrates

that the pore size of SMCS could be decreased from 110-130 nm to 5-15 nm.

List of tables

Tab. 4.1: Dextran molecular weights, concentrations, manufactures in the test solution

Dextran	MW (kDa)	Concentration (g/L)	Manufactur
T1	1	0.74	Pharmacosmos, (Holbaek, Denmark)
T10	10	0.54	GE Healthcare Biosciences Corp.(Piscataway, NJ)
T40	40	0.74	GE Healthcare Biosciences Corp.(Piscataway, NJ)
T70	70	0.34	GE Healthcare Biosciences Corp.(Piscataway, NJ)
T500	500	0.27	GE Healthcare Biosciences Corp.(Piscataway, NJ)
T2000	2000	3.15	Pharmacosmos.(Holbaek,Denmark)

Tab. 4.2: Dextran molecular weights and hydrodynamic radius(Rh)

Dextran	Mw(kDa)	Rh(nm)
T10	10	2.7
T40	40	5.7
T70	70	7.4
T500	500	15.3
T2000	2000	27.2

List of figures
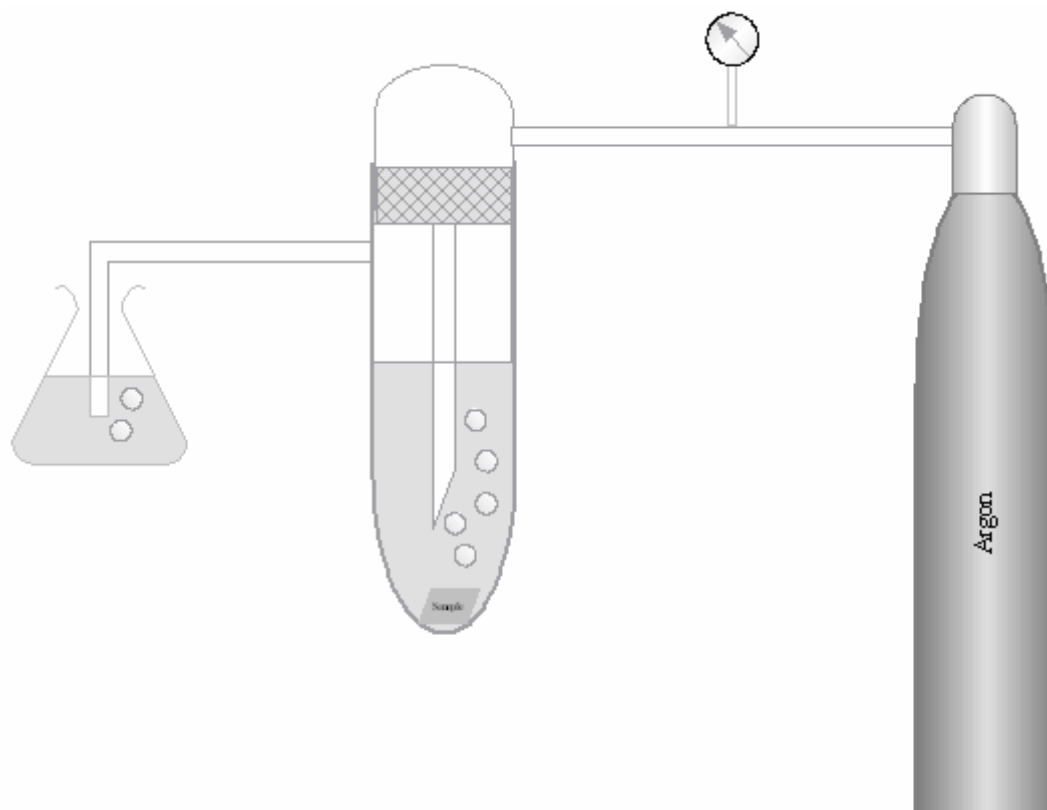


Fig. 4.1: Illustration of ATRP setup
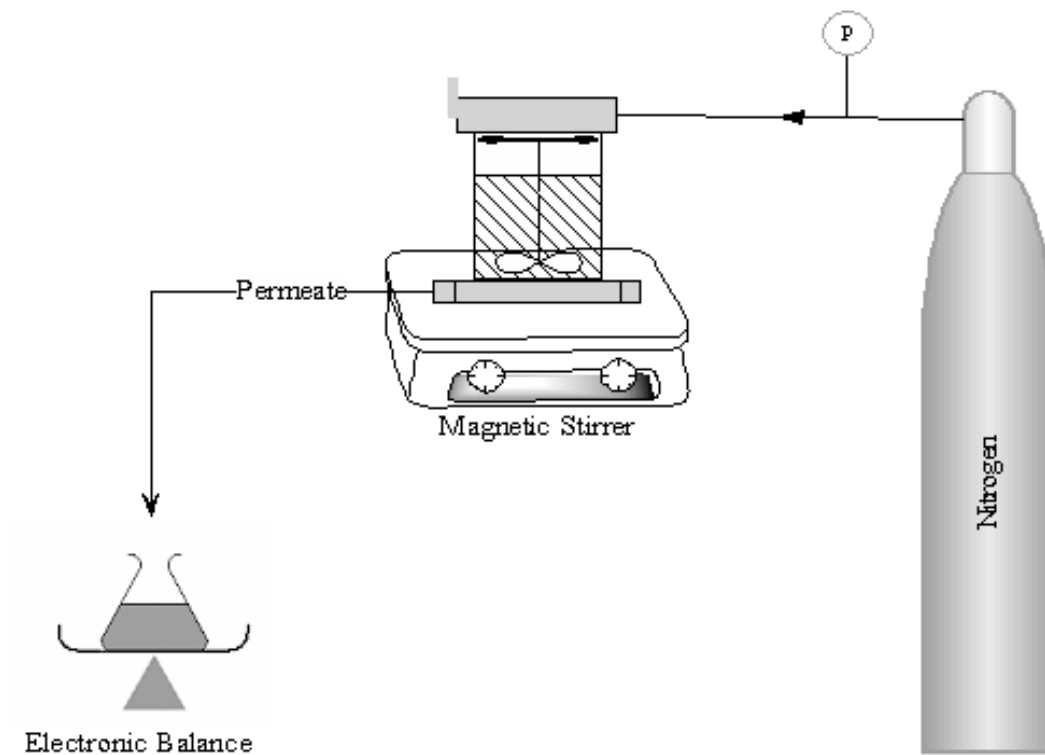
Fig. 4.2: Illustration of the filtration setup

Bibliography

[1] M. Moo-Yound, comprehensive biotechnology, Vol.2, Pergamon Press, Oxford 1985.

[2] K. Takita, K. Kono, T. Takashima, K. Okamoto, The preparation method for microporous polyolefin membrane, Japan Patent 364, 334, 1991.

[3] P. Apel, Track etching technique in membrane technology, Radiation Measurements, 34(2001) 559-566.

[4] W.S.W. Ho, K.K. Sirkar, Membrane handbook, van Nostrand Reinhold, New York, NY, 1992.

[5] H. Susanto, M. Ulbricht, Influence of ultrafiltration membrane characteristics on adsorptive fouling with dextrans, J. Membr. Sci. 266 (2005) 132.

[6] E. Matthiasson, The role of macromoleclar adsorption in fouling of ultrafiltration membranes, J. membr. Sci. 16 (1983) 23.

[7] K.J. Kim, A.G. Fane, C.J.D. Fell, D.C. Joy, Fouling mechanisms of membranes during protein ultrafiltration, J. Membr. Sci. 68 (1992) 79.

(A)

(B)

(C)

(D)

(E)

(F)
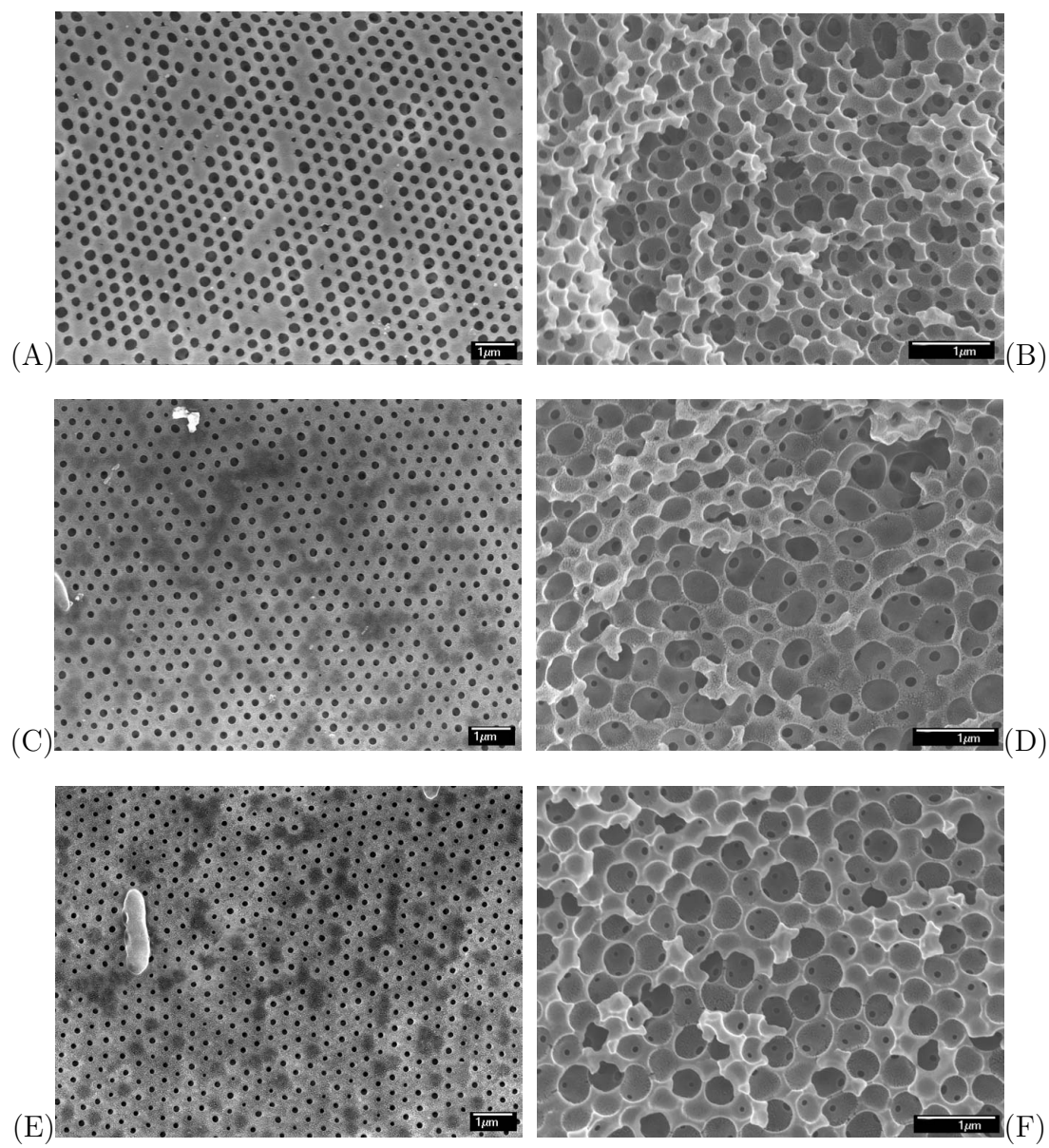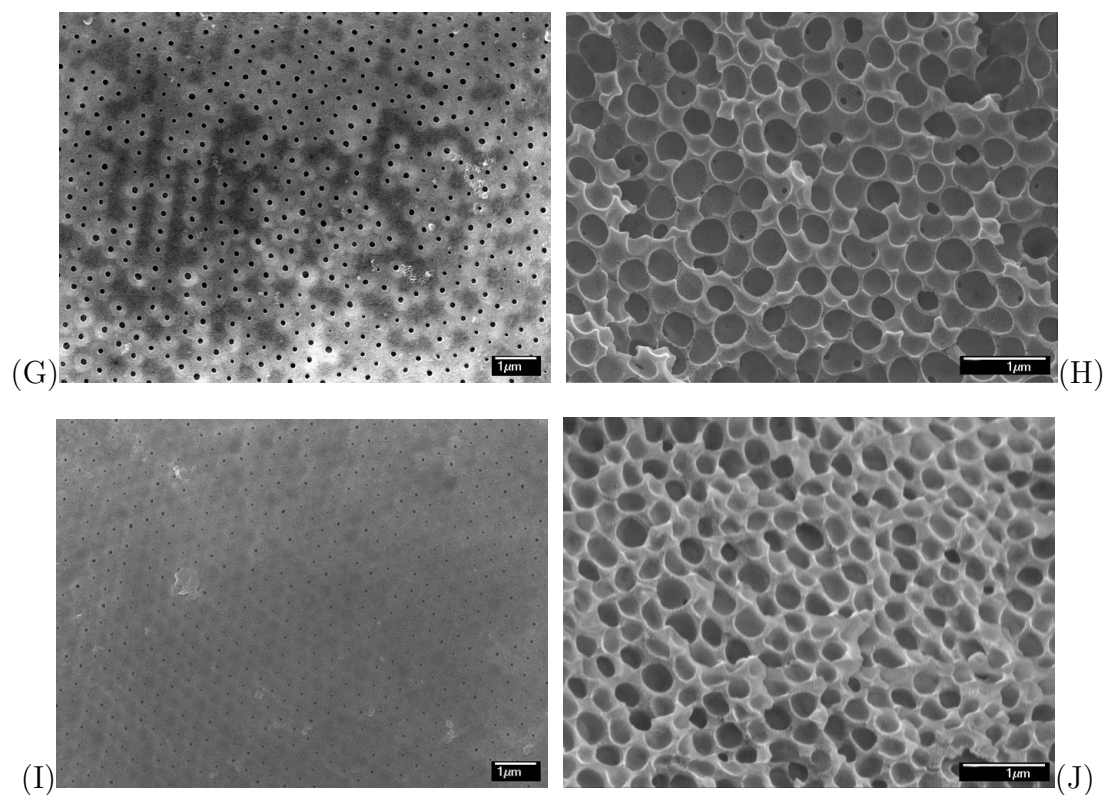
Fig. 4.3

Fig. 4.3: SEM images of unmodified and ATRP modified ICC membranes, unmodified ICC membranes (A) top view and (B) cross-section; ICC membrane modified for 0.5hr (C) top view and (D) cross-section; 1hr (E) top-view and (F) cross-section; 2hr (G) top-view and (H) cross-section; 3hr (I) top view and (J) cross-section
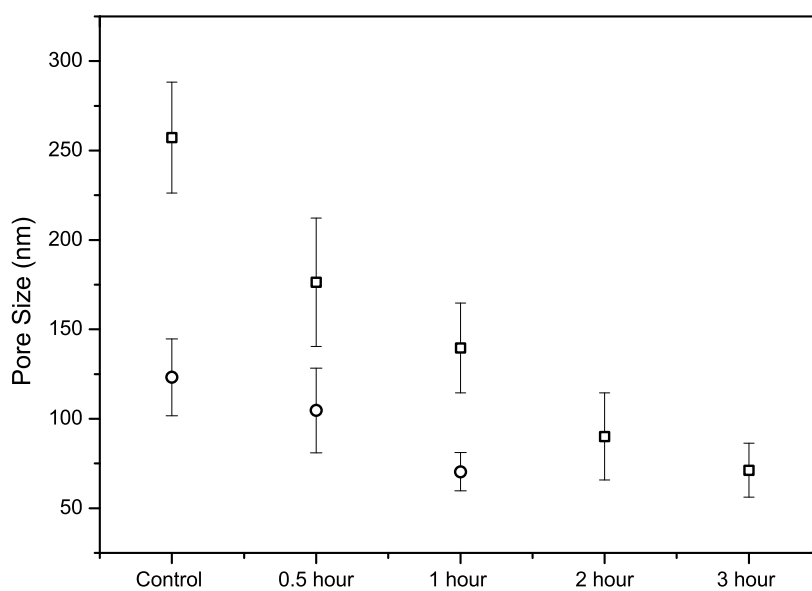
Fig. 4.4: POT (open square dot) and SPCS (open circle dot) Pore diameter for unmodified and modified membrane with modification time 0.5 hr, 1hr, 2hr, and 3hr.
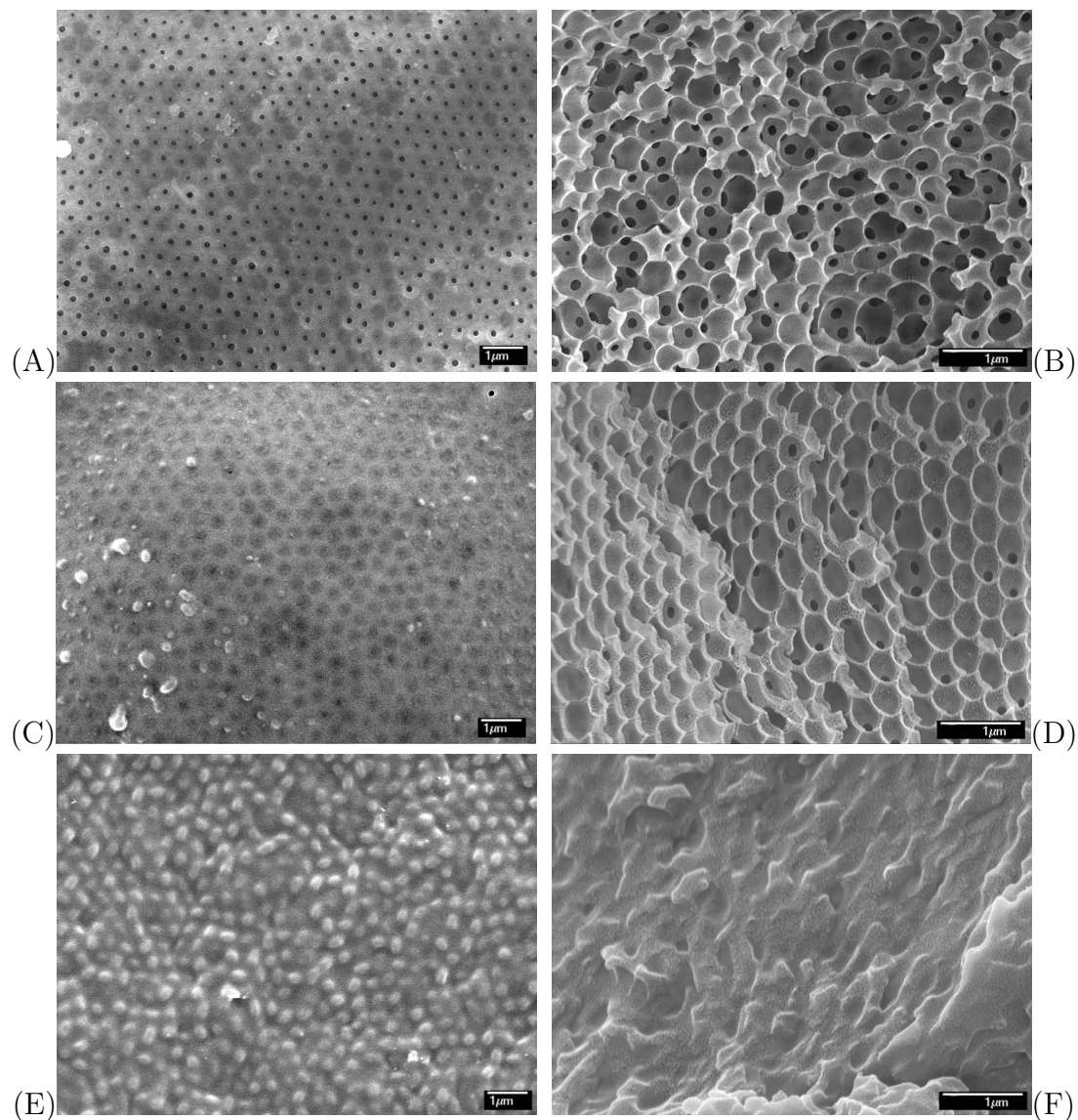
Fig. 4.5: SEM images of modified ICC membranes for 0.1M monomer concentration (A) top view and (B) cross-section; 0.2M monomer concentration (C) top view and (D) cross-section; 0.5M monomer concentration (E) top-view and (F) cross-section; reaction time 0.5 hour
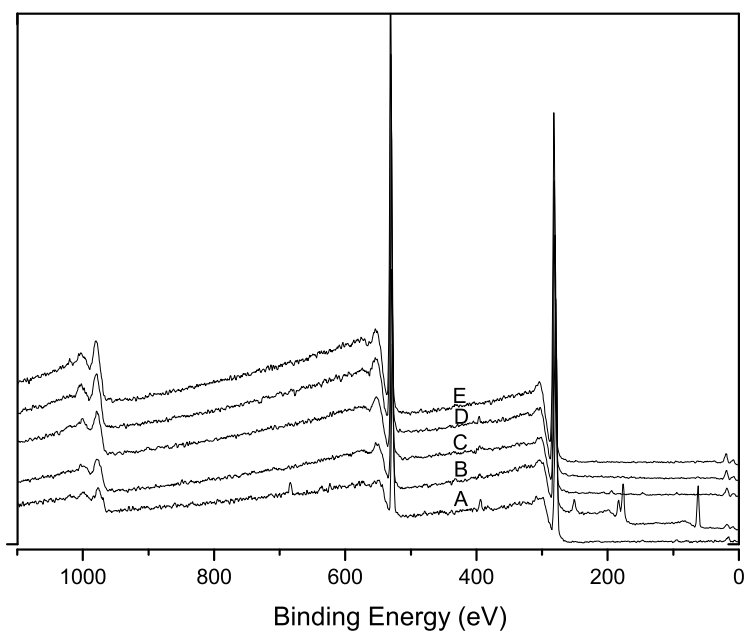
Fig. 4.6: Full scan of XPS peak for A)unmodified, B)initiator funcationlized and ATRP modified membranes from 0.05M monomer concentration and (A) 0.5 hr, (B)1hr, (C)3hr grafting time

(A)

(B)

(C)
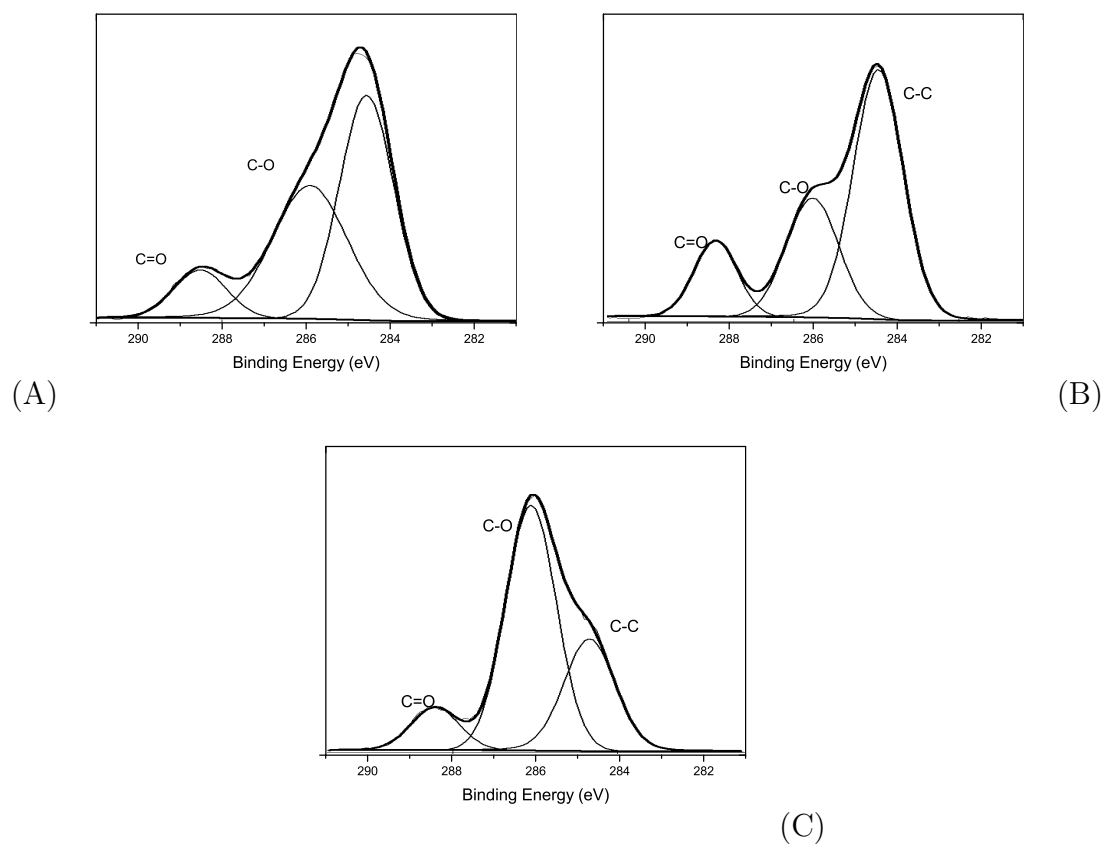
Fig. 4.7: C1s core level spectra for (A) unmodified control membrane (B) initiator function-alized membrane; modified membrane from 0.05M monomer concentration (C) 3 hr reaction time
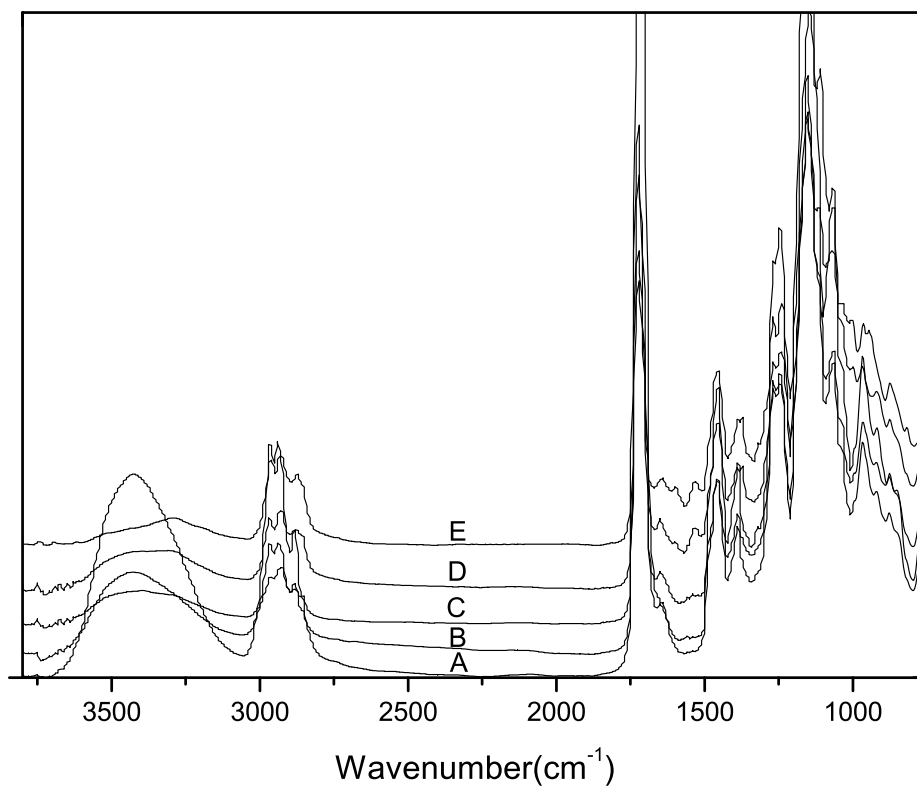
Fig. 4.8: ATR-FTIR spectra of (A) unmodified; B)initiator functionalized and ATRP modified membrane with modification time of (C)0.5hr, (D)1hr and (E)3hr
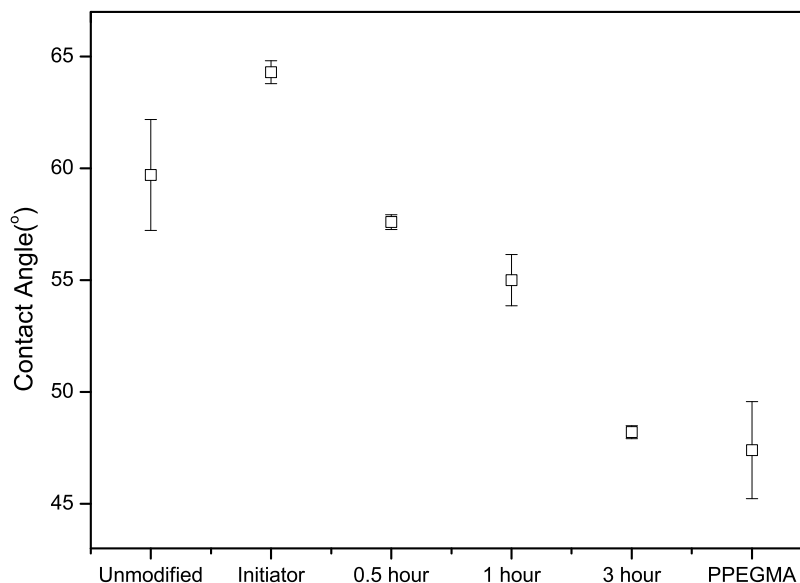
Fig. 4.9: Plot of contact angle degree versus membrane conditions

[8] M. Meireles, P. Aimar, V. Sanchez, Effects of protein fouling on the apparent pore size distribution of sieving membranes, J. Membr. Sci. 56 (1991) 13.

[9] J.A. Koehler, M. Ulbricht, G. Belfort, Intermolecular forces between proteins and polymer films with relevance to filtration, Langmuir 13 (1997) 4162.

[10] R. Chan, V. Chen, Characterization of protein fouling on membranes opportunities and challenges, J. Membr. Sci. 242 (2004) 169.

[11] A. Adout, S. Kang, A. Asatekin, A. M. Mayes, M. Elimelech, Ultrafiltration membranes incorporating amphiphilic comb copolymer additives prevent irreversible adhesion of bacteria, Environ. Sci. Technol., 44(2010)2406-2411

[12] A. D. Marshalla, P. A. Munrob, G. Tragardhc, The effect of protein fouling in microfiltration and ultrafiltration on permeate flux, protein retention and selectivity: A literature review, Desalination 91(1993) 65-108

[13] J. C. Lytle, A. Stein in: G. Cao, C. J. Brinker (Eds), Annual Review of Nanomaterials, World Scientific Publishing Company, Hackensack, NJ, 2006.

[14] J.S. Wang, K. Matyjaszewski, Controlled/"living" radical polymerization. atom transfer radical polymerization in the presence of transition-metal complexes, J. Am. Chem. Soc. 117 (1995) 5614-5915.
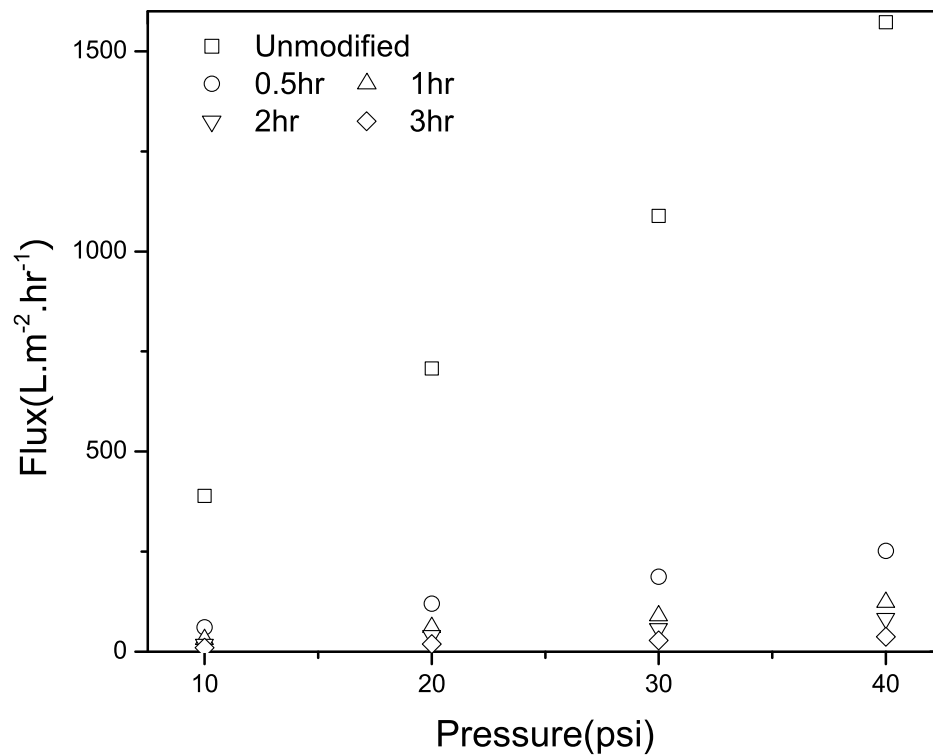
Fig. 4.10: Plot of pure water flux versus pressure for unmodified control membrane (open square), modified membranes with modification time of 0.5hr(open circle), 1hr(open up triangle), 2hr(open down triangle), and 3hr(open diamond); the calculated fluxes for modified membrane with modification time of 0.5 hr (solid square) and 1hr (solid diamond)
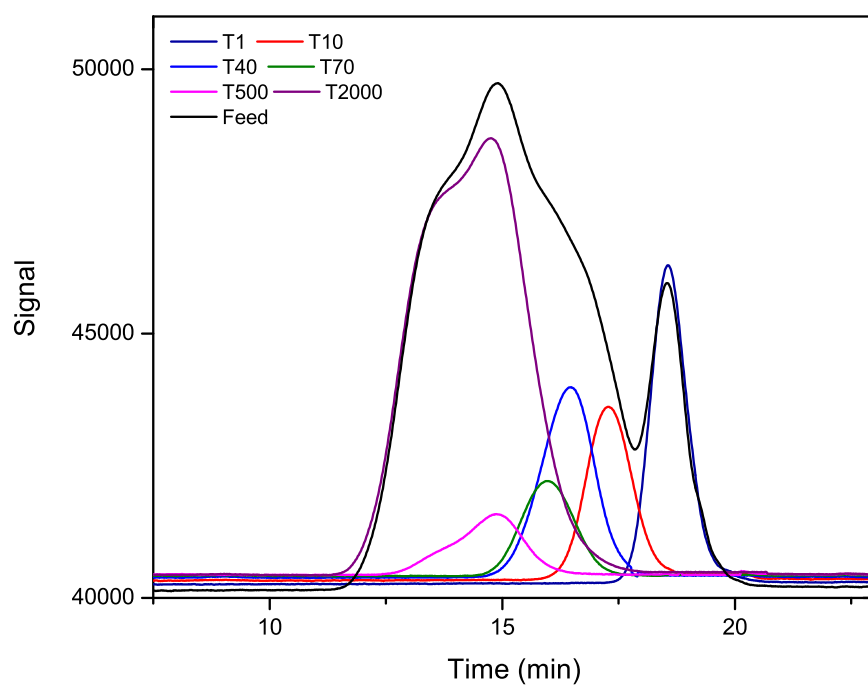
Fig. 4.11: Plot of peak strength verus time for feed solution and individual Dextranes
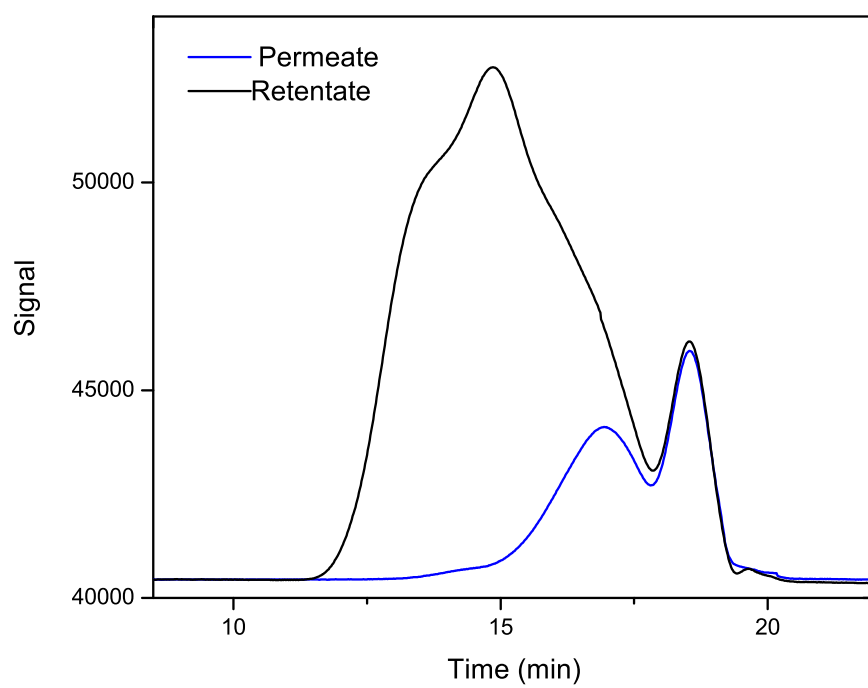
Fig. 4.12: Plot of peak strength verus time for retentate and permeate
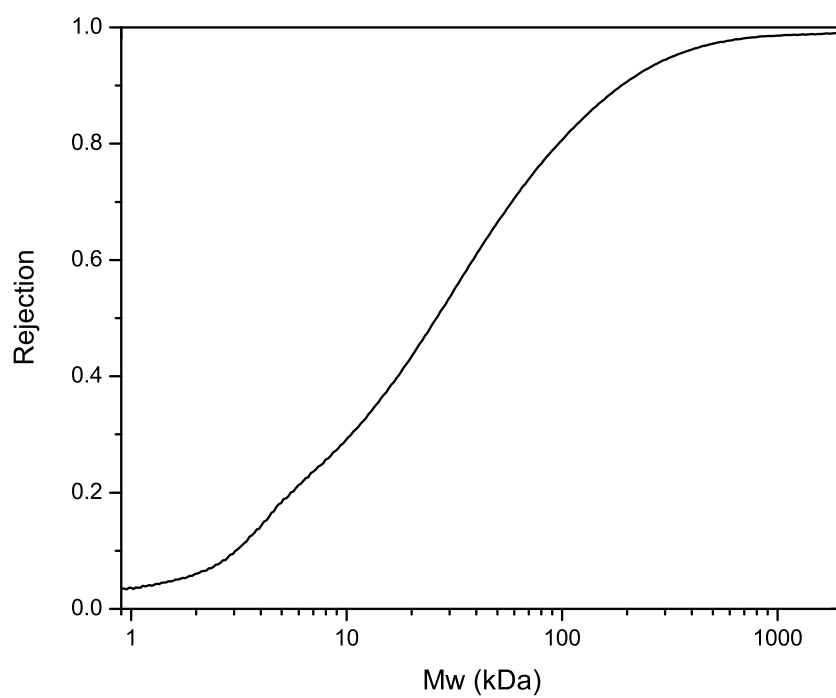
Fig. 4.13: Dextran rejection rate versus Dextran elution time for modified membrane with modification time of 3 hours

[15] V. Percec, B. Barboiu, "Living" Radical polymerization of styrene initiated by arenesulfonyl chlorides and CuI(bpy)nCl, Macromolecules 28 (1995) 7970.

[16] N. Ningh, Z. Chen, N. Toner, S.R. Wickramasinghe, N. Soice, S.M. Husson, Modification of regenerated cellulose ultrafiltration membranes by surface-initiated atom transfer radical polymerization, 311(2008) 225-234.

[17] L. P. Zhu, H.B. Dong, X. Z. Wei, Z. Yi, B.K. Zhu, Y.Y. Xu, Tethering hydrophilic polymer brushes onto PPESK membranes via surface-initiated atom transfer radical polymerization, J. Membr. Sci. 320 (2008) 407.

[18] Y. Chen, Q. Deng, J. Xiao, H. Nie, L. Wu, W. Zhou, B. Huang, Controlled grafting from poly (vinylidene fluoride) microfiltration membranes via reverse atom transfer radical polymerization and antifouling properties, Polymer 48 (2007) 7604-7613.

[19] W. Stober, A. Fink, E. Bohn, Controlled growth of monodisperse silica spheres in the micron size range, J. Colloid Interf. Sci. 26 (1968) 62-69

[20] C.Y. Liang, R.H. Marchessault, Infrared spectra of crystalline polysaccharides. I. Hydrogen bonds in native cellulose, J. Polymer Sci. 37(1959) 385.

[21] H. Younes, D. Cohn, Phase separation in poly (ethylene glycol)/poly (lactic acid) blends, Eur. Polym. J. 24(1988) 765.

[22] L. Lebrun, G. Junter, Diffusion of dextran through microporous membrane filters, J. Memb. Sci. 88 (1994) 253-261.

[23] A.L. Zydney and A. Xenopoulos, Improving dextran tests for ultrafiltration membranes: effects of device format, J. Membr. Sci. 291 (2007), 180-190.

5. CONCLUSIONS AND FUTURE WORKS

5.1 Research synopsis

5.1.1 Summary of vertical cell assembly method and ICC membrane formation

A vertical cell assembly method has been developed for fabrication of ICC membranes usable in separation field. The new assembly method provides a low cast, simple way to make such membrane. The colloidal crystal templates with controllable thickness were formed using the new-developed method. The thickest template was made up to be 100 μm. Different sizes of polystyrene particles were employed to make template using VC method. SEM images and UV-Vis spectra results showed that the bigger the particle was, less periodical the structure of the template was. When 2 μm particles were used, we found that the structures were mostly disordered.

The ICC membranes with controllable thickness were fabricated using the VC method. The thickness could be easily controlled by the thickness of the spacer. The pore size of the membrane could be controlled by the size of particles for assembling the template. The particles with size more than 1 μm and less than 0.3 μm might not be for making the ICC membranes. If the particles were too big, gravitational sedimentation was dominating during assembling, which resulting in no assembling. If the particles

were too small, the membranes had high porosity which resulted in poor mechanical strength. The ICC membranes made from different polymers were formed using the VC method easily. The ICC membranes made from the monomer solutions of HEMA and HBMA with different weight ratios showed variable water fluxes due to the hydrophobicity of the final polymer. The best recipe for making ICC membrane with best mechanical strength is HEMA: HBMA 1:3 by weight. The water fluxes were measured for the ICC membranes with different pore sizes and the ICC membranes made of different polymers.

5.1.2   Summary of ICC membrane surface modification using ATRP

A poly (poly ethylene glycol) methacrylate nano-layer was grew from the membrane surface using ATRP to control the membrane pore size and improve the membrane surface hydrophilicity. The reaction time and the monomer concentration were used as factors to control the thickness of the grafted polymer layer. The SEM images showed that the reaction time was a better way than monomer concentration to control the layer thickness. The water fluxes for modified ICC membrane under different times were measured. The ATR-FTIR and XPS results showed the successfulness of the modification chemically.

The membrane surface hydrophilicity for the unmodified, initiator immobilization and PPEGMA grafted membranes were characterized by water contact angle. The initiator immobilized membrane appeared more hydrophobic, which gave a higher contact angle, because of the loss of hydroxyl groups on the membrane surface. As

the modification time increased, the surface turned to be more hydrophilic.

5.1.3   Summary of the applications for ICC membranes and surface modified ICC membranes

The applications of the unmodified ICC membranes and modified ICC membranes focused on microfiltration and ultrafiltration. The ICC membrane was first used as microfiltration membrane for micro-size particles fractionation. The results showed that the ICC membrane made from 835 nm particles gives a good passage for the 60 nm particles in the bidisperse particle suspension of 60 nm and 835 nm while poor passage for the 60 nm particles in the bidisperse particle suspension of 60 nm and 440 nm.

The surface modified ICC membranes were tested as ultrafiltration membranes because the pore size had been reduced dramatically. The modified membrane with grafting time of 3 hours was tested using Dextrans with a variety of MW. The rejection rate for Dextran with certain MW was obtained. The rejection curve demonstrated that the pore diameter of the SPCS for ICC membrane produced form 440 nm particles could be reduced from 110-130 nm to 5-15 nm.

5.2   Future works

5.2.1   ICC Membranes for Hydrophobic Interaction Membrane Chromatography

The IgG antibodies are widely used in monoclonal antibody therapy for numerous serious diseases such as rheumatoid arthritis, multiple sclerosis and different types of cancers.[1] Q membrane chromatography is currently a widely used purification unit for commercial manufacture of a therapeutic IgG antibody.[2] However the disadvantages including the poor inlet flow distribution, broad pore size distribution and low protein binding capacity increase the antibody production cost dramatically.[3] Hydrophobic interaction membrane chromatography (HIMC) has drawn more and more attentions for protein[4, 5, 6] and DNA purification[7] due to its process relatively efficient and gentle. The binding mechanisms for HIMC is the same as hydrophobic interaction chromatography which have been discussed using several methods such as Solvophobic theory[8] and preferential interaction theory.[9]

By far, the purification of humanized monoclonal antibodies using HIMC has been discussed by Raja Ghosh who had used commercially available PVDF microfiltration membranes as membrane support for HIMC.[4, 5, 6] However the broad pore size distribution and low surface area of the commercially available PVDF membranes has limited their use in HIMC. The ICC membranes show many advantages over commercially available membranes as a membrane support used in membrane chromatography because of their highly uniform and controllable pore size, fully interconnected pores, and a large surface area. In previous chapters, the ICC membranes applicable

in MF and UF have been fabricated through a newly developed ICC membrane formation method, vertical cell assembly method. Preliminary tests for ICC membranes used as HIMC membrane supports for antibody IgG purification have shown the ICC membranes developed in our group a great alternative for PVDF membranes. Therefore, for the future work, application of ICC membranes in HIMC for purification of proteins could be a promising work.

5.2.2   Scale-up and commercialization

The ICC membranes have been fabricated using a low-cost, simple method. Commercialization of ICC membranes might be a valuable direction for the future work. Scale-up is one big problem before the commercialization. The biggest ICC membrane been made so far is about 5 cm^2 which is still too small. So, finding a way to make larger size membrane is very important for the successfulness of the commercialization.

One way to produce bigger ICC membrane is to customize the cover glass for making vertical cell. As the membrane size is limited by the cover glass size, obtaining bigger size cover glasses from manufacture is the first step to make bigger size ICC membrane. The other way to enlarge the membrane size is producing ICC anisotropic membrane. In this way, a porous support, which has greater pore size, will be used. A thin film of ICC is spreads on it. However, this way needs to explore a new membrane formation method to produce such an anisotropic ICC membrane. The new-developed ICC membrane formation method, VC method, will not be working in producing such membrane.

Bibliography

[1] T.A. Waldmann, Immunotherapy: past present and future, Nature Medicine, 9(2003) 269-277

[2] S. Brandt, R. Goffe, S.B. Kessler, J. L. O'Connor, S.E. Zale, Membrane-based affinity technology for commercial scale purifications, Bio/Technology 6(1988) 779-782

[3] D. K. Roper, E. N. Lightfoot, Separation of biomolecules using adsorptive membranes. J. Chromatogr. A. 702(1995) 3-26

[4] R. Ghosh, Separation of proteins using hydrophobic interaction membrane chromatography, J. Chromatogr. A, 923(2001) 59-64

[5] L. Wang, G. Hale, R. Ghosh, Non-size-based membrane chromatographic separation and analysis of monoclonal antibody aggregates, Anal . Chem., 78(2006) 6863-6867

[6] L. Wang, R. Gosh, Fractionation of monoclonal antibody aggregates using membrane chromatography, J. Membr. Sci., 318(2008)311-316

[7] L. R. Pereira, D. M. F. Prazeres, M. Mateus, Hydrophobic interaction membrane chromatography for plasmid DNA purification: Design and optimization, J. Sep. Sci. 33(2010)1175-1184.

[8] M. M. Diogo, J. A. Queiroz, D. M. F. Prazeres, Hydrophobic interaction chromatography of homo-oligonucleotides on derivatized sepharose CL-6B. Application of the solvophobic theory, J. Chromatogr. A 944(2002) 119-128

[9] S. luliano, J. R. Fisher, M. Chen, W. J. Kelly, Rapid analysis of a plasmid by hydrophobic-interaction chromatography with a non-porous resin, J. Chromatogr. A 972(2002) 77-86

APPENDIX

Fabrication of ICC membranes with various polymers

The ICC membranes fabricated with polystyrene (PS), poly methyl methacrylate (PMMA), poly butyl methacrylate (PBMA), and polyurethane (NOA-60) are demonstrated in this section. The silica particle preparation and the colloidal crystal template assembly have been described in chapter 3. The silica particles with 440 nm were used for assembling template. The spacer was 100 μm thick microfiltration membrane. The styrene (Aldrich, MA, Al_2O_3 column purified) and methyl methacrylate (MMA, Aldrich, MA, Al_2O_3 column purified) were used for fabrication of PS ICC membrane and PMMA ICC membrane, respectively. The styrene and the MMA are difficult to be polymerized using UV irradiation because the styrene absorbs UV light and the MMA has low boiling point. Thus, I used thermo-initiating to fabricate PS and PMMA ICC membranes. Azobisisobutyronitrile (AIBN, Aldrich, MA), which is a thermo-initiator, was used for initiating the polymerization. The monomer solution for fabrication of PS ICC membrane was styrene 2g and AIBN 0.04g, while the monomer solution for fabrication of PMMA ICC membrane was MMA 1.8 g, ethylene glycol dimethacrylate (EGDMA, Aldrich, MO) 0.2g, and AIBN 0.04g. The polymerization was conducted at 65 ºC for 2 hours. The template together with the cover

glasses were removed using 10% HF solution.

The PBMA ICC membrane was fabricated using butyl methacrylate (1.8 g, Aldrich, MO, Al_2O_3 column purified) as monomer, EGDMA(0.2g) as cross-linker, and benzoin isobutyl ether (0.02 g, BIE, Aldrich, MO) as initiator. The polymerization was conducted using a UV lamp (30 W with wavelength 254 nm) for 10 minutes. The template and the cover glasses were removed using 10% HF solution. For the polyurethane ICC membrane, NOA-60 (Norland Optical, NJ), which is UV curing polyurethane adhesive, was used as monomer solution. It is a little different with the monomer solutions for fabrication of other ICC membranes because the NOA-60 is a polymer already. Under UV irradiation, NOA-60 is cross-linked rather than polymerized. As I mentioned, NOA-60 is polymer. So it has a high viscosity. Therefore, the infiltration of NOA-60 is not easy. It takes 2 days for thoroughly infiltration. The UV cross-linking takes longer time (12 hours) as well. The template and the cover glasses were removed in a same way as fabrication of other ICC membranes.

Figure below shows the SEM images of the cross-section of the ICC membranes fabricated with various polymers. Figure (A)and (B) are ICC membranes fabricated with polystyrene and poly methyl methacrylate using thermal induced polymerization. Figure (C) and (D) are ICC membranes fabricated with poly butyl methacrylate using UV induced polymerization and NOA-60 using UV induced cross-linking. the PS ICC membrane and the PMMA ICC membrane were fabricated using thermo-initiating. However, the vaporization of the monomer at the beginning of the polymerization

was still sever. Therefore, monomer compensation at the beginning was needed. The way I did to compensate the monomer loss to vaporization was by adding a monomer 'reservoir'.

The reservoir was composed of another two pieces of cover glasses which 'sandwich' the assembly cell perpendicularly to form a cross. The two pieces of cover glasses were separated by the assembly cell. The space between the two pieces of glasses was used as the monomer reservoir which first filled with monomer solution by capillary force before the polymerization. At the beginning of polymerization, the monomer vaporization first took place from the reservoir to save time for the polymerization in the assembly cell. The PS and PMMA ICC membranes could be fabricated using this setup. But, the membranes were not integral after etched away the template and cover glasses. The PBMA ICC membrane can be fabricated easily. The SEM image of the PBMA membrane shows highly porous through the membrane. However, as seen from figure (D), the polyurethane ICC membrane loses the porosity. The reason is the softness of the polyurethane material. After removal of the particles, the pores are collapsed.
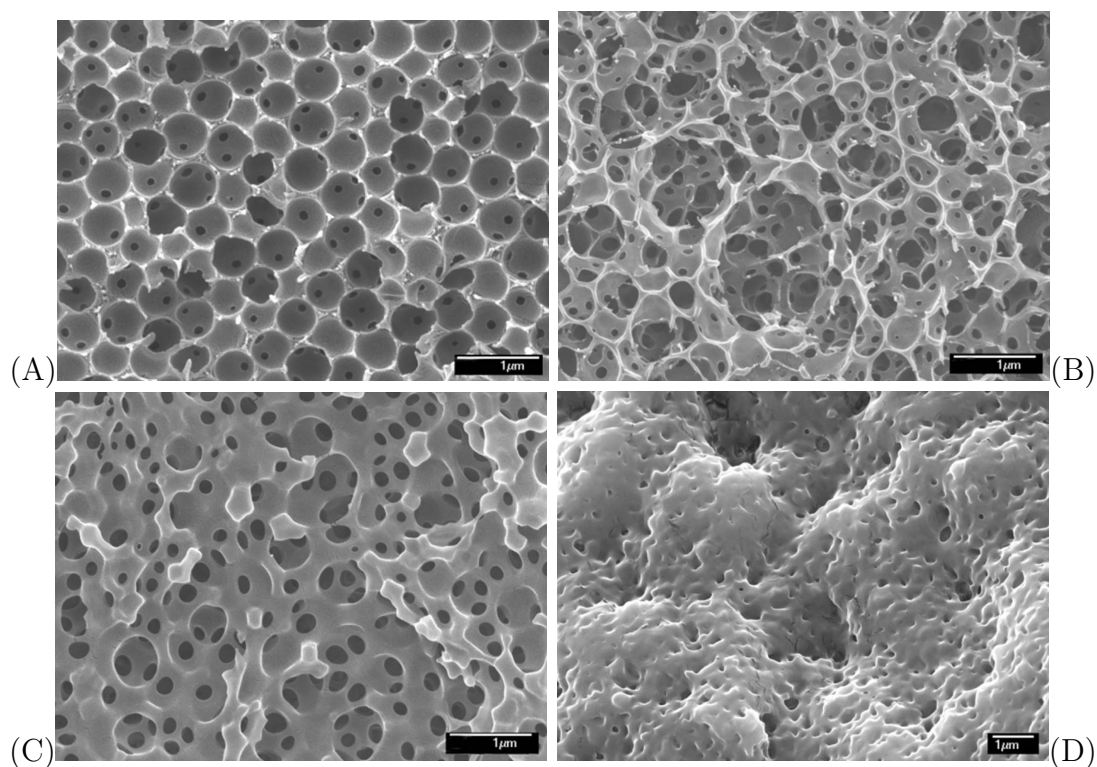
(A) (B) (C) (D)

FESEM image of inverse colloidal crystal membranes formed from colloidal crystal templates containing 440 nm silica particles. The microfiltration membrane was used as a 100 m spacer. Membranes were fabricated using (A)Polystyrene (B)Poly methyl methacrylate (C) poly butyl methacrylate (D) Poly urethane